2010

# Variability and Dynamics of Apoptotic Events in Single Cells

Patrick Bhola


# VARIABILITY AND DYNAMICS OF APOPTOTIC EVENTS IN SINGLE CELLS

A Thesis Presented to the Faculty of

The Rockefeller University

in Partial Fulfillment of the Requirements of

the degree of Doctor of Philosophy

By

Patrick Bhola

June 2010

# Variability and Dynamics of Apoptotic Events in Single Cells

Patrick Bhola, Ph.D.

The Rockefeller University 2010

Apoptosis is a form of programmed cell death that is necessary for development and organism homeostasis. The early stages of apoptosis are marked by the permeabilization of the mitochondrial outer membrane, the release of cytochrome *c* and Smac from mitochondria, and the activation of the caspase family of proteases. The permeabilization of the mitochondria outer membrane is thought to represent the commitment of a cell to an apoptotic fate, and the subsequent release of mitochondrial proteins is an "all or none" phenomenon that is completed in an individual cell within minutes. Although the cellular decision to commit to apoptosis is important for organism homeostasis, there is considerable variability in the onset of apoptosis between cells in culture, even in clonal populations. Here we developed a reporter (pmDEVD) for caspase activation in single cells. The pmDEVD reporter relocalizes from the plasma membrane to the cytoplasm after caspase activation. We find that the reporter has similar kinetic properties but better fold-increase properties than existing reporters. Using the pmDEVD reporter in single cells, we observe that the onset of caspase activity was tightly synchronized between nearby cells. This synchrony was not a consequence of secreted factors and was not correlated to the cell cycle. A similarity of apoptosis times was seen amongst sister and related cells and was lost over successive generations. The times of apoptosis also diverged within a

generation, but this was blocked by inhibiting protein synthesis before triggering apoptosis. These results suggest that the cell-cell variability of apoptosis times is due to the divergence of the molecular composition of the cell, and that the decision to commit to apoptosis at the time of drug addition has a deterministic component. We used the deterministic nature of apoptosis in single cells to monitor the release of mitochondrial release at a rapid temporal resolution. At a rapid time resolution, we find that the release of cytochrome *c* propagates throughout the cell as a spatially coordinated wave. The permeability of the outer membrane to Smac propagates with the same spatial pattern as cytochrome c but lagging in time. This is followed by a wave of increased permeability of the inner membrane to protons. Only afterward do the mitochondria fission. The spatial dependence of the permeability wave was inhibited by thapsigargin, an inhibitor of the endoplasmic reticulum calcium pumps, but buffering cytosolic calcium had no effect. Altogether, these results demonstrate the organized dynamics of apoptosis. First the onset of apoptosis in a single cell has a deterministic component, and second, the trigger for apoptosis is spatially localized, initiating at one or only a few mitochondria and then propagating across the cell.

To Peter, Jenifer, Priya,

Sarah and Lana

# Acknowledgements

I thank Dr. Sandy Simon for being a wonderful teacher and advisor during the past 5 years. I have appreciated and copied his views on the importance of observation in science, and the belief that there are many hidden biological processes waiting to be found.

I thank Dr. Alexa Mattheyses for being a wonderful collaborator. I deeply appreciate the propagated knowledge on imaging and quantification, as well as our many stimulating discussions.

I thank Dr. Marina Fix for being so supportive and helpful since the very beginning. I learned basic lab work from Marina including cloning, and cell culture, and I am very grateful for this.

I thank Shahrnaz Kemal for helping me integrate into the lab, as well as for helping me find things.

Dr. Shai Shaham and Dr. Hermann Steller for their guidance during the faculty advisory committees, and for the courses they taught and their stimulating discussions.

Dr. Richard Youle, the external member of the thesis committee. I am honored to have Dr. Youle given his contributions to the cell biology of apoptosis.

I thank the members of the Simon Lab for a lot of advice and technical help, and for the very active and stimulating lab meetings.

Finally, I appreciate the many reagents received from Roger Tsien, David Piston, Hermann Steller, Richard Youle, Junying Yuan, Douglas Green, Micheal Lenardo, Paul Greengard and Patrick Daugherty.

# Table of Contents

# List of Figures

# List of Tables

# List of Abbreviations

FRET – Forster Resonance Energy Transfer

NES – Nuclear Export Signal

NLS – Nuclear Localization Signal

EGTA - ethylene glycol tetraacetic acid

ROI – Region of Interest

TNFα – Tumor Necrosis Factor Alpha

CHX – Cycloheximide

ETO - Etoposide

STS - Staurosporine

SERCA - Sarco/Endoplasmic Reticulum $Ca^{2+}$- ATPase

$\Delta\Psi$ – Mitochondrial intermembrane space potential

EGFP – Enhanced Green Fluorescent Protein

TMRE – Tetramethyl rhodamine ester

GFP – Green Fluorescent Protein

CFP – Cyan Fluorescent Protein

YFP – Yellow Fluorescent Protein

TRAIL – TNF Related Apoptosis Inducing Ligand

pmDEVD – plasma membrane DEVD reporter

erDEVD – endoplasmic reticulum DEVD reporter

pmControl - plasma membrane Control reporter

erControl - endoplasmic reticulum Control reporter

DD – death domain

DED – death effector domain

PSLD – phosphorylated signal localization domain (from human DNA helicase B)

ER – endoplasmic reticulum

CARD – caspase activation recruitment domain

ANOVA – analysis of variance

# *Chapter1: Introduction*

Apoptosis is a form of programmed cell death which eliminates harmful or unwanted cells in multi-cellular organisms (Ellis et al., 1991). Generally, apoptosis is important for organism development and in the maintenance of organism homeostasis. Below is an overview of some of the early observations of cell death and apoptosis, and some of the organelles and molecules involved in apoptosis with an emphasis on aspects relevant to this thesis.

## *Early Observations of Cell Death*

Early reports of cell death date back to at least 1842 with experiments on cell death in insect metamorphosis (Clarke and Clarke, 1996). Over the next decades, studies on cell death focused on phagocytosis (the process where one cell engulfs another otherwise healthy cell) (Tauber, 2003), and necrosis (the death of injured cells) (Majno and Joris, 1995). Cell death was also observed in various developing organisms, and was eventually proposed to play a vital role (and not a detrimental role) in organism development (Glucksmann, 1951). Experimental manipulation of cell death in organisms was reported in the 1950's by Rita-Levi Montalcini and Viktor Hamburger on neuronal cell death in the chick embryo. These experiments described cell death in response to

limb bud removal (Levi-Montalcini, 1987; Hamburger and Levi-Montalcini, 1949), and they later identified the nerve growth factor (NGF) as a molecule that was preventing cell death (Levi-Montalcini, 1987).

### *Morphological Characterization of Cell Death*

The application of electron microscopy to biological specimens beginning in the 1940's enabled more detailed observations of the morphology and organelles present within cells (Porter et al., 1945). The application of electron microscopy to necrotic cell death showed swelling of organelles and of the cell (Kerr, 1969; Kerr, 1970). A separate type of cell death (autophagy) was characterized by the formation of lysosomes and vacuolar vesicles (Arstila and Trump, 1968). Later studies on cell death in developing tissues revealed the contraction of cells, and the condensation of chromatin which was in contrast to the morphology of necrotic cell death (Kerr et al., 1972). This developmental cell death was initially referred to as shrinkage necrosis (Kerr, 1971), and was later renamed apoptosis (Kerr et al., 1972).

### *Genetic Evidence of Apoptosis*

A genetic program underlying cell death was suggested by experiments showing that blocking protein and RNA synthesis inhibited cell death in insects and the tadpole tail (Lockshin, 1969; Tata, 1966). The identification of specific cell death genes was

initiated by the use of *C. elegans* as a model system for cell death. In these organisms 131 of 1090 cells undergo cell death (Sulston and Horvitz, 1977; Sulston et al., 1983). A close analysis of the lineage and fates of individual cells showed that the same cells were reproducibly eliminated (Sulston, 1976), indicating that the deaths were not only regulated on the organism level, but are also programmed at the level of single cells. Apoptosis genes were identified by mutagenizing somatic cells of *C. elegans,* and screening for cell death abnormal (*ced*) mutants (Ellis and Horvitz, 1986). Several mutants were found to have defects in apoptosis including *ced-3* and *ced-4*, both of which are absolutely required for cell death (Ellis and Horvitz, 1986).

A separate genetic analysis using insects as a model systems uncovered several proteins involved in programmed cell death. In cells from the moth *Spodoptera frugiperda* it was noted that mutations to the the baculovirus p35 gene could result in apoptosis after viral infection which could be rescued by a homologous gene termed *iap* present in another insect virus (Crook et al., 1993). Shortly afterwards, a genetic screen identified a cluster of genes required for almost all programmed cell death in *Drosophila* embryogenesis (White et al., 1994). The characterization of this locus resulted in the identification of the apoptosis genes *reaper, hid* and *grim* (Chen et al., 1996; Grether et al., 1995; White et al., 1994) which facilitate apoptosis. Later the physiological target of the proteins encoded by these apoptosis inducing genes was identified (Drosophila Inhibitor of Apoptosis Protein 1) which was shown to have homology to the apoptosis repressing baculovirus p35 gene (Goyal et al., 2000). Subsequent analysis of these

molecules suggested a system repressing programmed cell death, and a mechanism to relieve the repression (reviewed in (Kornbluth and White, 2005)).

Insights into the genetics of mammalian programmed cell death resulted from the cloning and characterization of the Bcl-2 proto-oncogene. The Bcl-2 gene was identified at the chromosomal breakpoint t(14;18) in human B cell lymphoma (Bakhshi et al., 1985). Unlike most other oncogenes identified at the time, Bcl-2 did not induce proliferation, but instead prevented cell death (Vaux et al., 1988). This was not only demonstrated in cell culture, but also in mice over-expressing Bcl-2 along with c-myc - which developed leukemia (McDonnell and Korsmeyer, 1991; Strasser et al., 1990), and in Bcl-2 knockout mice developed excessive cell death of lymphocytes and melanocytes (Veis et al., 1993). Importantly, the over-expression of Bcl-2 in *C. elegans* had had a protective effect on cell death in *C. elegans* (Vaux et al., 1992). This not only demonstrated a cell death defect in human pathology, but also that cell death components in vastly different species is functionally conserved (Vaux et al., 1992). Since the demonstration of an apoptotic genetic program, many apoptosis genes and molecules have been characterized.

## *Molecular Components of Apoptosis Signaling*

Below we give an overview of the molecules involved in mammalian apoptosis. Two non-distinct apoptotic pathways have been defined based on whether the triggering

mechanism is internal to the cell (intrinsic apoptosis), or whether the apoptotic trigger is external to the cell (extrinsic apoptosis) (Ow et al., 2008). Some intrinsic triggers include DNA damage, endoplasmic reticulum (ER) stress, or microtubule stress. External stimuli are often ligands which bind to receptors on the surface of the cells, and initiate signaling that culminates in the death of the cell (Fulda and Debatin, 2006). Example ligands include tumor necrosis factor α (TNFα) (Carswell et al., 1975), the TNF α related apoptosis inducing ligand (TRAIL) (Wiley et al., 1995), and Fas Ligand (Suda et al., 1993). Nonetheless, it is important to consider the overlap between molecules stimulated by different triggers, and that these pathways may not actually be distinct.

Below is a description of some of the molecules and processes which occur in response to apoptotic stimuli. These include the Bcl-2 family, mitochondrial associated proteins (including cytochrome c and Smac), and the caspase family of proteases.

### *Mitochondria Overview*

Mitochondria play a central role in the oxidative phosphorylation cycle and thus in the generation of cellular ATP (Slater, 1977). Electron microscopy studies of mitochondria revealed the substructure of mitochondria which includes the outer mitochondrial membrane (OMM), the intermembrane space (IM), the inner mitochondrial membrane (IMM), and the mitochondrial matrix (Palade, 1953). The IMM is organized in a manner that creates invaginations into the matrix called cristae spaces

(Palade, 1953; Frey and Mannella, 2000). Several membrane bound complexes exist on the IMM which transport protons and other ions in or out of the mitochondrial matrix (Schultz and Chan, 2001). The transport of protons creates a membrane potential ($\Delta\Psi$) across the IMM which is required for the synthesis of ATP. The presence of a potential across the IMM can be observed by the accumulation of lipophilic cations (such as TMRE and TMRM), which preferentially accumulate actively respiring mitochondria (Ehrenberg et al., 1988).

Mitochondria are highly dynamic organelles which fission and fuse with other mitochondria (Bereiter-Hahn and Voth, 1994). The fission and fusion of mitochondria are regulated by several proteins such as dynamin related protein 1 (Drp1), Fis1, Bax, and many other proteins (Hoppins et al., 2007). Several human disorders are associated with mutations in fission and fusion genes including Charcot-Marie-Tooth-subtype 2A and dominant optic atrophy (Alexander et al., 2000; Pedrola et al., 2005). Notably some of these fission/fusion proteins are also involved in apoptosis (Suen et al., 2008).

### *Mitochondrial Role in Apoptosis*

The mitochondrial localization of Bcl-2 in mammals and ced-4 in *C. elegans* suggested that the mitochondria play significant roles in apoptosis (Hockenbery et al., 1990). Since then various proteins associated with the mitochondria have been discovered to be involved in apoptosis. Some of these molecules include the Bcl-2

family of molecules, cytochrome c, Smac/DIABLO, and Omi, among many others (Ow et al., 2008). Furthermore, modifications to the mitochondria structure occur during apoptosis including mitochondrial fission and fragmentation (ROUILLER, 1957; Zhuang et al., 1998), loss of mitochondrial intermembrane space potential (Goldstein et al., 2000), and changes in the geometry of the mitochondria cristae spaces (Sun et al., 2007). Below we discuss some of the mitochondrial associated molecules relevant to this thesis and their involvement in apoptosis.

### *Bcl-2 Family*

The Bcl-2 family of proteins play critical roles in the release of mitochondrial proteins during apoptosis (Kluck et al., 1997; Yang et al., 1997). The expression and concentration of specific Bcl-2 molecules have been proposed to determine the sensitivity of cells to some apoptotic signals and some chemotherapies (Danial and Korsmeyer, 2004; Deng et al., 2007). Bcl-2 itself was identified at the chromosomal breakpoint of t(14;18) in human B cell lymphoma (Bakhshi et al., 1985; Cleary and Sklar, 1985). Further Bcl-2 related molecules were identified through protein-protein interactions or based on sequence homology. At least 19 Bcl-2 molecules have been identified to play a role in apoptosis (Wang and Youle, 2009). These molecules can be classified based on the presence of four Bcl-2 Homology (BH) domains, and their presumptive role in apoptosis (Table 1, Figure 1) (Danial and Korsmeyer, 2004).

**TABLE 1: Bcl-2 molecules**

| BH3 Only | Anti-Apoptotic | Pro-Apoptotic |
|---|---|---|
| Bad | Bcl-2 | Bax |
| Bim | Bcl-XL | Bak |
| Bid | Mcl1 | Bok |
| Noxa | A1 | |
| Puma | Bcl-W | |
| Bik | Bcl-Rambo | |
| Hrk | Bcl-L10 | |
| Bmf | Bcl-10 | |

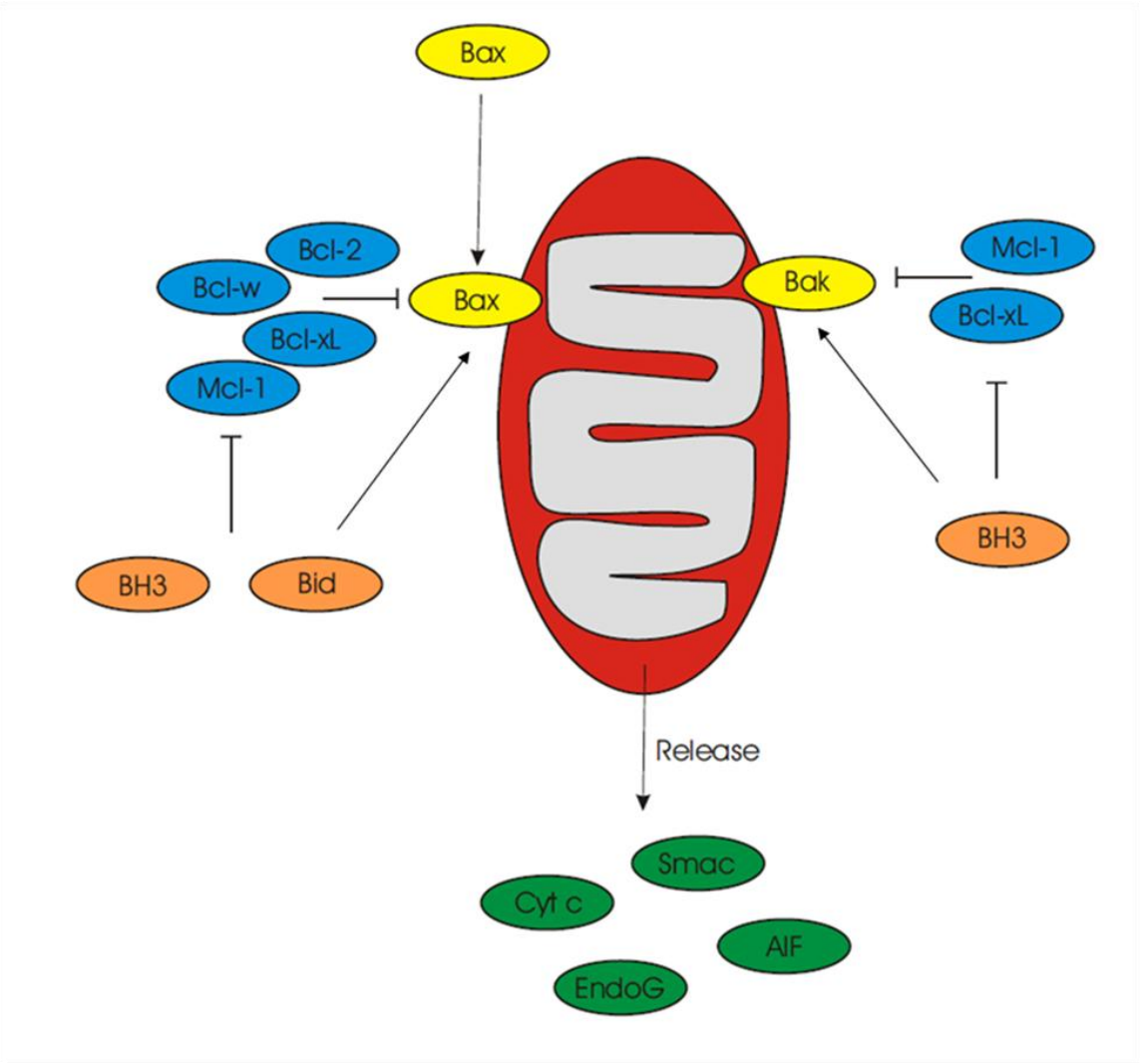


**Figure 1: Proposed roles of Bcl-2 and mitochondrial proteins during apoptosis. Anti-apoptotic (blue) and BH3-only (orange) molecules control the activity of the pro-apoptotic (yellow) Bcl-2 molecules. Oligomerization of pro-apoptotic molecules results in the release of mitochondrial proteins such as cytochrome c and Smac. The diagram does not include all known Bcl-2 molecules.**

Bcl-2 molecules have a variable number of the four distinct BH3 domains. The number of domains roughly correlates with the apoptotic function of the molecule (Danial and Korsmeyer, 2004). Pro-apoptotic molecules (such as Bax and Bak) possess BH domains 1-3, and are directly involved in the release of apoptotic mitochondrial proteins (Chittenden et al., 1995; Zha et al., 1996a). The BH3-only molecules enable the apoptotic function of Bax and Bak either by direct or indirect stimulation (Boyd et al., 1995; Lomonosova and Chinnadurai, 2008). The third category of Bcl-2 molecules possesses BH1-4 domains, and inhibit the pro-apoptotic or the BH3-only molecules (Muchmore et al., 1996; Danial and Korsmeyer, 2004). The subcategories of the Bcl-2 family are discussed in more detail below. Notably, there is significant controversy on the interactions of the Bcl-2 molecules and how they permeabilize the mitochondrial outer membrane (Antignani and Youle, 2006; Chipuk et al., 2010).

### *Bax/Bak*

During apoptosis Bax and Bak undergo conformational changes and oligomerize at discrete sites on the mitochondria (Nechushtan et al., 2001). The oligomerization of Bax and Bak is proposed to result in the permeablization of the mitochondria and the release of cytochrome c, Smac/DIABLO and other molecules involved in the execution of apoptosis. A double knockout of Bax and Bak blocks the release and inhibits caspase-3 processing and activity in response to intrinsic stimuli (Wei et al., 2001). While

extrinsic stimuli such as TNFα is still able to induce caspase activation in Bax/Bak double knockout cell lines, it is not able to induce cytochrome c release (Wei et al., 2001).

Bax is a monomeric protein that is localized in the cytoplasm and loosely associated with mitochondria (Hsu et al., 1997). It is comprised of 9 α-helices which form a hydrophobic pocket that is occupied by its C-terminal helix in its inactive state (Suzuki et al., 2000). During apoptosis Bax translocates to the mitochondria, and inserts into the outer membrane (Nechushtan et al., 2001; Gross et al., 1998), with liposomal assays suggesting that α-helices 5, 6, and 9 insert into the outer mitochondrial membrane (Annis et al., 2005). Bax then proceeds to oligomerize at discrete sites on the mitochondria rather than uniformly throughout the mitochondria (Nechushtan et al., 2001; Lovell et al., 2008). Although large Bax oligomers form on the mitochondria, experiments on isolated mitochondria or on liposomes suggest that only a few molecules are minimally required for permeabilization (Saito et al., 2000; Martinez-Caballero et al., 2009). Furthermore, live cell imaging of Bax fused to the green fluorescent protein (GFP) indicates that the majority of Bax accumulation at the mitochondria occurs after the permeabilization of the mitochondrial outer membrane (Dussmann et al., 2010).

Unlike Bax, Bak is constitutively associated with the mitochondrial membrane and the endoplasmic reticulum (Zong et al., 2003; Wei et al., 2000). Prior to apoptosis Bak can associate with anti-apoptotic proteins such as Mcl-1 and Bcl-xL (Willis et al., 2005), and also with VDAC (Cheng et al., 2003). However, co-immunoprecipitation

experiments suggest that Bax and Bak are not all be constitutively associated with anti-apoptotic Bcl-2 proteins, and may exist as monomers (Hsu and Youle, 1997; Cheng et al., 2001). The precise mechanism of how Bax/Bak is activated and regulated by other Bcl-2 members is unclear, though several models have been proposed to explain their regulation (Chipuk and Green, 2008); these are discussed in more detail in a later section. Nonetheless, during apoptosis Bak redistributes on the mitochondria and electron microscopy images indicate that Bak is found at discrete sites after apoptotic stimuli (Nechushtan et al., 2001). Bax and Bak double knockout lines also display altered mitochondrial morphology and mitochondrial fusion (Karbowski et al., 2006) which may suggest a link between mitochondrial morphology and apoptosis, or non-apoptotic functions of Bax and Bak.

Various mechanisms have been proposed for how Bax and Bak mediate the release of cytochrome c. These include the formation of a proteolipid pore or channel (Basanez et al., 2001; Martinez-Caballero et al., 2009), and the modification of an existing channel (Kroemer et al., 2007). Evidence supporting the role of a modified pore is based on the ability of Bax to accelerate the opening of a voltage dependant ion channel (VDAC) in liposomes (Shimizu et al., 1999). VDAC along with the adenine-nucleotide translocase (ANT) was proposed to form the permeability transition pore (PTP) which induces the swelling of the matrix, the rupturing of the mitochondria, and the release of cytochrome c. However, knockouts of VDAC or ANT do not recapitulate the phenotype of the Bax/Bak double knockout (Baines et al., 2007; Kokoszka et al.,

2004). Nonetheless it is possible that another modified channel is necessary for cytochrome c release but has not been identified.

Some evidence support the existence of Bax/Bak protein pores. First Bcl-2 proteins are structurally similar to bacteria pore toxins suggesting Bax and Bak may permeabilize the OM in a similar way (Muchmore et al., 1996). Furthermore, Bax can permeabilize synthetic liposomes which lack the additional proteins present in the mitochondrial membrane (Saito et al., 2000). However, while the existence of a channel or a pore has been proposed with Bax or Bak as the major component, key structural and biochemical evidence of a pore is lacking (Antignani and Youle, 2006; Chipuk and Green, 2008).

### *Bcl-2 Inhibitors*

Several Bcl-2 molecules inhibit the association of Bax and Bak into oligomers. These include Bcl-2, Bcl-xL, Bcl-W, MCL-1 and A1. Individual Bcl-2 anti-apoptotic molecules are proposed to have specific interactions with Bax and Bak (Willis et al., 2007) or with the BH3 only proteins (Chen et al., 2005; Letai et al., 2002; Kim et al., 2006). However there is some disagreement on the interactions between anti-apoptotic and pro-apoptotic proteins (Chipuk and Green, 2008). For example one immunoprecipitation study found that Bcl-$x_L$ is associated with Bak prior to apoptosis (Willis et al., 2005), whereas another study did not detect an interaction (Cheng et al.,

2001). Several possibilities explaining this difference could include an experimental difference in cell types, expression levels or in purification processes. More generally, the precise mechanism of inhibition, and the nature of these interactions remain unclear and are discussed in detail below (see Models of Bax/Bak Activation). Several drugs have been designed to inhibit Bcl-2 anti-apoptotic proteins to enable the progression of apoptosis in tumors or tumor cells (Oltersdorf et al., 2005; Nguyen et al., 2007).

### *Bcl-2 Sensitizers and BH3-Only Proteins*

The activation of Bax and Bak depends in part on the state of a subset of the Bcl-2 family called the BH3-only proteins (Wang et al., 1996). These include Bad, Bim, Bid and Noxa/Puma among other proteins (Giam et al., 2008). The activity of the BH3-only proteins can be modified post-translationally. These can include the inactivation of Bad and the activation Bim by phosphorylation events (Harada et al., 1999; Lei and Davis, 2003). Additionally, the pro-apoptotic function of Bid results from the cleavage of the amino terminal resulting in truncated Bid (tBid) (Zha et al., 1996b; Li et al., 1998; Hubner et al., 2008).

### *Models of Bax and Bak Activation*

Two often cited models have been proposed to explain the mechanism by which the Bcl-2 pro- and anti-apoptotic molecules proteins activate the Bax and Bak effector molecules. One model proposes that Bax and Bak can be directly activated by a subset of BH3 only molecules which interact with and structurally modify the effector proteins, and that the remaining BH3 molecules can alter the apoptotic sensitivity of mitochondria by inhibiting anti-apoptosis Bcl-2 proteins, but cannot themselves directly activate Bax or Bak (Kim et al., 2006). For example, it is thought that tBid (an activated and cleaved form of Bid) enables the association of Bax with mitochondria membrane based on *in vitro* liposomal experiments in the absence of other proteins (Lovell et al., 2008). More generally, of the BH3 peptides from BH3 only proteins, only Bid, Bim and Puma peptides were able to induce Bax mediated liposomal or mitochondrial permeabilization without the addition of other proteins (Letai et al., 2002). One of the objections to this model is the poorly detected interaction between Bax/Bak and the direct activator proteins (Willis et al., 2007) – which could indicate a transient interaction, but may also indicate that a direct activation of Bax and Bak is not a physiologically relevant signal.

Alternatively, it is possible that the BH3 only proteins interact with the Bcl-2 inhibitors, there by disengaging Bax or Bak from the anti-apoptotic inhibitor . In these models, Bcl-2 inhibitors would constantly keep Bax or Bak from being activated until disengaged by the BH3 only molecules (Adams and Cory, 2007). In support of this model is that while BH3 only peptides can engage Bax or Bak (Letai et al., 2002), there is

little or no interaction between these BH3 proteins and Bax/Bak in cells (Willis et al., 2007). Moreover, there is detectable interaction between over expressed anti-apoptotic proteins with Bak (Willis et al., 2005). One of the objections to this model is that several immunoprecipitation experiments indicate that Bax and Bak exist as monomers in vivo (Hsu and Youle, 1997; Cheng et al., 2001). These unattached and yet inactive Bax/Bak molecules are in apparent contradiction to this model – though one possibility is that there are other forms of Bax/Bak sequestering and inhibition that is not fully understood. Finally, another possibility is that both of these models are insufficient to explain the Bcl-2 family interactions, and a newer model is needed.

### *Cytochrome c*

Cytochrome c was initially discovered for its role in the electron transport chain and in the production of ATP (Slater, 1977). It is synthesized in the cytosol, and is imported into the mitochondria where it acquires a heme group. The heme group consists of an iron molecule which can covert between Fe2+ and Fe3+, thus enabling cytochrome c to serve as an electron donor and acceptor. In the context of the electron transport chain, cytochrome c transports electrons between Complex III and Complex IV (Schultz and Chan, 2001). Cytochrome c is predominantly localized to the intermembrane space of mitochondria and is thought that 85% of mitochondrial cytochrome c resides in the cristae spaces of the mitochondria (Bernardi and Azzone, 1981) where it associates with cardiolipin (Ott et al., 2007).

Early cell-free experiments indicated the depletion of mitochondria from Xenopus extracts reduced caspase activity suggesting that a mitochondrial protein is required for the activation of caspase-3 (Newmeyer et al., 1994). Using biochemical and centrifugation techniques caspase activation was shown to require cytochrome c, ATP, and another factor called the apoptosis protease activating factor-1 (Apaf-1) (Liu et al., 1996). Cell lines derived from knockout cytochrome c mice show reduced caspase-3 activation, however are able to undergo apoptosis in response to some stimuli (Li et al., 2000). Knocking in a mutagenized cytochrome c (K72A) that functions in the electron transport chain, but does not bind to Apaf-1 results in mice in which the majority died prenatally, but with a few that were able to survive for several weeks (Hao et al., 2005). Furthermore, while K72A MEFs are resistant to apoptosis induced by UV irradiation, K27A thymocytes display a similar apoptosis response as the wild-type cytochrome c thymocytes (Hao et al., 2005). Thus, the survival of some of the K27A mice, along with the similar apoptosis response of K72A thymocytes suggests that there may be cytochrome c independent mechanisms required for apoptosis.

Once in the cytosol, cytochrome c can interact with individual molecules of Apaf-1 (Zou et al., 1997). These molecules then oligomerize into a complex called the apoptosome which is able to induce caspase activity (Li et al., 1997; Zou et al., 1999). Furthermore, once cytochrome c relocalizes from the mitochondria to the cytosol, it can also interact with the inositol triphosphate receptor ($IP_3R$) which is embedded in the endoplasmic reticulum (ER) and controls calcium release (Boehning et al., 2003). The cytochrome c- $IP_3R$ interaction is proposed to enable the release of calcium from the ER,

which in turn can induce the release of cytochrome c from other mitochondria, thus amplifying the initial release cytochrome c (Boehning et al., 2003; Boehning et al., 2005).

Cytochrome c-GFP fusions have been found to localize to mitochondria prior to apoptosis, however this takes considerable time (>48 hours) to properly localize to mitochondria (personal communication D. Boehning). The release of cytochrome c GFP from mitochondria is complete within minutes, and is proposed to occur in a spatially invariant manner through the cell (Goldstein et al., 2000; Munoz-Pinedo et al., 2006). Coincident with the release of cytochrome c, mitochondrial intermembrane potential ($\Delta\Psi$) is also lost, though inhibitors of caspase activation can delay $\Delta\Psi$ loss (Munoz-Pinedo et al., 2006). Nonetheless, the acquisition frequency of the images in these studies is similar to the phenomenon that is being imaged, thus potentially masking finer dynamic behavior.

### *Smac/DIABLO*

During apoptosis, Smac/DIABLO (second mitochondria-derived activator of caspases / direct IAP-binding protein with low pI) is also released from the mitochondria (Du et al., 2000; Verhagen et al., 2000). Smac is synthesized in the cytosol and when imported into the mitochondria, the 55 N-terminal amino acids are cleaved resulting in the 4 amino acids at the N-terminal AVPI (Burri et al., 2005). The processing of Smac and the post-translocation AVPI amino terminal plays a role in promotion of caspase

activity (Wu et al., 2000). The processed form of Smac resides in the intermembrane space of mitochondria, with crystallography and biochemical data suggesting that it exists as a homodimer (Chai 2000). Once released into the cytosol, Smac can interact with Inhibitor of Apoptosis (IAP) proteins which themselves can directly inhibit or antagonize caspase activity (Verhagen et al., 2000; Du et al., 2000). Smac is proposed to inhibit IAP activity by substrate competition, direct IAP binding and inhibition or by inducing IAP degradation (Lacasse et al., 2008). The precise mode of inhibition is somewhat unclear and depends on the specific IAP; this is discussed in more detail in a later section.

Splice variants of Smac include Smac-beta, and Smac3. Smac-beta does not localize to the mitochondria, and does not bind to IAPs, however, its overexpression can predispose cells to certain apoptosis stimuli (Roberts et al., 2001). By comparison, Smac3 does localize to mitochondria, is released during apoptosis, and can trigger degradation of XIAP (Fu et al., 2003). Smac knockout mice are viable, and still undergo apoptosis in response to a variety of stimuli (Okada et al., 2002). One possibility explaining the viability of Smac knockout mice is the redundancy of Smac in apoptosis, or alternatively, a splice variant may compensate for the Smac knockout.

Smac release is presumed to occur at the same time as cytochrome c release (Munoz-Pinedo et al., 2006), and it has been suggested that they are released by the same mechanism. However this order may depend on the apoptosis inducing drug and the genetic background of the cell. For example in mouse embryonic fibroblasts (MEFs) from Bid, Bad or Bak single knockout mice, in response to TRAIL treatment, Smac

release is inhibited while cytochrome c release occurs (Kandasamy et al., 2003). This suggests that different mitochondrial modifications may be needed for Smac or cytochrome c release. Even more interesting is that Smac release is inhibited in cytochrome c KO mice (Hansen et al., 2006). This may indicate a feedback loop in which cytosolic cytochrome c is required for Smac release in single cells.

### *Apaf-1*

Apaf-1 forms a critical part of the apoptosome which activates the caspase-9, and in turn caspase-3 (Li et al., 1997; Zou et al., 1997). While the majority of Apaf-1 knockout mice are embryonic lethal, (depending on the genetic background of the mice), a small percentage can survive to adulthood (Yoshida et al., 1998; Honarpour et al., 2000). MEFs isolated from Apaf-1 knockout mice undergo apoptosis, and are more resistant to some apoptotic triggers than the cytochrome c K72A knockin mice suggesting that there may be cytochrome c independent but Apaf-1 dependant mechanisms to induce apoptosis (Hao et al., 2005).

Apaf-1 consists of a caspase recruitment domain (CARD) and two WD40 domains (Hu et al., 1998; Li et al., 1997). Prior to cytochrome c release from the mitochondria, Apaf-1 exists as a cytosolic monomer with its CARD domain bound to its WD40 domain (Acehan et al., 2002; Li et al., 1997; Zou et al., 1999). When released into the cytoplasm, cytochrome c binds to the Apaf-1 WD40 domain exposing the CARD

domain. The presence of ATP enables the oligomerization of Apaf-1 into a wheel like structure consisting of approximately 7 Apaf-1 proteins (Acehan et al., 2002; Li et al., 1997), with the Apaf-1 CARD domains located in the center. The CARD domains bind to caspase-9 thus forming the macromolecular complex called the apoptosome (Zou et al., 1999). It is proposed that the proximity of caspase-9 at the center of the apoptosome enables the activation of caspase-9 (Li et al., 1997; Rodriguez and Lazebnik, 1999; Stennicke et al., 1999)

### *Other Mitochondrial Modifications during Apoptosis*

During apoptosis, the structure of the mitochondria undergoes several changes. Mitochondria cristae junctions become wider, and at a later time the cristae structure changes from being long and tubular, to spherical and round (Sun et al., 2007). Opa1 – a protein that is localized in a macromolecular complex at the cristae junction – is cleaved during apoptosis enabling the widening of the cristae (Pellegrini and Scorrano, 2007). This is proposed to allow the passage of cytochrome c out of the cristae space (Scorrano et al., 2002). However, the temporal ordering of Opa1 cleavage and cytochrome c relocalization within the mitochondria has yet to be directly measured.

Mitochondria also become fragmented during apoptosis, and in some instances swell. This was initially thought to be a mechanism of release of cytochrome c, but direct imaging shows that cytochrome c release occurs before significant swelling (Goldstein et

al., 2005). Mitochondria also lose their membrane potential during apoptosis at a similar time as cytochrome c release (Munoz-Pinedo et al., 2006). However, the addition of caspase inhibitors delays loss of membrane potential, while still enabling cytochrome c release (Goldstein et al., 2000).

### *Caspases*

Caspases are a family of proteases that are involved in apoptosis, inflammation, differentiation, and neuronal pruning, among other functions (Kumar, 2007). In mammalian cells, at least fourteen caspases have been identified and are referred to as caspase-1 through caspase-14 according to defined nomenclature (Alnemri et al., 1996). The caspases are characterized by a cysteine nucleophile in their active site, and the requirement for cleavage of substrates after aspartic acids (aspase) (Thornberry et al., 1992). Caspases are translated as inactive precursors called zymogens or procaspases which zymogens contain an inhibitory N-terminal prodomain of variable size, and a large and small subunit (17-20 kDa and 10-12 kDa respectively) (Yan and Shi, 2005). The activation of caspases represents a critical step in the progression of apoptosis resulting in the cleavage of transcription factors, translation factors, cellular structures, among other vital cellular components (Dix et al., 2008; Timmer and Salvesen, 2007).

Caspase-1 was the first identified mammalian caspase as the protease responsible for the cleavage and activation of the precursor of IL-1β, and was accordingly named IL-

1β Converting Enzyme (Cerretti et al., 1992). Shortly afterwards, the molecular characterization of the protein encoded by the *C. elegans ced-3* gene resulted in identification of an enzyme with significant homology to the active region of caspase-1 (Yuan et al., 1993). Since these initial discoveries, families of caspases have been discovered in various organisms identified and were found to play a role in apoptosis (and other processes) (Vaux and Korsmeyer, 1999).

Caspases-2,-3,-6,-7,-8,-9 and -10 play roles in response to various apoptotic stimuli. These are classified as initiator caspases or as executioner caspases based on the length of their prodomains, and on their presumed function in apoptosis (Table 1) (Yan and Shi, 2005). Initiator caspases are activated early in apoptosis and have prodomains that are longer than 90 amino acids. These pro-domains enable the association with other molecules required for caspase activation (Yan and Shi, 2005). In contrast executioner caspases have significantly shorter prodomains (20-30 amino acids), are active late in apoptosis, and when activated, cleave a large number of cellular substrates (Dix et al., 2008; Timmer and Salvesen, 2007). The early/late involvement is largely based on genetic evidence (Kumar, 2007) and immunodepletion of in vitro cultures (Slee et al., 1999). Thus, these experiments do not preclude the existence of overlapping activities, or of a synergistic relationship between initiator and executioner caspases.

***Table 2: Classification of Apoptotic Caspases***

| Initiator | Executioner |
|---|---|
| Caspase-9 | Caspase-3 |
| Caspase-8 | Caspase-6 |
| Caspase-10 | Caspase-7 |
| Caspase-2 | |

***Caspase-9***

Once released from the mitochondria, cytochrome c and Apaf-1 associates with caspase-9 to form the apoptosome which in turn processes and activates caspase-3 (Li et al., 1997). After translation, caspase-9 is localized in the cytosol and exists as a monomer (Stennicke et al., 1999; Renatus et al., 2001). It consists of an N-terminal pro-domain with a caspase recruitment domain (CARD) which is responsible for the association of caspase-9 with Apaf-1 (Li et al., 1997). Caspase-9 knockout mice reveal excessive brain tissue resulting from decreased apoptosis, and are embryonic or perinatal lethal depending on the genetic background (Hakem et al., 1998; Kuida et al., 1998).

While caspase-9 can be cleaved, the activation of caspase-9 does not require the removal of its N-terminal prodomain (Stennicke et al., 1999). Two hypothesis exist for the activation of caspse-9: the induced proximity model and the allosteric model

(Boatright and Salvesen, 2003; Shi, 2004). The allosteric model proposes that caspase-9 monomers are activated directly (Rodriguez and Lazebnik, 1999), while the induced proximity model proposed that the association of caspase-9 monomers in the apoptosome brings caspase-9 close together which enables the multimerization of caspase-9 and thus its activation (Boatright et al., 2003).

### *Caspase-3 and Caspase-7*

In mammalian cells, caspase-3 is presumed to be the major executioner caspase that cleaves the majority of cellular substrates. Caspase-3 can be processed and activated by initiator caspases such as caspase-8, and -9, or by executioner caspases such as caspase-7 and caspase-3 itself (Pop and Salvesen, 2009). Several substrates of caspase-3 include poly(ADP-ribose) polymerase (PARP), actin, and many other vital cellular proteins (Dix et al., 2008; Timmer and Salvesen, 2007). Caspase-7 is highly similar to caspase-3 based on sequence homology, and based on the cleavage of preferred substrates (Fuentes-Prior and Salvesen, 2004; Thornberry et al., 1997). Furthermore, their inactive and active structures show similar features (Chai et al., 2001; Mittl et al., 1997; Riedl et al., 2001; Rotonda et al., 1996).

Shortly after translation, caspase-3 and caspase-7 zymogens form inactive dimers in the cytosol (Yan and Shi, 2005). In this pre-apoptotic form, the activity of executioner caspases is inhibited by the presence of the prodomain and by spacers between the large

and small subunits (Boatright and Salvesen, 2003). Executioner caspases are processed by the initiator caspases, resulting in the removal of the pro-domain and cleavage of the small and large subunits. Structural studies indicate that the cleavage of the linker between the small and large subunit enables a structural rearrangement and formation of the catalytic site (Yan and Shi, 2005). The result is an active executioner caspase is a tetramer consisting of two large and two small subunits (Chai et al., 2001; Mittl et al., 1997; Riedl et al., 2001; Rotonda et al., 1996).

Caspase-3 knockout mice were initially thought to be embryonic lethal, with significant cell survival in the central nervous system (Kuida et al., 1996). However, in different genetic backgrounds, caspase-3 knockout mice survive to birth, with cardiovascular defects (Lakhani et al., 2006). Similar results are seen of caspase-7 (Lakhani et al., 2006). These single knockout experiments suggest that caspase-3 and caspase-7 are not absolutely necessary for apoptosis in all tissues, and that they may have overlapping functionality. While caspase-3 and -7 double knockout mice can survive to birth, they die shortly afterwards, and display significant heart development problems (Lakhani et al., 2006). Furthermore, the double knockout mice show delayed mitochondrial permeabilization suggesting that there may be a caspase feedback loop to amplify cytochrome c release (Lakhani et al., 2006).

### *Caspase-8 and Caspase-10*

Caspase-8 and caspase-10 are important components of apoptosis induced by extracellular ligands such as TRAIL, sFasL or TNFα (Muzio et al., 1996; Boldin et al., 1996). Caspase-8 knockout mice are embryonic lethal with defects in cardiac and T-cell development (Varfolomeev et al., 1998). The defects in the KO mice result in a lack of apoptosis induced by death receptors, however apoptosis still occurs in response to intrinsic stimuli (Varfolomeev et al., 1998). Caspase-8 consists of an N-terminal prodomain with 2 repeats of the death effector domain (DED). The DED enables association with the death domains (DD) in the adaptor proteins FADD and TRADD (Boldin et al., 1996; Carrington et al., 2006). In response to sFasL, caspase-8 associates with a macromolecular complex called the death induced signaling complex (DISC) at the plasma membrane resulting in caspase-8 activation (Lee et al., 2006). In contrast, when cells are treated with TNFα, caspase-8 does not associate with the DISC at the plasma membrane, but instead forms an oligomer with FADD in the cytosol where caspase-8 is activated (Micheau and Tschopp, 2003). The mechanism of caspase-8 activation remains unclear and is proposed to auto-activate upon close proximity (Lee et al., 2006). Once activated casapase-8 can cleave and activate Bid which enables the association of Bax with mitochondria and release of cytochrome c from the mitochondria (Li et al., 1998). Alternatively, caspase-8 can directly process and activate caspase-3 (Stennicke et al., 1998).

### *Caspase-2*

Caspase-2 is an apical caspase that is response the activation of cell death in response to DNA damage, TRAIL and heat shock stimulus (Tinel and Tschopp, 2004; Tu et al., 2006). Like other apical caspases, it contains a long pro-domain, which has a CARD protein-protein interaction domain (Baliga et al., 2004). The activation of caspase-2 is thought to occur in a similar manner to caspase-9. Prior to apoptosis, caspase-2 is a monomer, and after an apoptotic stimulus, it binds to the protein RAIDD in a multimeric scaffolding platform called the PIDDosome (Tinel and Tschopp, 2004). Here multiple caspase-2 molecules are brought into close proximity which is thought to activate it.

### *Cleavage Preferences of Caspases*

Several studies have been performed to identify the optimal substrates that will be processed by caspases for the purposes of creating specific reporters of caspase activity. The initial studies identifying substrate preference were based on fluorogenic substrates with four amino acids that bind to the active sites of caspases (Thornberry et al., 1997). Caspase-9 prefers the four amino acid sequence 'LEHD', and caspase-8 prefers the sequence 'IETD'. Caspase-3 and -7 have similar substrate preferences for the sequence 'DEVD', however they are also able to efficiently cleave both LEHD and IETD (Thornberry et al., 1997). Extending the substrate size beyond four amino acids results in greater substrate specificity, however there is still considerable overlap (Stennicke et al.,

2000). This redundancy is likely a beneficial feature in the event that a particular caspase is mutagenized and inactivated, however it makes the design of a reporter for specific caspase activity difficult (McStay et al., 2008).

### *Inhibitor of Apoptosis Proteins*

In contrast to the molecules involved in the activation of caspases, the activation of caspases can be inhibited by a class of proteins called the inhibitor of apoptosis family (IAP). The IAP family consists of eight distinct molecules which contain several BIR (baculovirus IAP repeat) domains, and in some instances a CARD domain, and a RING domain (Salvesen and Duckett, 2002). The proposed mechanisms of IAP-caspase inhibition is specific to an IAP member, and can occur via direct inhibition of active caspases, inhibition of caspase processing, or in promoting the degradation of caspases (LaCasse et al., 2008). These are discussed in detail below.

In Drosophila, the IAP homolog Drosophila IAP-1 (Diap1) functions as a ubiquitin ligase which marks Dronc (caspase-9 homolog) for degradation (Wilson et al., 2002). In mammalian cells, the clearest demonstration of IAP-caspase inhibition is the interaction between caspases-3, 7, and 9, and XIAP (Deveraux et al., 1998). XIAP can bind to caspase-3, 7 and 9, and is proposed to interfere with the active sites of the caspases, or with dimerization (Scott et al., 2005; Shiozaki et al., 2003). Some evidence suggests that cIAP1 and cIAP2 can also inhibit caspase activity, though this may occur

through a different mechanism than XIAP. Specifically, studies in yeast indicate that activation of exogenous mammalian caspase-3 can be inhibited by the expression of cIAP1 and cIAP2 (Wright et al., 2000). Initially, it was thought that cIAP1 and cIAP2 are able to bind and directly inhibit caspase activation (Roy et al., 1997), but later studies suggest that while cIAP1/2 can bind to caspases-3/7, the direct inhibition may be an experimental artifact (Eckelman et al., 2006). Alternatively, cIAP1 and 2 may antagonize caspase activation by ubiquitination (LaCasse et al., 2008).

The relief of XIAP inhibition during apoptosis can be in part attributed to the release of Smac from mitochondria (Du et al., 2000; Verhagen et al., 2000). Initially, it was thought that Smac antagonizes the XIAP inactivation of caspase-9 by competition (Srinivasula et al., 2001). However Smac is unable to relieve the inhibition between BIR3 of XIAP and caspase-9, but is able to relieve the inhibition of caspase-9 by XIAP lacking BIR1, suggesting that simple substrate competition may not be the mechanism of Smac-XIAP inactivation (Huang et al., 2003).

### *Genetically Encoded Fluorescent Proteins*

We extensively use light and fluorescence microscopy to observe the dynamics of various apoptotic events in single cells. The characterization and cloning of the green fluorescent protein (GFP) was a technological advance in the fluorescent tagging of proteins (Prasher et al., 1992) (Shimomura, 2009). GFP is a fluorescent molecule found in the jellyfish Aequeora Victoria (Shimomura, 2009). The application of GFP to imaging in organisms first enabled the observation of single cells in *C. elegans* which had specific active promoters (Chalfie et al., 1994), and more recently has been applied to simultaneously image many distinct cells in fixed tissues (Livet et al., 2007).

GFP has a specific excitation and emission spectra. The wild type GFP required UV excitation which is not ideal for the long term imaging of cells (Heim et al., 1994). Significant work was performed to mutagenize GFP, to improve its spectral properties as well as its brightness and photostability (Heim et al., 1995; Heim et al., 1994). Further mutagenesis altered the emission spectra of GFP resulting in the development of the cyan fluorescent protein (CFP), the yellow fluorescent protein (YFP) and other fluorescent proteins with similar fluorescent properties such as mCerulean, mCitrine (Griesbeck et al., 2001; Rizzo et al., 2004). The discovery of DsRed enabled visualization of proteins at longer wavelengths (Matz et al., 1999; Baird et al., 2000). The mutagenesis of DsRed improved its spectral properties, but also enabled the characterization of a monomeric red fluorescent protein (mRFP) (Campbell et al., 2002), and later the generation of several fluorescent proteins with varied emission wavelengths (mCherry, mOrange,

mStrawberry, mPlum) (Shaner et al., 2004). A diverse set of proteins can be used in combination with the appropriate set of spectral filters to separately image different molecules. For example, it is easily possible to image mCerulean, mCitrine, and mCherry (Shaner et al., 2005).

***Table 3: Genetically Encoded Fluorescent Proteins***

| Fluorophore | Excitation | Emissions |
|---|---|---|
| Cerulean | 433 | 475 |
| EGFP | 488 | 507 |
| mCitrine | 516 | 529 |
| mCherry | 587 | 610 |

(Shaner et al., 2005)

### *Caspase and Protease Reporters*

Various reporters of caspase reporters exist which involve a change of fluorescence or fluorophore localization upon caspase activation (Figure 2). Existing reporters for live caspase activity include a reporter which undergoes a change in Forster Resonance Energy Transfer (FRET) after caspase activation (Nguyen and Daugherty, 2005; Xu et al., 1998), and a separate reporter that transitions from being in both the cytoplasm and the nucleus to being solely in the nucleus after caspase activation (pCaspase-3 Sensor, Clontech).

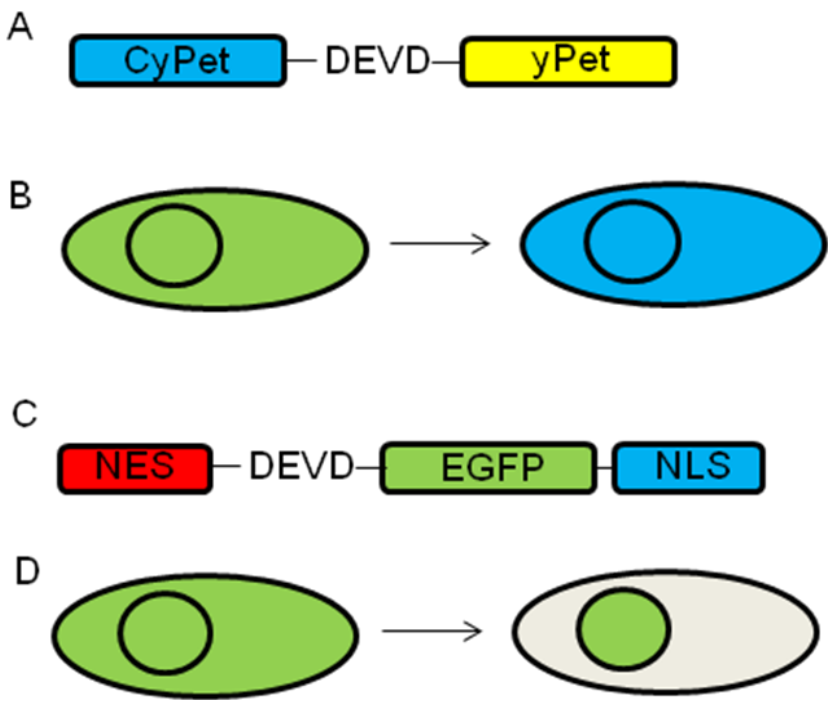


**Figure 2: Image of existing caspase reporters. (A) Design of the FRET caspase reporter. (B) Prior to caspase activation, CFP and YFP molecules are proximal resulting in an energy transfer between CFP and YFP. After caspase activation, CFP and YFP are separated resulting in significantly less energy transfer and less YFP emission. (C) Design of the pCaspase-3 sensor. This consists of a fluorophore and a nuclear localization signal (NLS) which are separated from a nuclear export signal (NES) by a DEVD amino acid linker. (B) The pCaspase-3 sensor initially exists in both the cytoplasm and the nucleus. After caspase activation, the nuclear export signal is removed and the fluorophore relocalizes to the nucleus.**

The FRET reporter consists of two fluorophores which are held together by a linker region which contains the amino acids DEVD (Figure 2A,B). The close proximity of the two fluorophores enables a non-photon mediated energy transfer (Andrews, 1989) from an excited donor fluorophore to the acceptor fluorophore, and thus emission from the acceptor fluorophore at its characteristic emission signature. Upon caspase activity the DEVD linker is cleaved resulting in the separation of the fluorophores, loss of the energy transfer, and therefore the loss of emission from the acceptor fluorophore. Although monitoring the activation of caspase-3/7 can be achieved with FRET reporters, these reporters require the use of two fluorescent proteins, and therefore use a significant portion of the visible spectrum (Nguyen and Daugherty, 2005; Xu et al., 1998). As result, they limit the ability to use additional independent fluorophores to probe signaling molecules or other cytosolic activities. Such probes might include reporters for the cell cycle, phosphorylation, and various tagged proteins.

A separate reporter sold by Clontech called the pCaspase-3 sensor is an alternative genetically encoded caspase reporter (figure 2C,D). This reporter consists of a nuclear export signal (NES), a DEVD linker, a fluorophore, and a nuclear localization signal (NLS). After caspase activation, the NES is removed and the reporter relocalizes from the nucleus and cytosol to the nucleus alone after caspase activation. However one of the concerns is the various strengths of the NES or NLS in different cells can lead to improper nuclear localization prior to caspase activation.

### *Variability in Commitment to Apoptosis*

Cells destined to undergo apoptosis in response to internal stresses and some external stresses release cytochrome c and Smac from mitochondria (Ow et al., 2008), and within minutes activate caspases-3 and -9 (Rehm et al., 2003). In contrast to the tight timing between these events, the duration of events preceding cytochrome c release and caspase activation can vary from 1 hour to over 20 hours within a clonal population of cells (Goldstein et al., 2000). This variation is striking considering that the biochemical events within this delayed and variable stage determine whether the cell will die.

Population variability has also been documented for other phenotypes including phage lambda infection (Arkin et al., 1998), bacterial chemotaxis (Spudich and Koshland, Jr., 1976), cell differentiation (Abkowitz et al., 1996; Enver et al., 1998), and HIV-1 Tat transactivation (Weinberger et al., 2005). Understanding the sources and dynamics of apoptotic variability can lend insight into the precision with which cells are able to process extracellular signals. A number of different factors could contribute to population variability of apoptosis including differences in the composition of single cells, the local environment of single cells, or stochasticity in biochemical reactions triggered by apoptotic stimuli.

One source of *in vitro* variability in response to an apoptotic drug could be inhomogeneities in extracellular concentrations of secreted pro- and anti-apoptotic factors. Apoptotic factors play a role in apoptosis signal transduction in cultured cells

(Janes et al., 2006). However, it is unclear how much the secreted factor contributes to the apoptosis variability, or to the shift of apoptosis time of the entire culture. It also possible that these factors act mainly on the secreted cell itself (Loewer and Lahav, 2006).

A second source of variability could result from stochasticity of the biochemical reactions in response to apoptotic stimuli. A stochastic transduction of an apoptotic signal could be the consequence of just a few molecules being involved in a particular stage of apoptosis (Rao et al., 2002). During apoptosis, factors may re-localize to sub-cellular regions of the cell including the plasma membrane (Siegel et al., 2004), and the endoplasmic reticulum (Boehning et al., 2003). Along with the synthesis and degradation of molecules (Barkett and Gilmore, 1999; Wertz and Dixit, 2008), this may create situations where the activation of certain apoptotic factors or complexes may be limiting, resulting in stochastic onset of apoptosis, and therefore variability in the population (Raychaudhuri et al., 2008). Thus, even when the same initial conditions are reproduced, the reaction does not necessarily produce the same result (McAdams and Arkin, 1998).

A third source of population variability is a heterogeneity of cellular factors amongst the population (Kaern et al., 2005). In some instances, variation of protein expression has been correlated to the cell cycle (Sigal et al., 2006a). However, in other instances variation in protein expression is uncoupled to the cell cycle, and is a function of the time since cells last shared a common ancestor (Sigal et al., 2006b). The commitment of a

single cell to apoptosis likely depends on the concentrations and post-translational modifications to the many molecules involved in apoptosis.

# *Chapter Two: Design of Caspase Reporter*

## *Introduction*

We first sought to design a probe for caspase-3/7 activity that was genetically encoded facilitate the generation of stable cell lines and for reporting the caspase activity in organisms. Existing reporters for live caspase activity include a reporter which undergoes a change in Forster Resonance Energy Transfer (FRET) after caspase activation (Nguyen and Daugherty, 2005; Xu et al., 1998), and another reporter that transitions from being in both the cytoplasm and the nucleus to being solely in the nucleus after caspase activation (pCaspase-3 Sensor, Clontech).

The FRET reporter consists of a donor fluorophore and an acceptor fluorophore which are separated by a DEVD amino acid sequence. The DEVD sequence is preferably cleaved by caspase3/7, though is cleaved by other proteases (Thornberry et al., 1997). Prior to caspase activation, excitation of the donor fluorophore results in emission from the acceptor fluorophore owing to the close physical proximity of the fluorophores. After caspase activation and cleavage of the DEVD sequence, the fluorophores are separated resulting in a change of the emission spectra when the donor fluorophore is excited. FRET reporters have been used to monitor caspase activation in cell culture (Nguyen et al., 2007) and in organisms (Takemoto et al., 2007). However, the FRET reporter requires two fluorophores which limits the use of orthogonal fluorophores for

simultaneously monitoring other processes. The pCaspase-3 sensor consists of a nuclear export signal (NES) at its N terminal, followed by the DEVD sequence, a fluorescent protein, and a nuclear localization signal (NLS). Upon caspase activation, the NES is removed and the fluorescent protein is exclusively localized to the nucleus. One of the drawbacks of this reporter is that it depends on strengths of the NES and the NLS in a particular cell line. This is known to have considerable variation, and in our hands results in different localization of the reporter prior to caspase activation (data not shown).

In this chapter, we describe the generation and characterization of two single fluorophore caspase reporters (termed the pmDEVD and erDEVD reporters). These reporters are based on the principle of re-localization. We compared the kinetics of these reporters to exiting reporters, and determined the effect on downstream steps of apoptosis.

## *Results*

### *Reporter Design*

In creating single fluorophore reporters of caspase activity we sought to create reporters that changed cellular localization upon caspase activity. Two reporters were constructed: the first reporter was designed to re-localize from the plasma membrane to the cytoplasm (pmDEVD) (Figure 3), whereas the second reporter relocalizes from the cytoplasmic surface of the endoplasmic reticulum to the nucleus (erDEVD) (Figure 4).

The pmDEVD reporter consists of an N-terminal plasma membrane (pm) targeting palmitoylation domain from Growth Associated Protein 43 (GAP-43) (Skene and Virag, 1989) and a fluorescent protein, which are separated by a linker region containing the DEVD caspase-3/7 cleavage site (Figure 3A). The linker region contains the amino acid sequence DEVD that has been used to detect caspase-3/7 activity (Thornberry et al., 1997). Though other caspases will cleave 'DEVD' - albeit with a lower efficiency (Thornberry et al., 1997) - for the sake of consistency of terminology with previous publications, we refer to the designed DEVDase reporters as a caspase-3/7 reporters. The pmDEVD reporter was designed so that the fluorophores and the linker region are easily interchangeable (see plasmid design in Chapter Six).

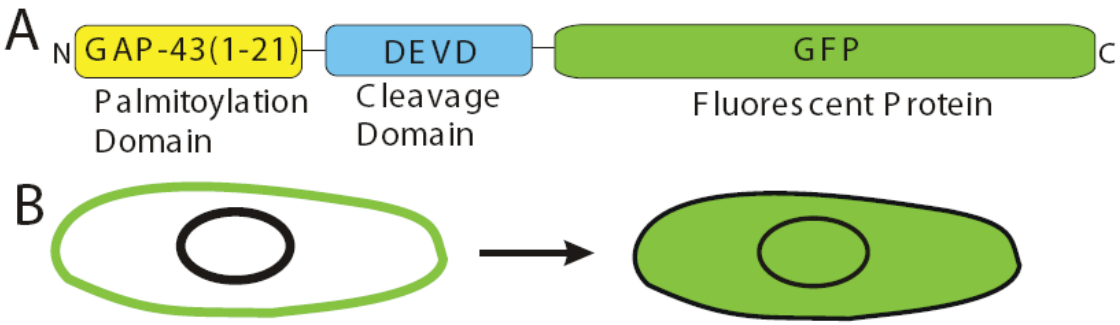


**Figure 3: Design of the plasma membrane DEVD reporter (pmDEVD). (A) The reporter consists of a membrane targeted palmitoylation domain (amino acids 1-21 from GAP-43), a linker containing the DEVD amino acid sequence, and a fluorescent protein (in this case GFP). (B) Prior to caspase activation the fluorophore (green) is localized to the plasma membrane, and after caspase activation it becomes cytosolic.**

The erDEVD reporter contains the first endoplasmic reticulum (er) transmembrane domain of Sec63 as its N-terminus (Meyer et al., 2000) followed by the DEVD linker region, a fluorescent protein, and finally a triple repeat of the SV40 nuclear localization signal (NLS) at the C-terminus (Kalderon et al., 1984; Lanford et al., 1986) (Figure 4). The Sec63 domain consists of amino acids 1-63 of Sec63, and this contains a protein translocation consensus sequence (Meyer et al., 2000), and a few amino acids following the transmembrane domain. Similar to the pmDEVD reporter, the fluorophore in the erDEVD reporter is interchangeable.

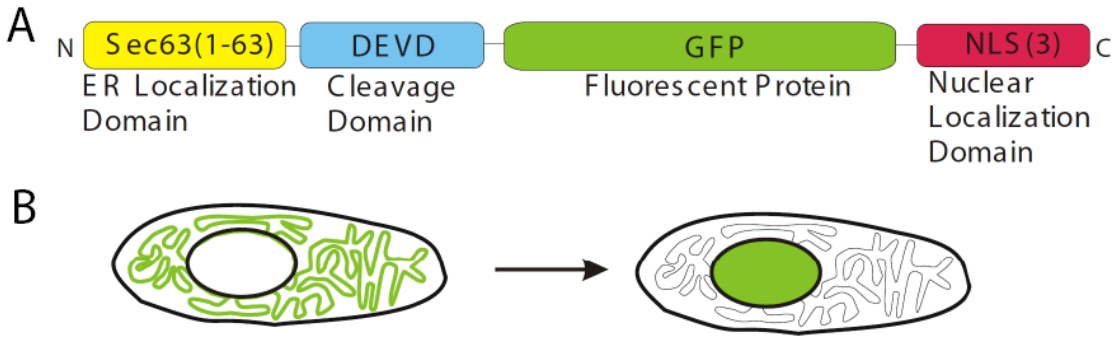


**Figure 4: Design of the endoplasmic reticulum DEVD reporter (erDEVD). (A) The reporter consists of the endoplasmic reticulum translocation domain from Sec63, a DEVD amino acid sequence, a fluorescent protein (in this case GFP), and a triple repeat of the nuclear localization tag from SV40. (B) Prior to caspase activation the fluorophore (green) is localized to the endoplasmic reticulum, and after caspase activation it becomes localized to the nucleus.**

Each reporter is named by its initial localization (er or pm) as well as its fluorophore. For example, when the mCherry fluorescent protein is linked via the caspase sensitive sequence DEVD to the plasma membrane, the resulting probe is referred to as pmDEVD-mCherry. Upon caspase activation the reporters should shift their location owing to cleavage of the DEVD caspase sensitive linker. As a control for whether the caspase-sensitive linker region was responsible for any changes in localization, we created reporters (pmControl or erControl) that only differed from the pmDEVD or erDEVD reporters by the absence of the DEVD cleavage site in the linker region.

To test the pmDEVD reporter, we co-expressed the pmDEVD-mCherry and pmControl-Cerulean reporters in HeLa cells (Figure 5). Prior to any treatment, Golgi localization of the pmDEVD reporter is observed, which is consistent with earlier observations of the palmitoylation localization tag (Figure 5A) (McLaughlin and Denny, 1999). After treatment with STS (2 μM), the mCherry fluorescence is relocalized from the plasma membrane to the cytosol (Figure 5A). This was quantified by monitoring the fluorescence in a region within the cytoplasm over time (Figure 5B). In contrast, pmControl-Cerulean remained at the plasma membrane (images in Figure 5A and quantification in Figure 5B) indicating that the DEVD cleavage site is responsible for the change in localization and not the palmitoylation domain. The lack of change in the pmControl-Cerulean signal also indicates that the contraction of apoptotic cells is not responsible for the increase in the pmDEVD-mCherry signal. Thus, the cytosolic fluorescence of mCherry could be used to quantify the DEVDase activation.

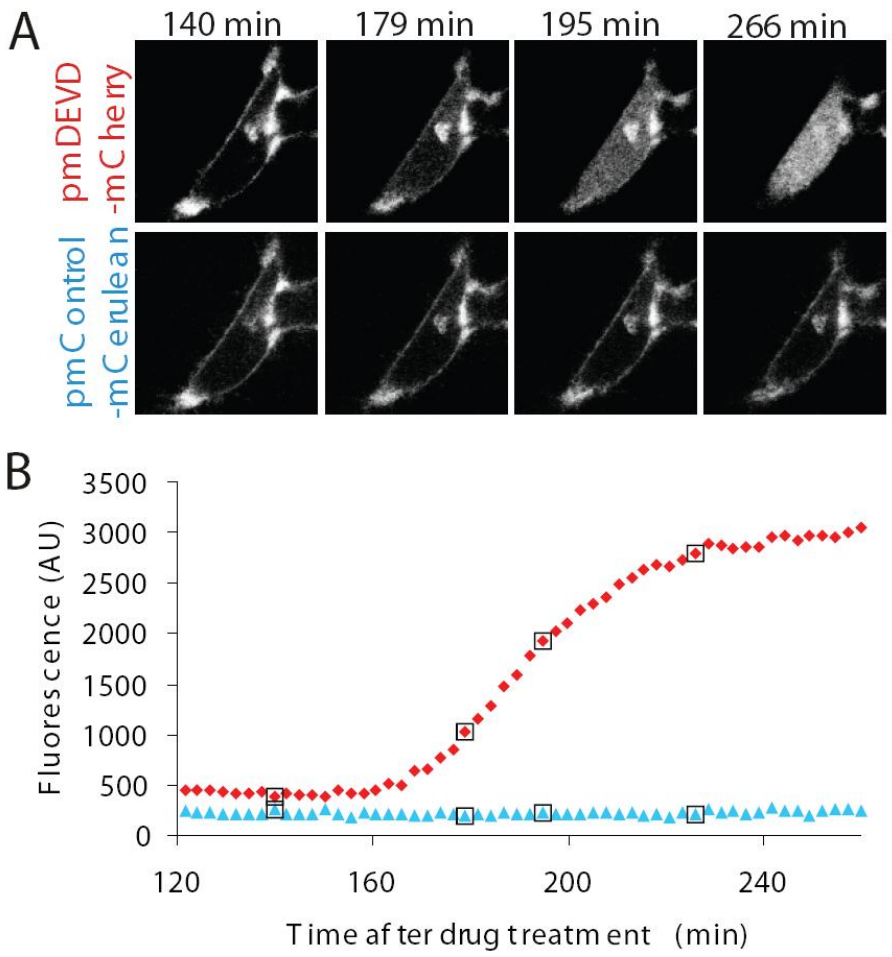


**Figure 5: Time lapse images and quantification of the pmDEVD reporter. (A) pmDEVD-mCherry and pmControl-mCerulean reporter expressed in the same HeLa cell and treated with 2µM of STS. The pmDEVD reporter relocalizes to the cytosol (top panel) and the pmControl reporter remains membrane associated (lower panel). (B) Quantification of cytosolic fluorescence for the cells in A shows and increase in the pmDEVD reporter (red diamonds), but no significant change in the pmControl reporter (blue triangles). Time points with squares correspond to the images in A.**

Similar results were observed when apoptosis was triggered by the addition of TNFα (50ng/mL) and cycloheximide (5μg/mL) (data not shown). Notably with TNFα and CHX treatment, the contraction of the cell occurs approximately 30 minutes after detectable caspase activity (data not shown). Though these results were observed with confocal microscopy, a similar increase in fluorescence could be observed with wide-field microscopy (Figure 6). With wide-field microscopy, prior to any treatment, there is an apparent cytosolic fluorescence which is likely out of focus plasma membrane associated fluorescence. When treated with STS (2 μM), there was an increase in the cellular fluorescence of the cell as the probe was released from the plasma membrane. This net increase in fluorescence suggests that the reporter may be at a high enough density at the plasma membrane to partially self-quench. Alternatively, this may indicate out of focus fluorescence entering the focal plane.

To test the utility of the erDEVD reporter, we transfected HeLa cells with the erDEVD-mCherry reporter and the erControl-mCerulean reporter, and treated cells with TNFα (50ng/mL) and CHX (5μg/mL) (Figure 7). While the mCherry fluorescence re-localized to the nucleus (Figure 7A upper panel; Figure 7B red trace), no change was seen in the localization of the erControl-Cerulean reporter (Figure 7A lower panel, 7B blue trace). Therefore, in both the pmDEVD and the erDEVD reporters, the linker region was responsible for the re-localization of the fluorophore during induction of apoptosis. Similar results were observed in cells treated with STS (2μM) (data not shown). Notably, the erDEVD reporter does not completely relocalize from the ER to the cytosol after caspase activation. This could indicate that the reporter is inaccessible at the plasma

membrane. Inaccessibility could also be an issue of the pmDEVD reporter, but would not be detectable owing to the cytosolic (and not nuclear) relocalization which would mask the presence of some plasma membrane fluorescence.

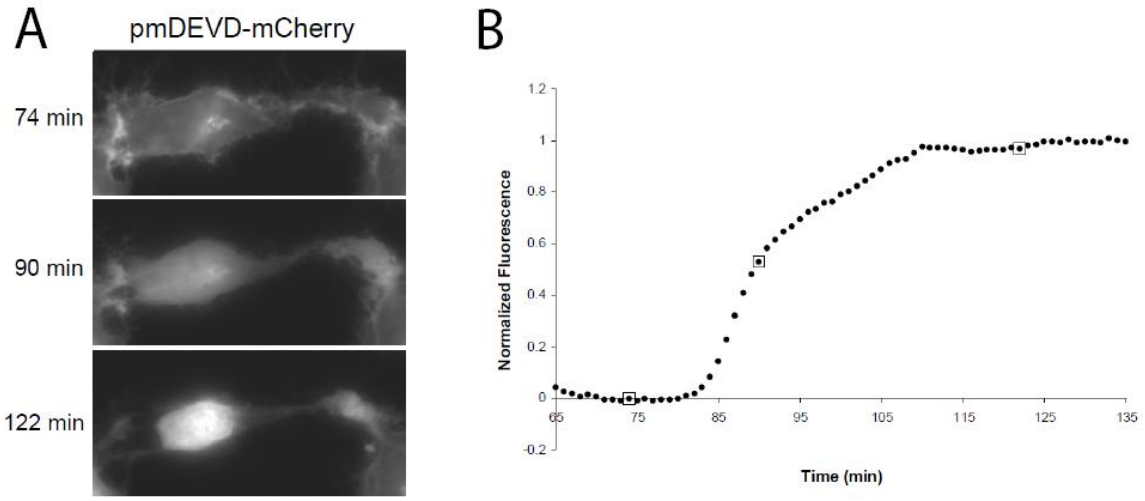


**Figure 6: Time lapse images and quantification of the pmDEVD reporter in widefield microscopy. (A) pmDEVD-mCherry expressed in HeLa cells and treated with 2μM of STS. Caspase activation is indicated by an increase in total fluorescence. (B) Quantification of cytosolic fluorescence for the cells in (A) shows and increase in fluorescence of pmDEVD reporter. Time points with squares correspond to the images in A.**

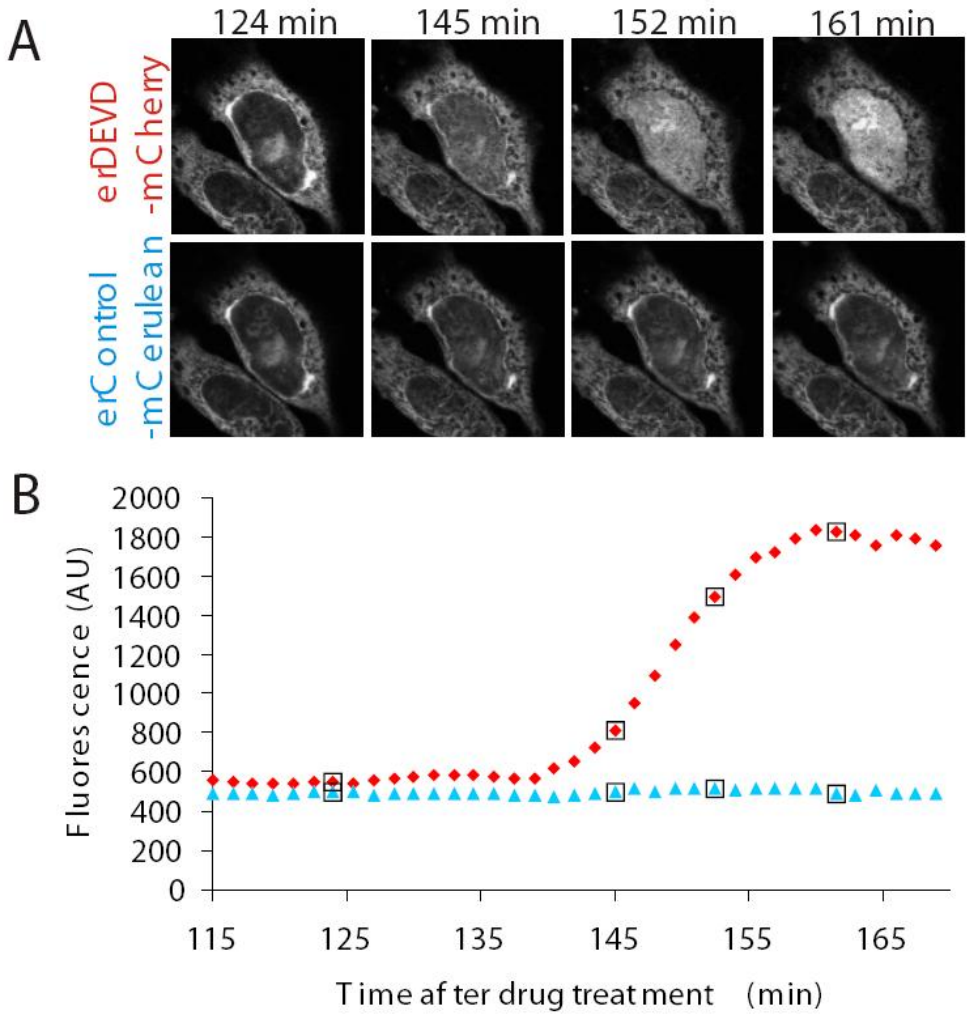


**Figure 7: Time lapse images and quantification of the erDEVD reporter. (A) erDEVD-mCherry and erControl-mCerulean reporter expressed in the same HeLa cell and treated with 2μM of STS. The erDEVD reporter relocalizes to the nucleus and the erControl reporter remains associated with the ER. (B) Quantification of nuclear fluorescence for the cells in A shows and increase in the pmDEVD reporter (red diamonds), but no significant change in the pmControl reporter (blue triangles). Time points with squares correspond to the images in A.**

### *Comparison to Existing Reporters*

We next compared the developed re-localization reporters to existing reporters on the basis of signal strength and kinetic sensitivity. One existing reporter has a caspase-3/7 targeted DEVD linker between two fluorophores and yields a change of FRET upon caspase activity (FRET-DEVD) (Nguyen and Daugherty, 2005). This reporter consist of the fluorophores CyPet and yPet which were optimized FRET fluorophores derived from CFP and YFP respectively (Nguyen and Daugherty, 2005). A second existing reporter has a fluorescent protein and a nuclear localization signal (NLS) which are separated by DEVD linker from a nuclear export signal (NES). This reporter localizes to the nucleus upon activation of caspase-3/7 and removal of the nuclear export signal (pCaspase-3 sensor, Clontech).

To compare the signal strength properties of the reporters, we monitored both the fold increase of the signal of the reporters in different cells, and determined the ratio of magnitude of the increase relative to the noise of the initial signal ($n>10$ cells). The fold increase of the pmDEVD reporter ($4.5\pm1.9$) was similar to the erDEVD reporter ($4.2\pm1.5$), but was significantly greater than the increase of the pCaspase-3 and FRET reporters ($2.2\pm0.7$, $p=0.003$, and $2.4\pm0.4$, $p=0.0006$ respectively) (Figure 8).

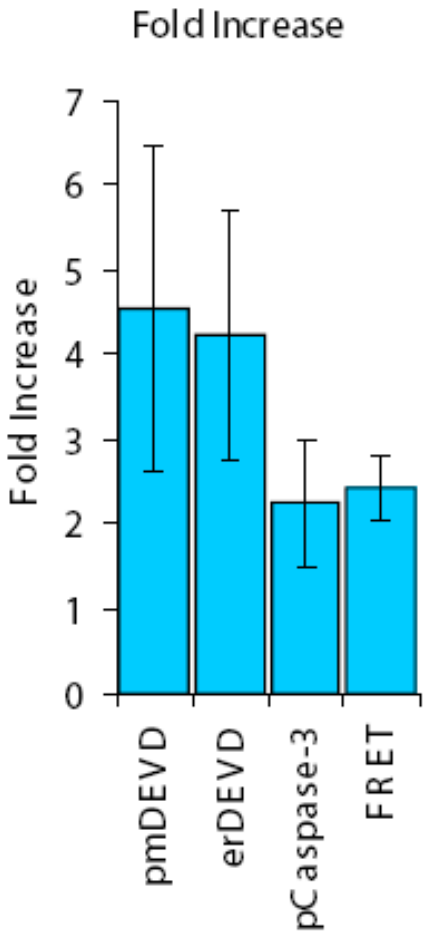


**Figure 8: Comparison of the fold increase properties of the different reporters. The pmDEVD reporter shows the largest fold increase, and the erDEVD reporter is within error. By comparison the pCaspase-3 sensor and the FRET sensor show less of an increase (p=0.003 and p=0.0006 respectively). All error bars represent standard deviation.**

We next wanted to assess the signal to noise ratio of the reporter which gives an approximate measure of the dynamic range of the reporter. The signal to noise is defined as the increase in fluorescence divided by the standard deviation of the reporter signal prior to caspase activation (Figure 9A). The pmDEVD has the highest ratio (80±50), and erDEVD has the second lowest ratio (65±34). The ratios of the pCaspase-3 sensor and the FRET-DEVD (39±9, and 22±11 respectively) reporter are significantly smaller than the pmDEVD ratio ($P$=0.009 and $P$=0.0007 respectively) (Figure 9B). Thus in comparing the reporters on their fold increase an in the signal to noise ratio, the pmDEVD reporter showed better signal strength than the pCaspase-3 sensor and the FRET reporter.

The reporters were next compared based on the kinetics of their response: specifically the time of the first detectable signal of the reporters, and the time to the half-maximum point of the activity curves. The first detectable signal was quantified as the time when the signal was two standard deviations above the noise of the basal signal. In all cases we made kinetic comparisons between different reporters expressed simultaneously in the same cell, to avoid potential variability between cells. Possible variability could result from the amount of caspase present in different cells or the degree of caspase activation from cell to cell. We induced apoptosis in cells transfected with both the pmDEVD and FRET-DEVD reporter, or in cells expressing the pmDEVD, erDEVD and pCaspase-3 reporters simultaneously and quantified the signal of each. Example kinetic traces of the simultaneous use of these reporters are shown in Figure 10.

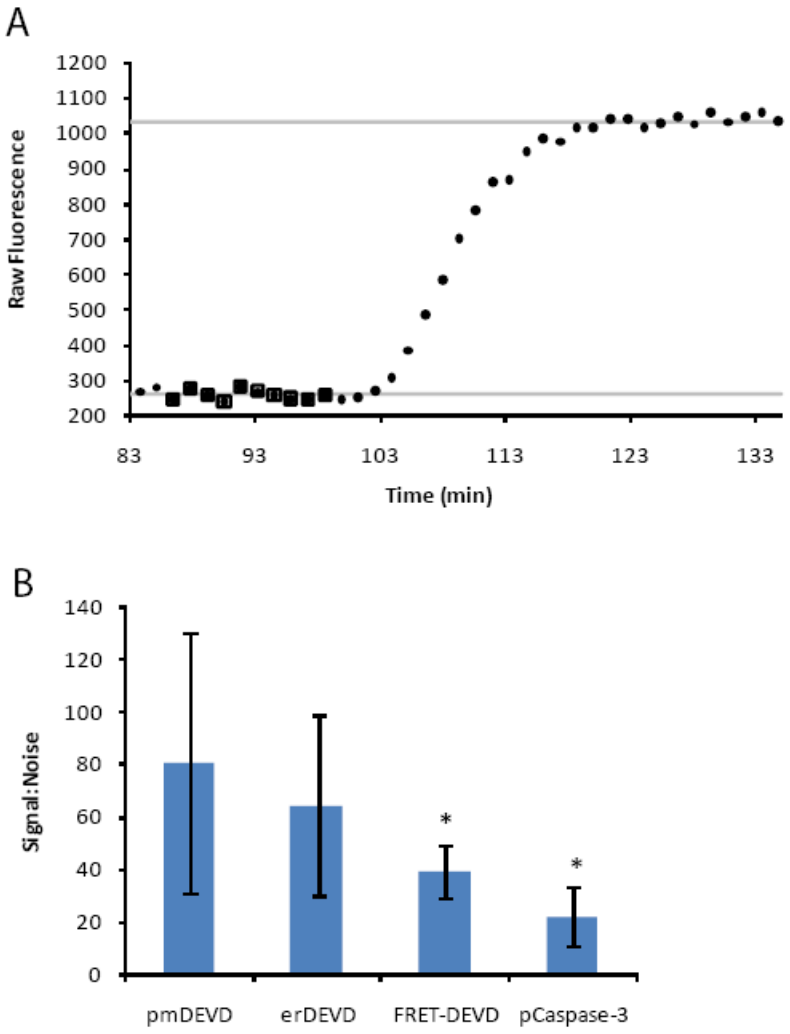


**Figure 9: Comparison of the signal to noise of the different reporters. (A) Signal to noise is calculated as the standard deviation of the ten points before caspase activation divided by the fold increase. (E) Comparison of signal to noise for the different reporters. The pmDEVD has the highest ratio (80±50), and erDEVD has the second lowest ratio (65±34). The ratios of the pCaspase-3 sensor and the FRET-DEVD (39±9, and 22±11 respectively) reporter are significantly smaller than the pmDEVD ratio (p=0.009 and p=0.0007 respectively).**

**Figure 10: Comparison of the different reporters in the same cell. To check the differences in the kinetics of the reporters we made comparisons of reporters in the same cell. (A) Kinetics of a pmDEVD (red triangles) and FRET-DEVD (yellow circles) reporter in the same cell. The reporters show similar kinetics. (B) Kinetics of the pmDEVD (red triangles), erDEVD (yellow squares) and pCaspase-3 (blue circles) reporters expressed in the same cell shows slightly differences in kinetics of the reporters.**

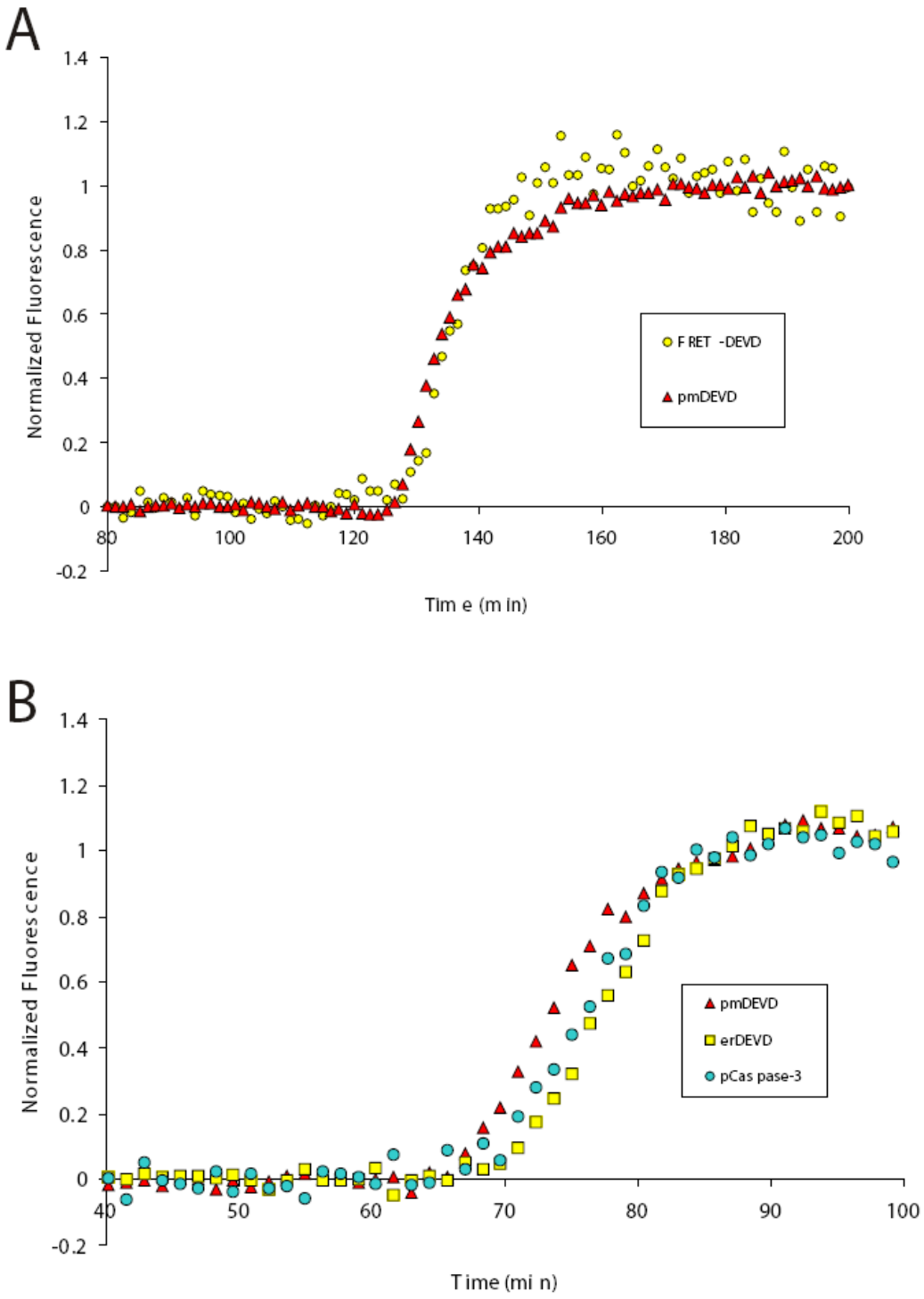
A
1.4
1.2
1
0.8
0.6
0.4
0.2
0
-0.2
Normalized Fluorescence
80
100
120
140
160
180
200
Tim e (m in)
F RET -DEVD
pmDEVD
B
1.4
1.2
1
0.8
0.6
0.4
0.2
0
-0.2
Normalized Fluorescence
40
50
60
70
80
90
100
Time (mi n)
pmDEVD
erDEVD
pCas pase-3

**Figure 10**

The first detectable caspase activation signal was consistently observed with the pmDEVD reporter (Figure 11). We therefore made comparisons of the pmDEVD reporter to each of the other reporters. There was a time lag between the pmDEVD and the erDEVD reporter (100±41s for first detectable signal, and 247±118s to half-maximum activation). The pCaspase-3 sensors were significantly delayed relative to the pmDEVD reporter (delay to first detectable signal = 154±80s, delay to half-maximum = 186±133s). For the FRET-DEVD reporter the delay to the first detectable signal (31.9±88s) or to half-maximum (141±169s) was not statistically significant. Therefore, the pmDEVD reporter preserves the kinetic properties of the FRET-DEVD reporter, while only using a single fluorophore, and having a larger fold increase in the signal.

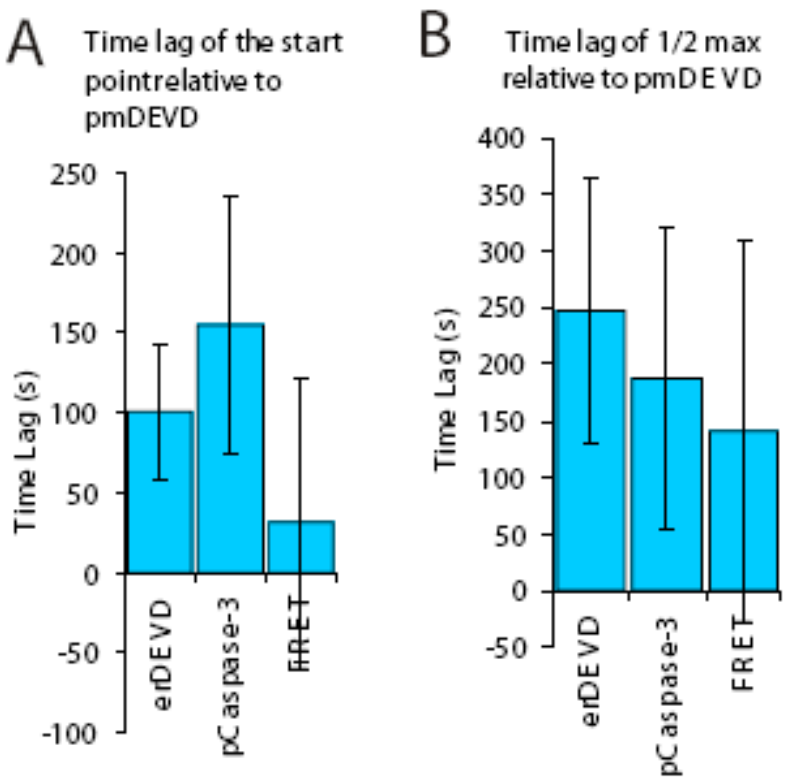


**Figure 11: Quantification of the kinetic properties of the different reporters, (A) The first detectable signal of the pmDEVD reporter was observed before the erDEVD reporter (100±41seconds), the pCaspase-3 sensor (154±80 seconds), and at the same time as the FRET reporter (31.9±88 seconds). (B) The pmDEVD reporter reached the half-maximum faster than the erDEVD reporter (247±118 seconds), the pCaspase-3 sensor (186±133 seconds). For the FRET-DEVD reporter the delay to half-maximum (141±169 seconds) was not statistically significant. All error bars represent standard deviation.**

To determine that the release of the reporter coincides with other apoptotic events, we monitored the release of cytochrome c-GFP along with the pmDEVD reporter. Observations of the release of mitochondrial proteins suggest that caspase activation occurs approximately 10 minutes before caspase activation (Rehm et al., 2003). We expressed the pmDEVD-mCherry reporter in HeLa cells along with cytochrome c-GFP and induced apoptosis with 2μM of STS. Cytochrome c release from mitochondria occurred before the detected pmDEVD caspase activation (Figure 12A). We quantified the release of cytochrome c release by monitoring the standard deviation of the pixels divided by the total intensity (referred to as the punctuate diffuse index) (Figure 12B). Thus when cytochrome c is aggregated in mitochondria, the standard deviation should be high, and when released, the standard deviation should decrease. This quantification also demonstrated cytochrome c-GFP release occurred a few minutes before caspase activation (Figure 12B).

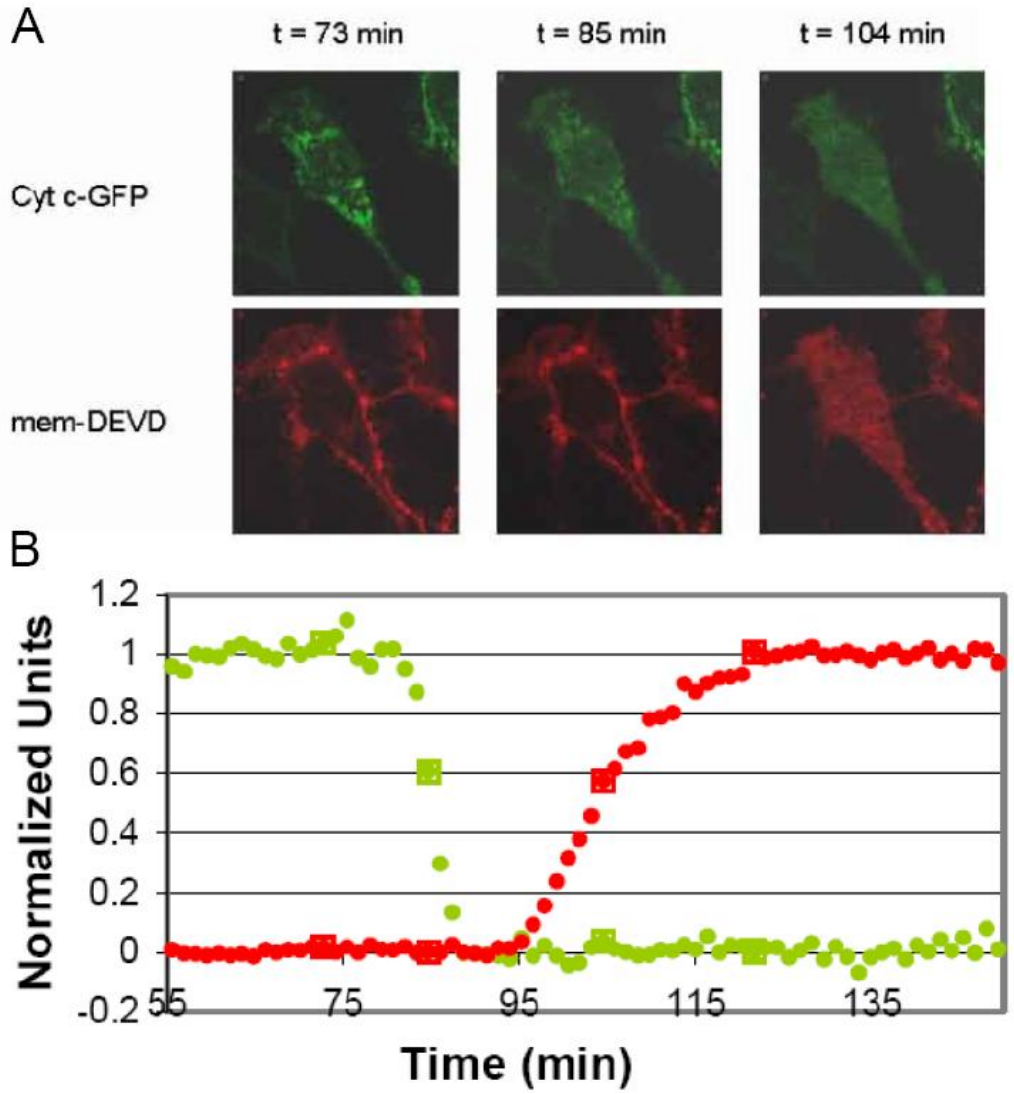


**Figure 12: Release of cytochrome c-GFP and pmDEVD-mCherry in the same cell. HeLa cells treated with 2µM STS. (A) Images of cytochrome c release (top panel) and caspase activation (lower panel). (B) Quantification of the release of cytochrome c-GFP (green) measured as the standard deviation/total intensity of the cell, and cytosolic mCherry fluorescence (red). Squares indicate data points corresponding to the images in A.**

### *Effect of pmDEVD on the Progression of Apoptosis*

A potential concern with any reporter is that it might perturb the event that it is designed to assay. To determine whether the expression of the pmDEVD reporter, which is a caspase-3 and -7 target, would affect the progression of apoptosis, we assayed whether expression of pmDEVD delayed chromatin condensation – an event downstream of caspase-3/7 activation (Liu et al., 1997). Cells were transiently transfected with the pmDEVD reporter, treated with STS (2μM), fixed at different time points, and were stained with TUNEL – which marks apoptotic cells. Expression of the pmDEVD reporter had no detectable effect on the kinetics of TUNEL staining (Figure 13). This result illustrates that the pmDEVD reporter records the kinetics of caspase-3/7 activation without a detectable effect on subsequent apoptotic steps.

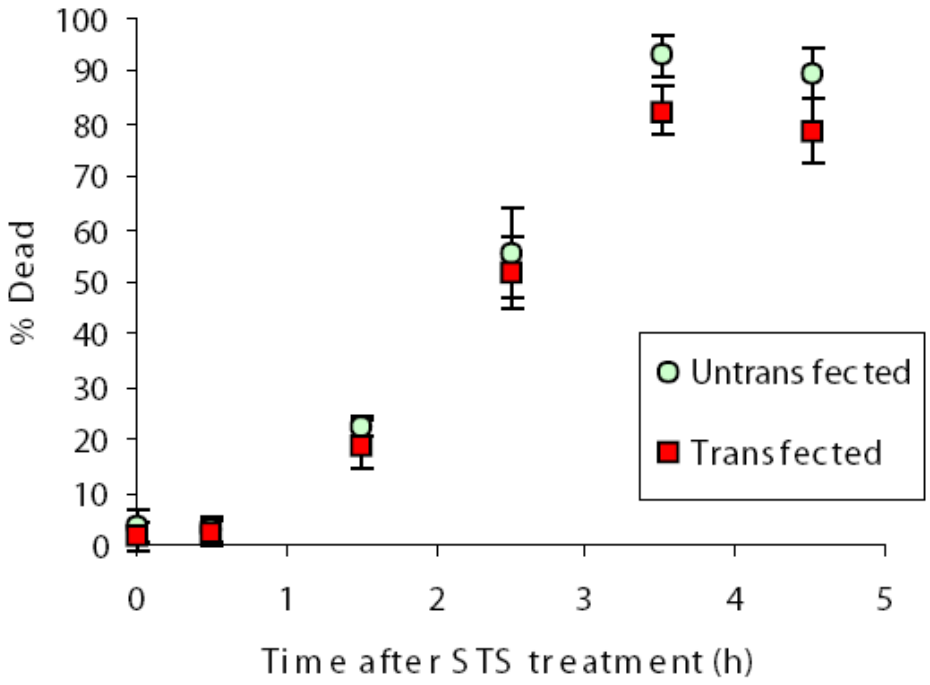


**Figure 13: Test of potential effects of the pmDEVD reporter on DNA fragmentation. Cells were transiently transfected with the pmDEVD reporter, treated with staurosporine (2µM), fixed at different time points, and were stained with TUNEL. Percentage of dead cells transfected with pmDEVD-mCherry (red square); Percentage of dead untransfected cells (yellow circle). Each data point represents the average from three wells − with >50 cells analyzed per well.**

## *Summary*

We created two reporters for assaying caspase activity in single cells. One of the reporters relocalizes from the plasma membrane to the cytosol (pmDEVD), and the

other reporter relocalizes from the ER to the nucleus (erDEVD) (Figure 3,4). Each reporter requires the use of only a single fluorophore, and is genetically encoded which enables use in organisms and the creation of stable cell lines. In comparing the signal strength and kinetic properties of each of the reporters, we find that the pmDEVD reporter had similar kinetic properties to the FRET reporter, but showed a greater signal increase (Figures 8-11). We also demonstrate that the pmDEVD reporter can be monitored with confocal or widefield microscopy in single cells (Figures 5,6). This probe reports activity after cytochrome c release which is consistent with existing data, and does not have an effect on DNA fragmentation (as assayed by TUNEL staining) which is downstream of caspase activity (Figure 13). This suggests that the pmDEVD reporter assays caspase activity without noticeably affect the progression of apoptosis.

# *Chapter Three: Similarity of Sister Cell Apoptosis*

## *Introduction*

Cells destined to undergo apoptosis in response to internal stresses and some external stresses release cytochrome c and Smac from mitochondria (Ow et al., 2008), and within minutes activate caspase-3 and caspase-9 (Rehm et al., 2003). In contrast to the tight timing between these events, the duration of events following exposure to an apoptotic agent but preceding cytochrome c release and caspase activation can vary from 1 hour to over 20 hours within a clonal population of cells (Goldstein et al., 2000). This variation is striking considering that the biochemical events within this delayed and variable stage determine whether the cell will die or survive.

Population variability has also been documented for other phenotypes, including phage lambda infection (Arkin et al., 1998), bacterial chemotaxis (Spudich and Koshland, Jr., 1976), cell differentiation (Abkowitz et al., 1996; Enver et al., 1998) and HIV-1 Tat transactivation (Weinberger et al., 2005). Understanding the sources and dynamics of apoptotic variability can lend insight into the precision with which cells are able to process extracellular signals. A number of different factors could contribute to population variability of apoptosis, including differences in the composition of single cells, the local environment of single cells, or stochasticity in biochemical reactions triggered by apoptotic stimuli.

Here, we observe that when and whether cells entered apoptosis were synchronized between cells in close proximity. Entry into apoptosis did not correlate with the distance between unrelated cells, or with the phase of the cell cycle. Entry into apoptosis was strongly correlated for sister cells, and this correlation diverged over subsequent generations. The divergence of apoptosis times was inhibited by blockade of protein synthesis. These results indicate that there is a persistent cellular state underlying the susceptibility of a single cell to apoptosis. These results are similar to a separate study published while our work was in review (Spencer et al., 2009).

## *Results*

### *Neighboring Apoptosis*

To gain insight into the cell-to-cell variability in the onset of apoptosis, we developed HeLa cell lines that stably expressed the pmDEVD-mCherry caspase-3/7 reporter and a nuclear marker (YFP-NLS) to facilitate cell tracking. Using wide-field microscopy, we monitored cellular fluorescence in cells that were plated 40 hours prior to treatment with STS (2μM). Cells were imaged every 5 minutes with a 10x objective using an Olympus IX81 widefield microscope. The onset of caspase-3/7 activation was indicated by a large increase in cellular fluorescence of pmDEVD-mCherry when observed by wide-field microscopy (Figure 14A: mCherry false colored green, YFP-NLS false colored blue). A map of nuclei which are color coded to represent the time of

caspase-3/7 activation indicates that groups of spatially clustered cells undergo apoptosis at similar times, and thus a localized synchronization of apoptosis (Figure 14B).

To quantify the local synchronization of caspase-3/7 activation observed in Figure 14 for all pairs of cells we plotted the difference in the time of caspase-3/7 activation as a function of the distance between cells. When cells were closer to each other it was more likely that their caspase activation would be synchronized (Figure 15C - blue). To determine potential artifacts of the analysis that could generate a spatial correlation, we randomly reassigned apoptosis times to different cellular positions and no correlation was reported, thus demonstrating that the analysis did not contribute to the spatial correlation between caspase-3/7 activation and intercellular distance (Figure 15C - red).

**Figure 14: Local synchronization of apoptosis. (A) HeLa cells expressing pmDEVD-mCherry (green) and YFP-NLS (blue) treated with 2μM of STS. Onset of DEVDase activation is marked by the increase in fluorescence. (B) Nuclei of HeLa cells in A. Nuclei are color coded to represent the times of apoptosis. Clusters of cells with white outlines indicate examples of neighboring cells undergoing DEVDase activation at similar times.**

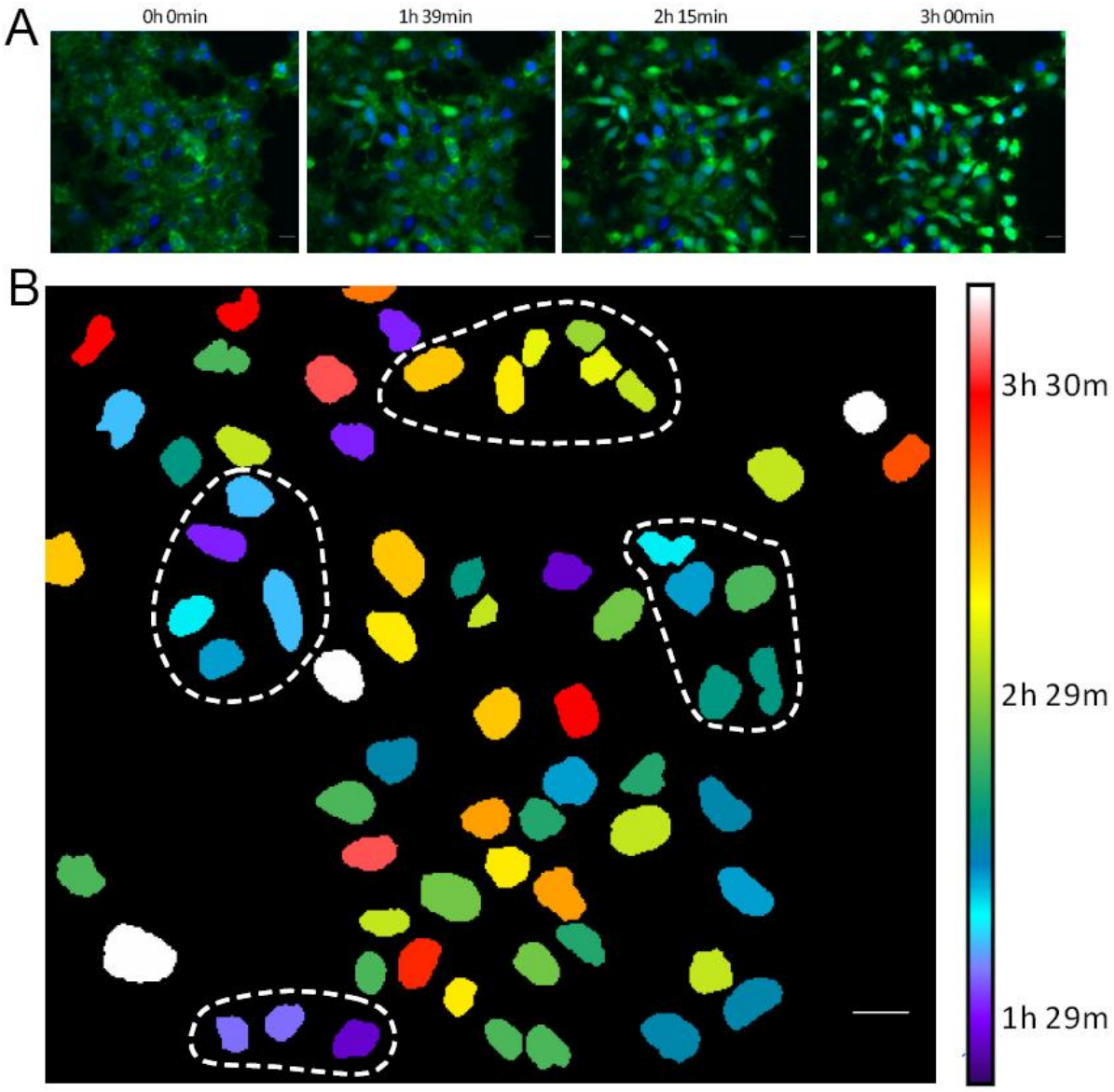


**Figure 14**

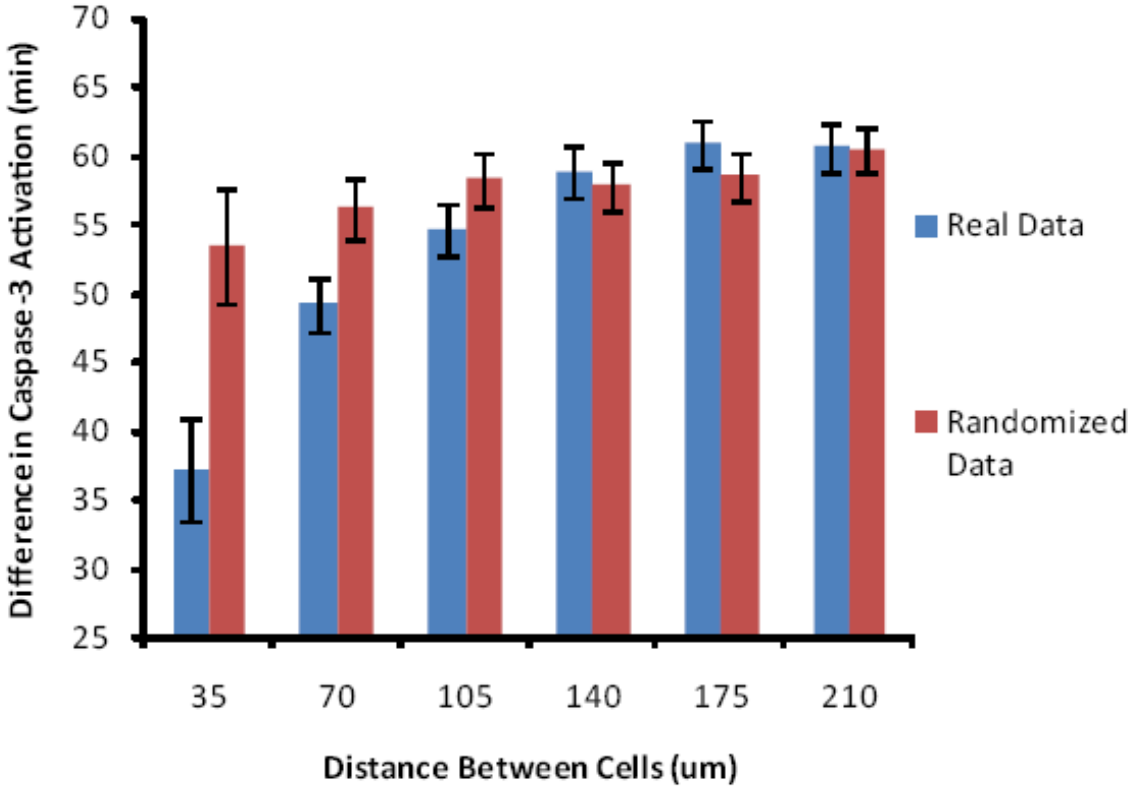


**Figure 15: Plot of the difference in time of apoptosis between HeLa cells as a function of their distance reveals a correlation between apoptosis and distance. (Error bars represent 95% confidence interval of the mean.)**

The following are three possibilities that could explain the correlation of the distance between cells and the time of caspase activation: First, cells that are near each other may be sister cells which are at a similar phase of the cell cycle. If there is a cell cycle dependant susceptibility to apoptosis this could account for the local synchronization of the activation of caspases. Second, cells may secrete factors that promote or hinder apoptosis in a local neighborhood. Third, sister cells may have similar molecular compositions uncoupled from the cell cycle that affects their sensitivity to entering apoptosis.

### *Cell Cycle and Apoptosis Correlation*

To investigate the role of the cell cycle in locally synchronized apoptosis, we monitored fluorescent reporters for both apoptosis and the cell cycle stage in single cells. Two approaches were taken. The first was to synchronize the cell cycle. HeLa cells expressing pmDEVD were subjected to a double thymidine block (15 hr block, 10 hr release, 15 hr block), and released for variable intervals before treatment with STS (2μM). No correlation was observed between the time to apoptosis and the time cells were treated after release (One way ANOVA: $F=1.26 < F_{crit}=2.40$; Figure 16).

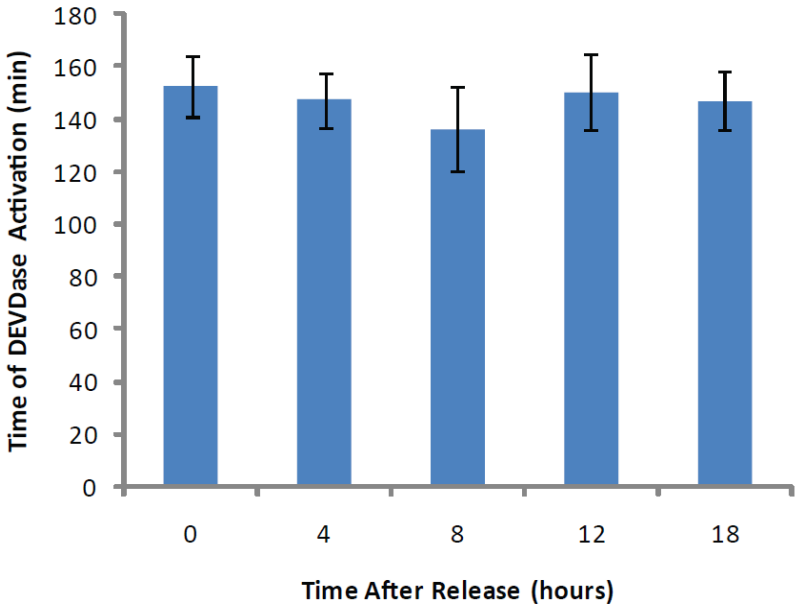


**Figure 16: Cell Cycle Synchronization Experiment. HeLa cells expressing pmDEVD were subjected to a double thymidine block (15 hour block, 10 hour release, 15 hour block), and released for variable intervals before treatment with 2 µM STS. No correlation was observed between apoptosis and the time cells were treated after release. One way ANOVA performed to determine significant differences between apoptosis at different time points. F=1.26<Fcrit=2.40; therefore there is no significant difference between inducing apoptosis at different times after release from a double thymidine block.**

One potential concern of the cell cycle synchronization experiment is the effect of cell cycle synchronizing agents on apoptosis (Ji et al., 1997), which might mask a cell

cycle sensitivity. Thus, the second approach was to observe an asynchronous population in which the state of the cell cycle could be characterized in each individual cell with a fluorescent reporter. For this purpose we observed the G1/S cell cycle transition using a fluorescent fusion to the PSLD domain of human DNA Helicase B (referred to as PSLD-mCitrine) (Gu et al., 2004; Taneja et al., 2002). This PSLD-mCitrine reporter is localized to the nucleus in G1 phase and transitions to the cytosol upon cyclinE CDK phosphorylation, which marks the G1/S transition (Gu et al., 2004) (Figure 17) .

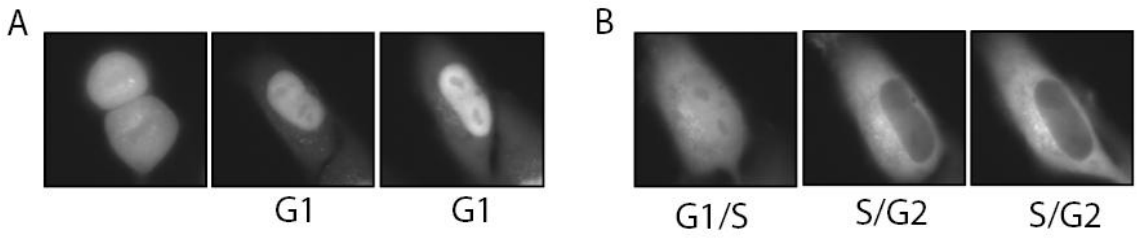


**Figure 17: PSLD-mCitrine cell cycle reporter. This reporter transitions out of the nucleus owing to cyclin E-CDK2 phosphorylation at the G1/S transition. It begins in the nucleus in G1 phase , then transitions to being in both the nucleus and the cytoplasm during the G1/S transition, and the reporter becomes cytosolic in the S/G2 phase.**

To facilitate identifying and tracking individual cells we used a Cerulean-NLS as a nuclear marker. The nuclear fluorescence was determined by tracking Cerulean-NLS

using the Spot Module in Imaris. A mask of the Cerulean NLS fluorescence was created and the PSLD-mCitrine fluorescence was monitored in that mask. An example of the quantification of PSLD-Citrine nuclear fluorescence is shown in Figure 18 A and B. Here a mother cell (green trace) divides into two daughter cells (blue and red trace), both of which undergo the G1-S transition. At time $t$=1.8 hours the mother cell enters M phase − the fluorescence associated with the nuclear marker increases owing to a breakdown of the nucleus and rounding of the cell. The cell divides at time $t$=3.5 hours, and later at approximately $t$=9 hours, the cells start to undergo the G1-S transition, resulting in a decrease of nuclear fluorescence. The duration of G1 phase was determined by the time difference between division, and the decrease in nuclear fluorescence of the PSLD-Citrine. A histogram was created for $n$=143 cells. The duration is 4.7±2.3 hours (standard deviation) indicating considerable variability in the duration of G1 (Figure 18C).

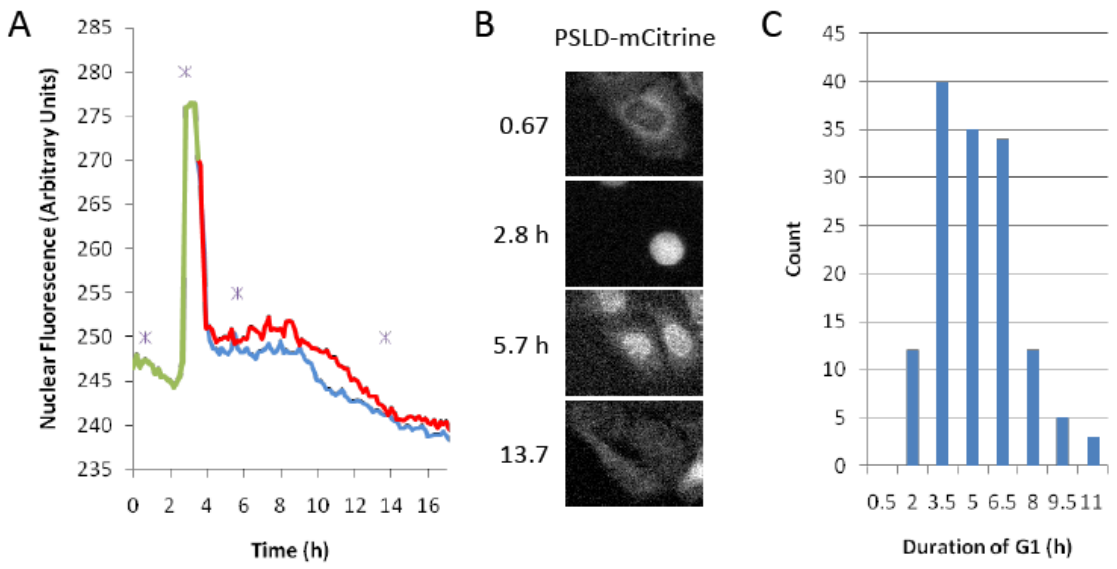


**Figure 18: Quantification of the PSLD cell cycle reporter. (A) The PSLD-mCitrine nuclear fluorescence of the mother cell is indicated by the green line; the nuclear fluorescence of the daughter cells is indicated by the red and blue lines. At time *t*=1.8 hours the mother cell enters M phase and the cell divides at time *t*=3.5 hours. At approximately *t*=9 hours, the cells start to undergo the G1-S transition, resulting in a decrease of nuclear fluorescence. (B) Fluorescence images corresponding to the quantification in A. (C) The duration of G1 phase was determined by the time difference between division, and the decrease in nuclear fluorescence of the PSLD-Citrine. A histogram was created for *n*=143 cells. The duration is 4.7±2.3 hours (standard deviation) indicating considerable variability in the duration of G1.**

To monitor both the stage of the cell cycle and the onset of caspase activation we co-expressed Cerulean-NLS, PSLD-Citrine and pmDEVD in HeLa cells and treated cells with 2 µM STS (Figure 19). Here, the nuclear outline in the upper panel indicates the mask created by the Cerulean-NLS fluorescence. We tracked cells for several hours prior to the addition of STS (time *t*=0 indicates when STS is added). The activation of caspase-3/7 is indicated by an increase in fluorescence (Figure 19 – lower panel).

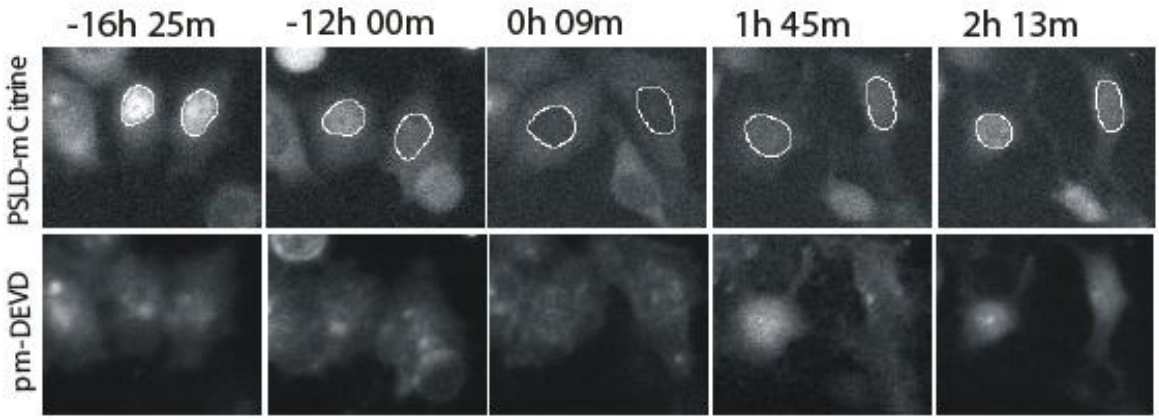


**Figure 19: Monitoring the cell cycle and caspase activity in the same cell. (Top Panel) Expression of the PSLD-mCitrine cell cycle reporter. Cells transition out of G1 (nuclear to cytosolic localization). (Bottom Panel) Caspase activity of the pmDEVD mCherry reporter indicated by the increase in fluorescence.**

The phase of the cell cycle was determined relative to either the G1/S transition, or the time of last division. The time of apoptosis was plotted as a function of the position in the cell cycle at the time of STS treatment since the reporter becomes localized in both the nucleus and cytoplasm after STS treatment. No correlation could be detected between the phase of the cell cycle at the time of STS addition, and the time of caspase activation after treatment with STS (Figure 20). These results indicate that the correlation of the distance between cells and when cells enter apoptosis in response to STS is not related to the cell cycle.

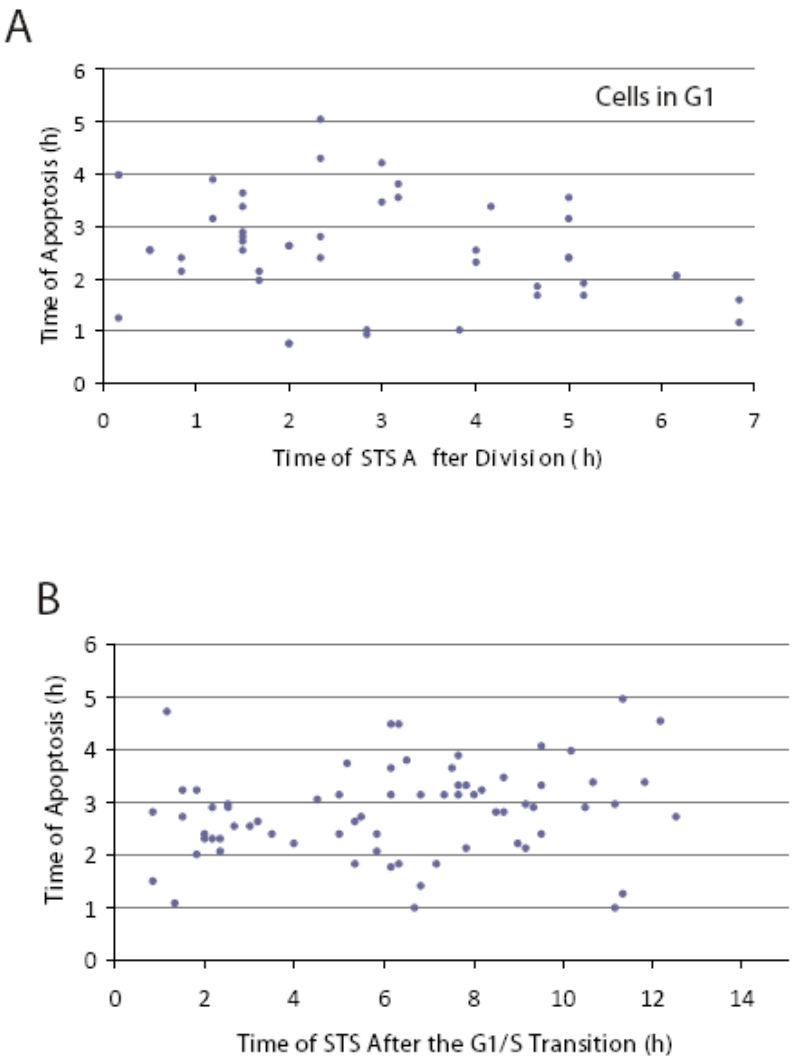


**Figure 20: Correlation of the stage of the cell cycle and the onset of caspase activation in single cells. HeLa cells expressing the PSLD-mCitrine reporter and the pmDEVD-mCherry reporter were monitored to determine the stage of the cell cycle, then treated with 2µM of STS. There was no clear correlation between the phase of the cell cycle at the time of treatment and the time to caspase activation.**

### *Separation of Distance and Genealogy*

To determine if the local synchronization in activation of caspases was the effect of secreted factors or of a similarity of molecular composition of sister cells, we performed three different tests. The first test was to monitor the activation of caspase in the rapidly moving HT1080 cell line that was stably expressing pmDEVD-mCherry and YFP-NLS. HT1080 migrate after division such that average distance between nuclei of sister cells was 223±39 μm (compared to 66±13 μm for HeLa pairs; Figure 21). In the HT1080 cells there is a lower probability that neighboring cells are also sister cells which would uncouple effects of possible secreted factors from similarities in the molecular composition of the cell. The rapid movement also created situations where a pair of sister cells were separated by an unrelated cell. In these situations we determined whether the time of caspase activation in each sister cell was correlated with the nearer unrelated cell or the more distant sister cell.

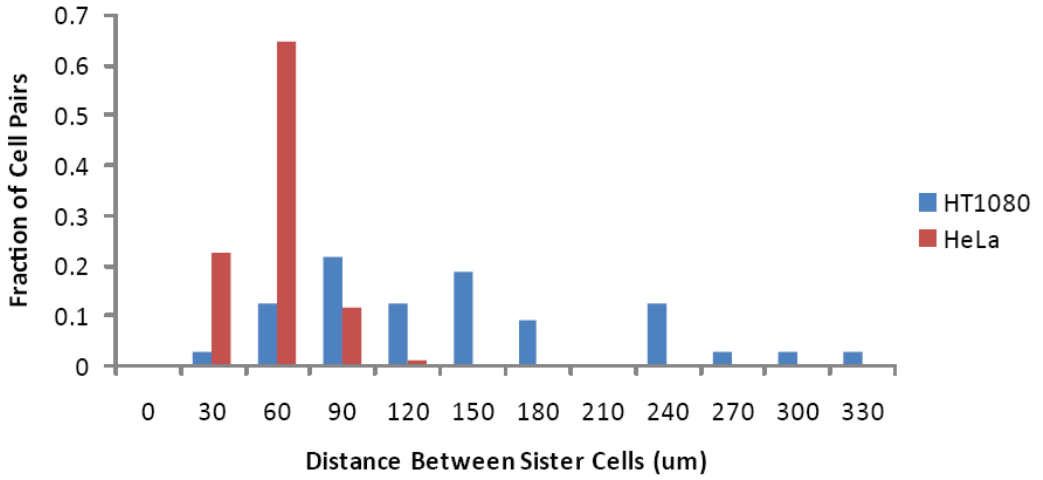


**Figure 21: Distance correlation for the HT1080 cell line. (A) A histogram of the distance between sister cells at the time of drug treatment indicates that the distance between HT1080 sister cell pairs is larger than the distance between HeLa cell pairs. The average distances are 223±39 µm for HT1080 cells, and 66±13 µm for HeLa cells.**

An example of HT1080 sister cells that are separated by other cells at the time of STS (2µM) treatment is shown in Figure 22A. While the sister cell pair undergo apoptosis at similar times, a cell that had migrated so that it was between the sister cells does not undergo apoptosis until much later (Figure 22B).

**Figure 22: (A) Time lapse images of HT1080 cells before and after treatment with STS. T=0:00 indicates the time of STS addition. HT1080 cells express the pmDEVD caspase-3/caspase-7 reporter (grey-scale), and YFP-NLS (shown as a colored nuclear outline). An instance of sister cells that are physically separated is indicated by cells with a red nuclear outlines. The separating cell is indicated with a yellow nuclear outline. All other nuclei are in blue. (B) Time course of caspase-3/caspase-7 activation of the sister cells in (A), and a cell between the sister cells. Color of the data points corresponds to cells with the same colored nuclear outline in (B). Cells undergo apoptosis at a similar time relative to the distribution of apoptosis, and relative to the middle cell.**

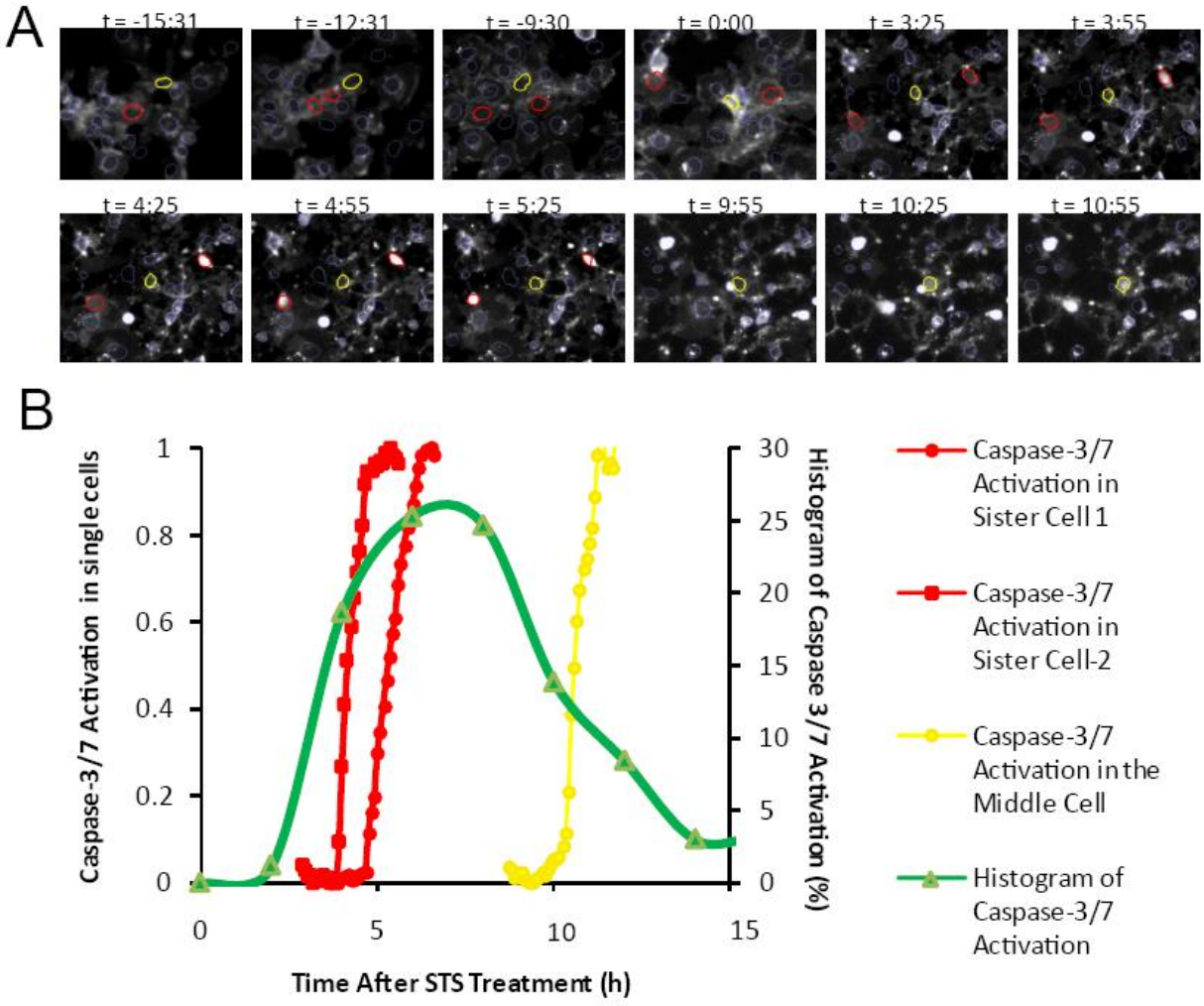
A
t = -15:31
t = -12:31
t = -9:30
t = 0:00
t = 3:25
t = 3:55
t = 4:25
t = 4:55
t = 5:25
t = 9:55
t = 10:25
t = 10:55
B
Caspase-3/7 Activation in single cells
Histogram of Caspase 3/7 Activation (%)
Time After STS Treatment (h)
Caspase-3/7 Activation in Sister Cell 1
Caspase-3/7 Activation in Sister Cell-2
Caspase-3/7 Activation in the Middle Cell
Histogram of Caspase-3/7 Activation

**Figure 22**

Furthermore, for HT1080 cells, there was no correlation between inter-cellular distance and the onset of apoptosis (Figure 23). This suggests that a secreted factor cannot be entirely responsible for the correlation between caspase activation and distance. However this does not exclude the partial contribution of secreted factors to the correlation seen in HeLa cells (Figure 14).

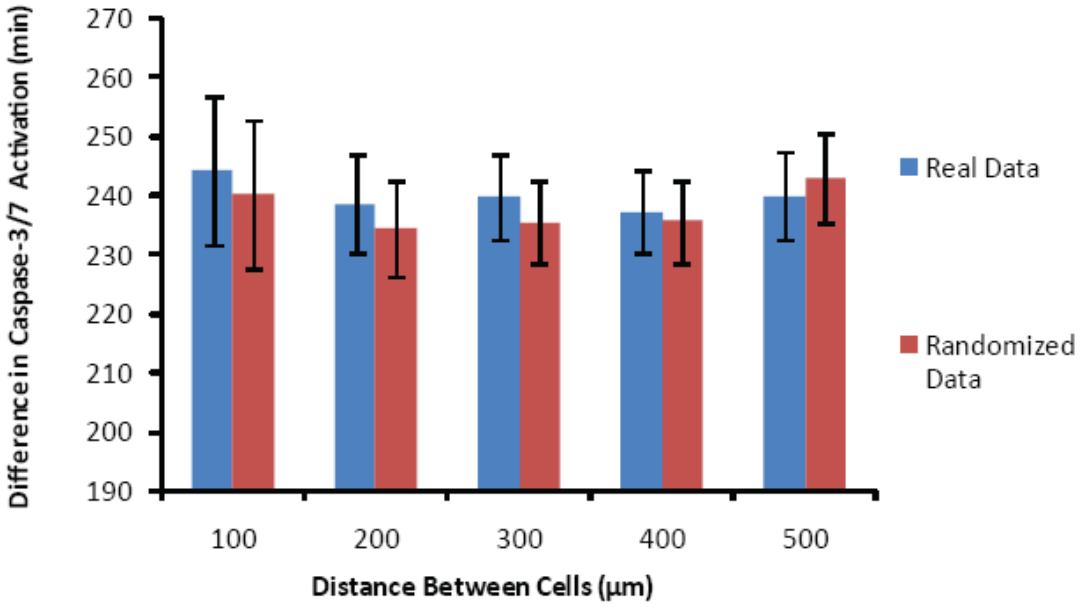


**Figure 23: Plot of the difference in time of apoptosis between HT1080 cells as a function of their distance. (*n*=195 cells in three fields). Error bars represent 95% confidence interval of the mean.**

The second test was to uncouple distance and genealogy by dissociating cells from their dish, and then re-plating them so their positions are randomized (Figure 24). If the genealogical relationship between cells was responsible for the local synchronization of apoptosis, then when cells were dissociated and then re-plated at a high density, the local effects should be lost. In contrast, effects of secreted factors on neighboring apoptosis should be unaffected.

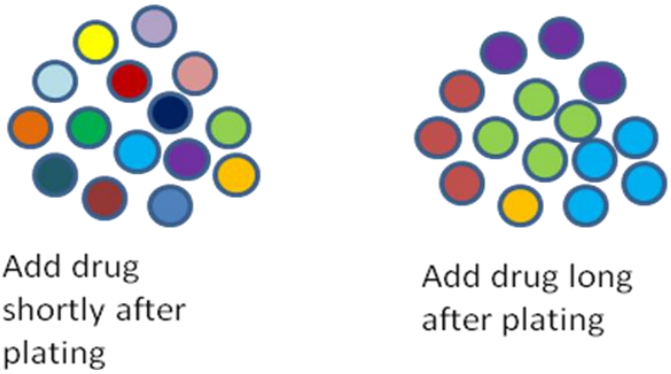


**Figure 24: Scheme of plating experiments. Cells in which apoptosis is induced shortly after plating are unlikely to be related; by comparison cells that are treated with a drug long after plating are more likely to have divided and thus be related. Cells of similar colors are related cells.**

Cells that were plated 48 hours or 80 hours prior to STS treatment showed a strong distance correlation (Figure 25): The delay between two cells entering apoptosis that were 50 µm apart was 24% less than cells 200 µm apart for cells plated 48 hours prior to treatment. However, for cells plated 14 hours prior to STS treatment, the decrease in the delay for entering apoptosis for cells at a distance of 50 µm was reduced

only 8%, indicating a weaker local effect. This residual degree of synchronization could be due to the presence of a few neighboring sister cells which divided within 14 hours after plating (data not shown).

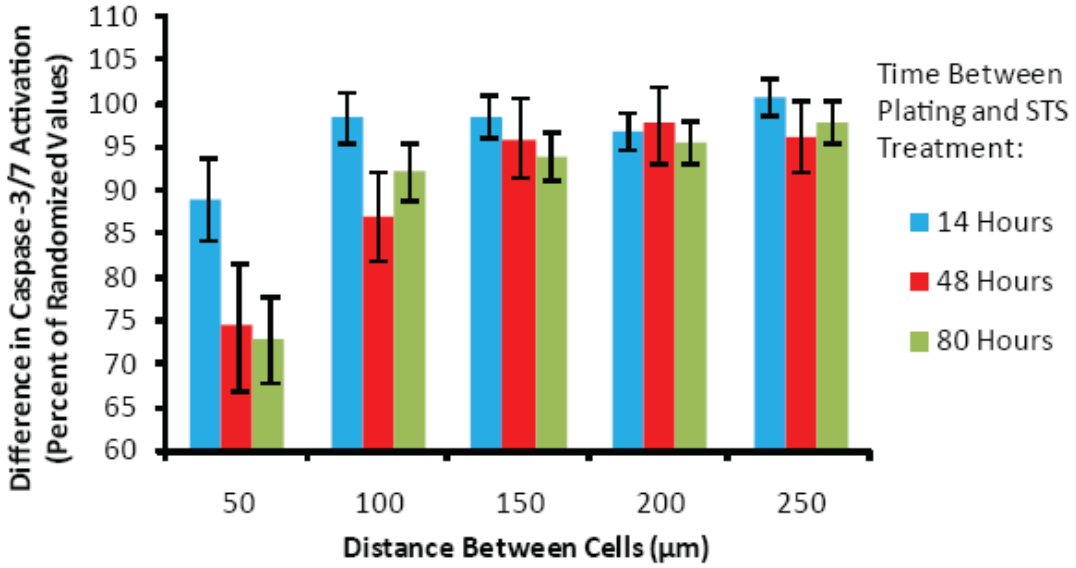


**Figure 25: Analysis of time difference of DEVDase activation as a function of distance for cells plated at various times prior to STS addition (number of cells>385 for each time point).**

The third test was to separate the effects of HeLa cell genealogy and inter-cell distance by determining the correlation between caspase-3/7 activation and distance after excluding comparisons between related HeLa cells. Cells at closer distances demonstrate a higher similarity of their times of caspase-3/7 activation than cells further apart indicating a correlation between caspase-3/7 activation and distance (Figure 26 - red).

However, when sister cells were excluded from the comparison the correlation was weaker (Figure 26 - green) and further weakened when sister and cousin cells are excluded (Figure 26 - purple). To determine whether the spatial correlation to apoptosis was only between sister cells, we plotted time of caspase-3/7 activation between sister cells as a function of their inter-cell distance (Figure 26 - blue). While these showed a high degree of similarity between time of entering apoptosis, they did not show correlation with distance. The lack of spatial correlation between sister cells further indicates that a secreted factor between sister cells does not contribute to the correlation between caspase activation and intercellular distance. The combination of the above experiments suggests that secreted factors do not play a role that we can detect in the local synchronization in the activation of caspases.

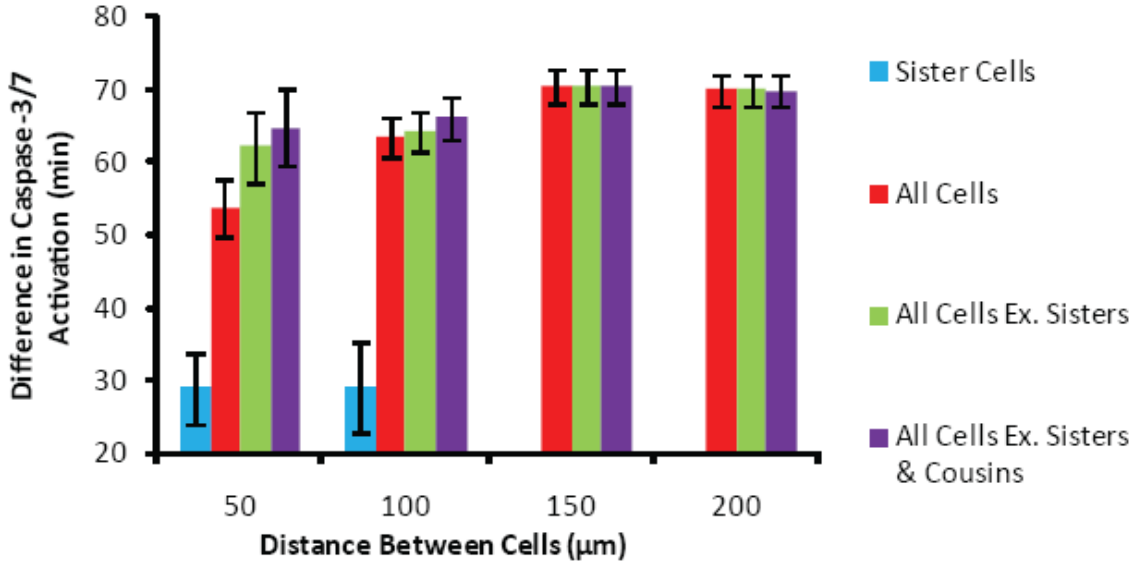


**Figure 26: Analysis of the time difference of DEVDase activation as a function of distance between cells for sister cell cells (blue), between all cells (red), between all cells that are not sister cells (green), and between all cells that are not sister cells or cousin cells (purple) (*n*=562 cells in three fields).**

### *Similarity of Apoptosis Timing Between Sister Cells*

The observation that in unrelated cells there is no correlation between distance and when cell undergoes apoptosis implicates cell lineage and an underlying source for the local synchrony of apoptosis. This was further tested by quantifying the difference in caspase activation between sister cells (Figure 27 - blue). As a control we measured the distribution of the differences in the time of caspase activation between randomly paired cells (Figure 27 – red). When HeLa cells were treated with STS (2µM), the difference in

caspase-3/7 activation between randomly paired cells was significantly greater than the difference in caspase-3/7 activation between sister cells ($p=6.2x10^{-34}$; Figure 27). This is an independent confirmation of the role of lineage in determining when a cell undergoes apoptosis.

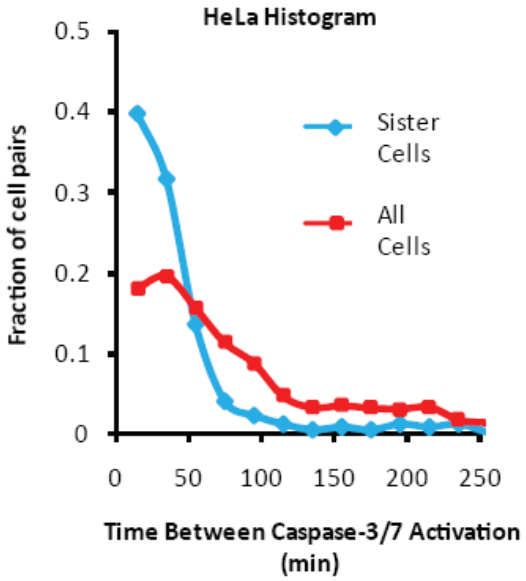


**Figure 27: Histogram of the difference in time of DEVDase activation between HeLa sister cells, and between randomly paired cells (n=265 pairs).**

To determine whether the similarity in apoptosis times between sister cells was specific to a cell type or apoptotic stimuli, we calculated the average difference in the onset of caspase-3/7 activation between sister cells, and between randomly paired cells for HeLa, NIH3T3, HT1080, and mouse embryonic fibroblasts (MEF) cells. These cells were treated with STS (2μM), TNFα (250μg.mL) + CHX (5μg/mL), or etoposide (ETO,

50μM) (Figure 28). In all cases the average time difference of caspase-3/7 activation between sister cells was significantly less than the average time difference of caspase-3/7 activation between randomly paired cells. These results, obtained in multiple cell types and with multiple drugs, indicate that the similarity of caspase-3/7 activity between sister cells is not a cell type specific or drug-specific effect.

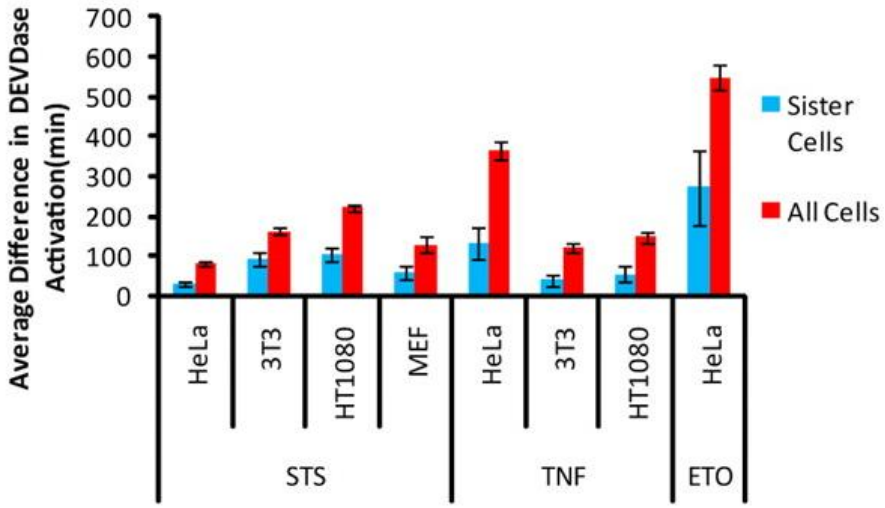


**Figure 28: Average difference in DEVDase activation between sister cells (blue), and randomly paired cells (red) for HeLa, NIH3T3 and HT1080 cells treated with 2 μM STS, 250 ng/μl TNFα + 5 μg/ml CHX, or 50 μM ETO. Differences between sister and random distributions are significant for all cell types (STS: HeLa, $P=6.2\times10^{-34}$; 3T3, $P=0.0011$; HT1080, $P=2.1\times10^{-10}$; MEF, $P=9.9\times10^{-4}$. TNFα+CHX: HeLa, $P=1.4\times10^{-16}$; 3T3, $P=4.7\times10^{-14}$; HT1080, $P=5.8\times10^{-10}$. ETO: HeLa, $P=1.2\times10^{-11}$. For MEFs, $n_{pairs}=21$; for all other cells: $n_{pairs}$ is between 54-106 pairs for different conditions).**

### *Similarity of Sister Cell Fate*

To determine whether the cellular fate was similar between sister cells, we used a milder apoptotic treatment which only killed a fraction of cells, and determined whether both sister cells underwent apoptosis or survived, or whether only one of the sister cells underwent apoptosis. HeLa cells were transiently treated with of STS (1μM) for 45 minutes, and during the subsequent 36 hours, 44% of the cells underwent apoptosis. If there was no linkage in the fate between sister cells, then of 72 total cell pairs, 14 pairs should both undergo apoptosis, 22 pairs should both survive, and 36 pairs should have only one cell undergoing apoptosis (Figure 29 - red). Instead we observed that 27 sister pairs both underwent apoptosis, 35 pairs both survived, and there were 10 pairs where only one cell underwent apoptosis (Figure 29 - blue). Of the cells that did not undergo apoptosis, a few did not divide again, and it is possible that even 36 hours after treatment, apoptosis will still continue to occur. Nonetheless, given that 44% of all cells die, the probability that there are only 10 pairs of sister cells of which only one undergoes apoptosis is $p<0.0005$ ($\chi^2= 37.2$, 2 degrees of freedom). This indicates that not only the timing of apoptosis between sister cells is similar (Figure 27), but also when given a mild apoptotic treatment, the fates of sister cells are similar (Figure 29).

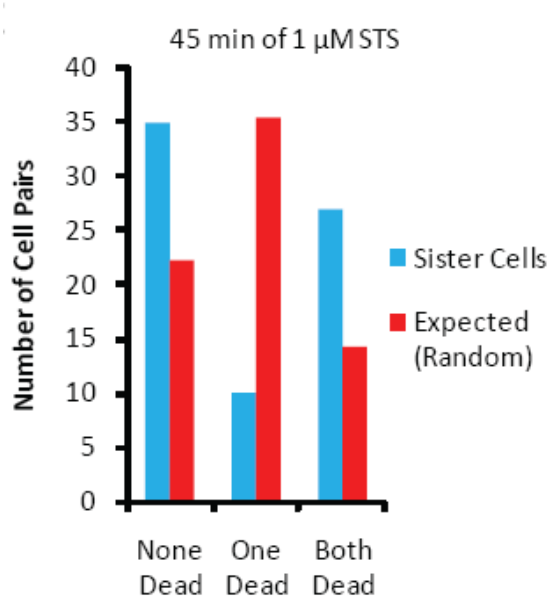


**Figure 29: HeLa cells treated with 1 µM STS for 45 minutes. In blue are counts of sister cell pairs where both cells die, only one cell dies and where both survive. In red is the expected value of the counts if there were no apoptosis similarity between sister cells, and given that 44% of all cells underwent apoptosis. All error bars represent the 95% confidence interval of the mean.**

### *Intergenerational Divergence of the Apoptosis Susceptibility*

The similarity of the apoptosis between related cells could be stable – resulting from the inheritance of genes. Thus the similarity of whether and when related cells undergo apoptosis could result from the presence of a mixture of difference cell lineages. However, the similarity could also be transient – arising from the division of proteins from the mother cell. Alternatively, the similarity may be a combination of these factors.

To distinguish between these possibilities, we monitored the lineage of cells up to four generations prior to apoptosis treatment. We reasoned that if the similarity resulted from a temporary inheritance of proteins, then the difference in the time of caspase-3/7 activation between two cells should become larger as the cells are more distantly related. Alternatively, if it were a stable genetic alternation, then the differences in the time of caspase activation should remain constant for the different lineages. To assay differences and similarities in apoptosis susceptibility for a time longer than four generations, we created clonal cell lines and compared the distribution of the time of caspase-3/7 activation between these lines. If similarity of apoptotic state resulted from a stable genetic inheritance, we expected a significant difference in the time of caspase-3/7 activation between different cell lines. We monitored cells for up to 90 hours prior to apoptosis treatment to determine the lineage of cells. We defined sister cells as being one generation apart and cousin cells as being two generations apart (Figure 30).

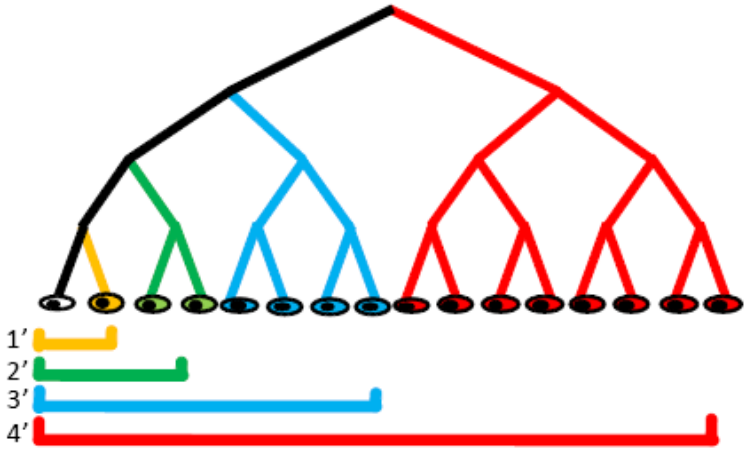


**Figure 30: Lineage of cells. We monitored cells for up to 90 hours prior to apoptosis treatment to determine the lineage of cells. We defined sister cells as being one generation apart and cousin cells as being two generations apart.**

After monitoring the lineage of HeLa cells for four generations, we treated cells with STS (1 μM) and compared the time of apoptosis between cells that shared a common ancestor (Figure 31). A histogram of the apoptosis time differences, as well as the apoptosis time difference between randomly paired cells is shown in Figure 31. As the relation between cells becomes more distant (from gold, to green to blue to red), the histogram flattens, approaching the histogram of randomly paired cells (Figure 31).

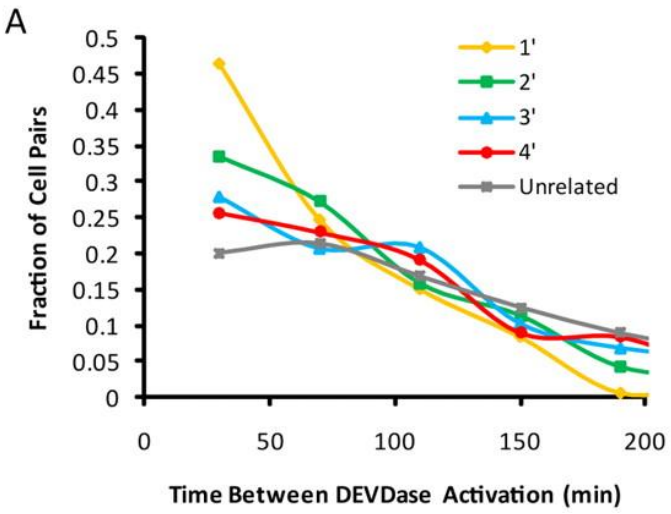


**Figure 31: Divergence of apoptotic susceptibility. (A) The difference in time of apoptosis between cells from different generations. As the number of generations between cells increases, the curve flattens.**

To determine the dynamics of the divergence of the apoptotic susceptibility, we fit the mean difference of the time to enter apoptosis between cells from different generations to an exponential recovery curve (Figure 32). This curve was selected on the assumption that cells lost a proportional fraction of their apoptotic susceptibility during division or over time. The fit was of the form $y=42.5+43.2(1-e^{-(g-1)/1.94})$ with $y$ minutes, and $g$ in generational difference between cells. Analysis of the fitted parameters revealed that the half-time of loss of apoptosis susceptibility was 1.3±0.6 generations, and as cells become more distantly related, the difference in their time of apoptosis approaches the asymptote of 86±9 minutes. The calculated half-time is similar to half-times of the mixing of gene expression in related mammalian cells (Sigal et al., 2006b), suggesting

that the similar apoptosis times of sister cells may reflect the similarity of gene expression levels. Furthermore, the calculated time of apoptosis between distantly related cells (86±9 min) is within error of the measured apoptosis time differences between unrelated cells (90±1 min), indicating that the similarity of the apoptotic state of related cells is transient, and does not result from genetic differences.

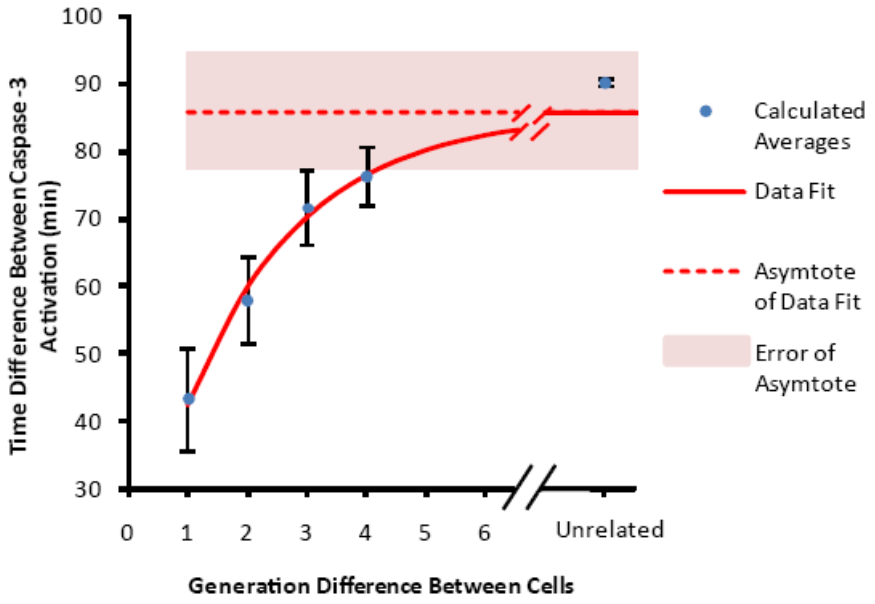


**Figure 32: Analysis of the difference in DEVDase activation between cells from different generations and between unrelated cells (blue circles). Cells are fit to an exponential recovery curve (solid red line). Exponential fit is: $y=42.5+43.2(1-e^{-(g-1)/1.94})$ with $y$ minutes, and $g$ in generational difference between cells; $R^2=0.988$ for the shown data points. Red dotted line is the asymptote of exponential recovery fit. Pink overlay is the error of the asymptote.**

To examine the persistence of apoptosis susceptibility over more than four generations, we analyzed the distributions of the onset of caspase-3/7 activation in clonal cell lines (Figure 33). The overlap in the distributions was significant (One way ANOVA: $F=1.29$, $F_{crit}=2.38$, $F>F_{crit}$) indicating that the similarity in apoptosis susceptibility does not persist indefinitely, and is unlikely a result of genetic variation or the presence of multiple cell lineages.

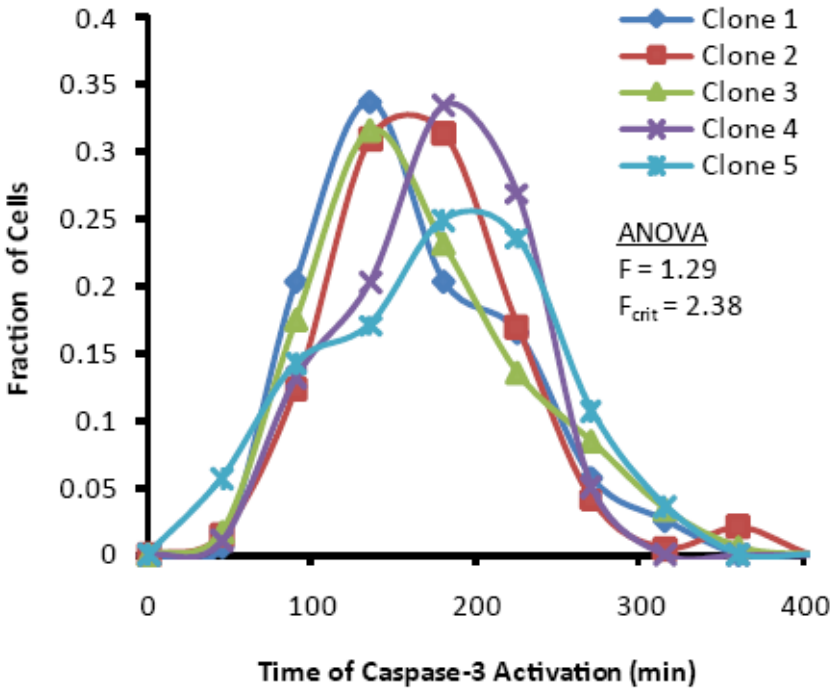


**Figure 33: Kinetics of apoptosis in clonal populations. Clonal cells expressing the pmDEVD-mCherry reporter treated with 2 µM STS. Overall distribution of apoptosis was similar according to One Way ANOVA.**

### *Intragenerational Apoptosis Divergence*

To gain insight into the divergence of apoptosis susceptibility, we plotted the difference in caspase activation as a function of the time since sister cells or cousin cells divided from their last common ancestor (Figure 34). An exponential recovery curve was fit to the data; this was of the form: $y=5.8+68.5(1-e^{-t/1256})$. To assess intragenerational trends, cell pairs were binned according to the time since division (500 minute bins; Figure 34). We found that apoptosis times between newly divided sister cells was more similar than sister cells that had divided long before STS treatment (1μM STS – Figure 34). Thus, the varied susceptibility to apoptosis is a function of the time that cells spend apart. These results indicate that the loss of correlation of apoptosis between sister cells occurs continuously and not as a discrete step during mitosis, or another phase of the cell cycle.

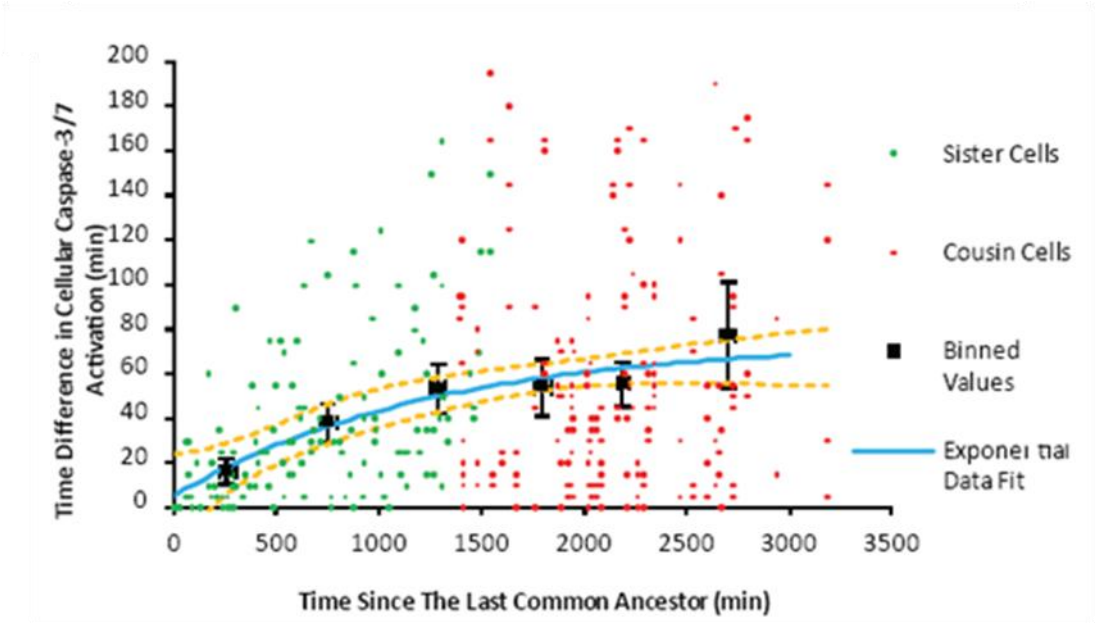


**Figure 34: Difference in DEVDase activation between related cells (sister cells, green; cousin cells, red) as a function of time since cells shared a common ancestor. Recovering exponential fit (blue line), confidence interval of fit (yellow line) are plotted as well as individual time points from a 500 minute binning (black squares). Exponential fit is: $y=5.8+68.5(1-e^{-t/1256})$ with $y$ and $t$ in minutes; $R^2=0.122$.**

### *Inhibition of Divergence*

One possibility for the divergence of apoptosis susceptibility in sister cells is a difference in gene expression after division. To determine whether new protein expression was responsible for the divergence of apoptosis susceptibility, we inhibited protein expression in newly divided cells using cycloheximide (CHX) - an inhibitor of protein translation (ENNIS and LUBIN, 1964; SIEGEL and SISLER, 1963). We sought

to inhibit protein synthesis prior to apoptosis treatment but after cell division, Thus in an asynchronous culture we monitored newly divided HeLa cells under the following conditions: (1) in the presence of CHX (20 µg/mL) for 9 hours, (2) in the absence of CHX for 3 hours, followed by the presence of CHX for 6 hours, (3) in the absence of CHX for 6 hours, followed by the presence of CHX for 3 hours, and (4) in the absence of CHX for 9 hours. Cells were then treated with CHX (20 µg/mL) and STS (1µM) (Figure 35).

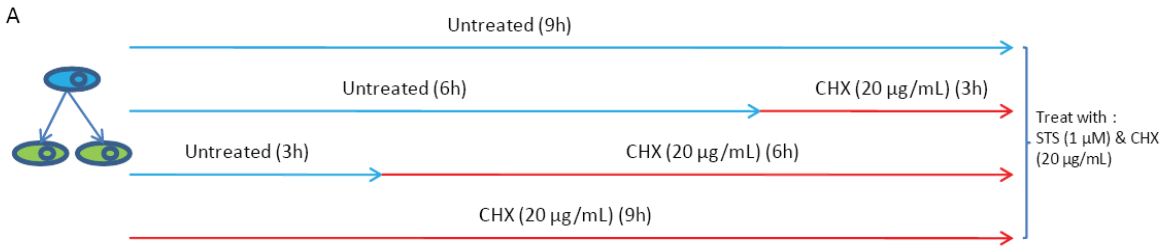


**Figure 35: Schematic of the protein inhibition experiment. (1) in the presence of CHX (20 µg/mL) for 9 hours, (2) in the absence of CHX for 3 hours, followed by the presence of CHX for 6 hours, (3) in the absence of CHX for 6 hours, followed by the presence of CHX for 3 hours, and (4) in the absence of CHX for 9 hours. Cells were then treated with CHX (20 µg/mL) and STS (1µM)**

The difference in apoptosis times was determined for sister cells. We plotted the histograms of the time difference of apoptosis between sister cells. The longer time that sister cells spent in the absence of CHX, the greater the difference in apoptosis times (Figure 36A,B). The difference in sister cell apoptosis times for different CHX

treatments was not a result of an overall difference in the time of apoptosis in the population (Figure 36C).

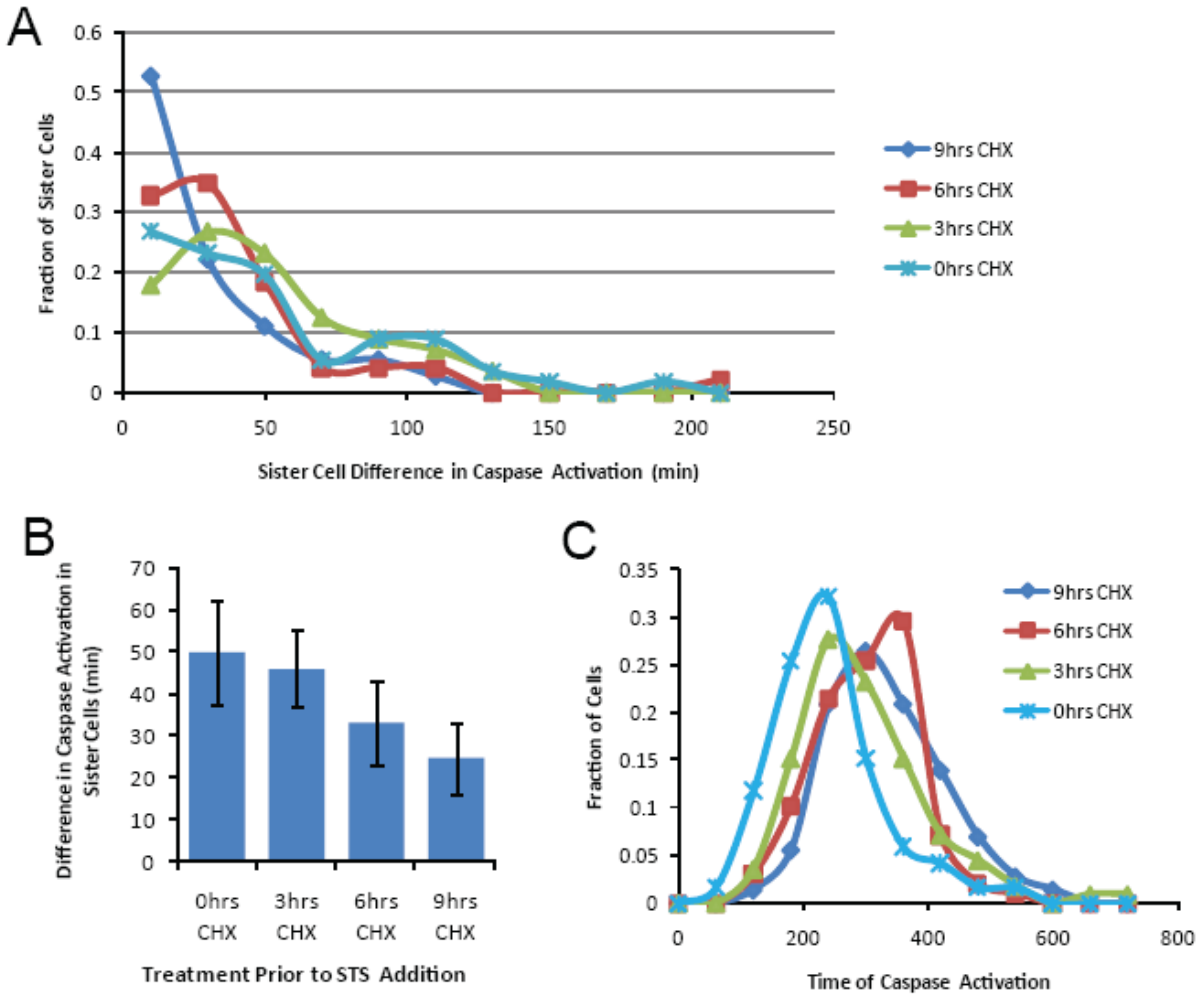


**Figure 36: Difference in DEVDase activation between newly divided sister cells for different treatments with cycloheximide (see text). Relative to untreated cells, the difference is smaller for cells in CHX for 9 hours (*P*=0.0039). Error bars represent 95% confidence intervals**

One of the concerns of using cycloheximide is that it may have a non-specific effect that may alter another aspect of apoptosis. Thus we sought to inhibit protein synthesis with another inhibitor to determine if we got the same effect. Similar results were also observed with puromycin, another inhibitor of protein synthesis that works through a different mechanism from cycloheximide (Traut and Monro, 1964) (Figure 37). We could only extend the pre-treatment of cells in puromycin to 6 hours since at 9 hours, some cell death started to occur without STS treatment (data not shown). These results suggest that the divergence of apoptosis times between sister cells is partially a result of new protein expression.

## *Summary*

In this chapter we provide experiments demonstrating that sister cells undergo apoptosis a few minutes apart (Figure 27). The similarity in apoptosis times could not be correlated to the cell cycle (Figure 20), or the distance between cells (Figure 22-26). Furthermore, not only are the apoptosis times between sister cells similar, but the fates of sister cells are more similar that random (Figure 29). We also find that for related cells that there is divergence in the times of apoptosis as cells become more unrelated (Figure 32). This divergence is also observed within single generations (Figure 34) and is limited by blocking protein synthesis after division (Figure 36).

**Figure 37: Divergence of apoptosis times in sister cells in inhibited by puromycin. (A) Experiment overview. We monitored the division of sister cells in a 3 hour interval prior to puromycin (1 µg/ml) treatments. These newly divided cells were followed under three different conditions which differed in the time that cells were untreated with puromycin. All cells were then treated with staurosporine (STS) (1 µM) in the presence of puromycin (1 µg/ml). The duration of the puromycin experiment is shorter than the cycloheximide (CHX) owing to greater cell death prior to STS treatment, whereas cell death is negligible in the CHX experiment prior to STS treatment. (B) Distributions of the difference in caspase activation of sister cells under the three different puromycin treatments. The distribution appears to flatten the longer the cells are not in the presence of puromycin. Data binned in 30 minute intervals. Total number of cell pairs for each treatment is between 32 and 37. (C) Average time of apoptosis under the three different puromycin conditions. Error bars represent the 95% confidence interval of the mean. (D) Population distribution of apoptosis times under the three different puromycin conditions.**

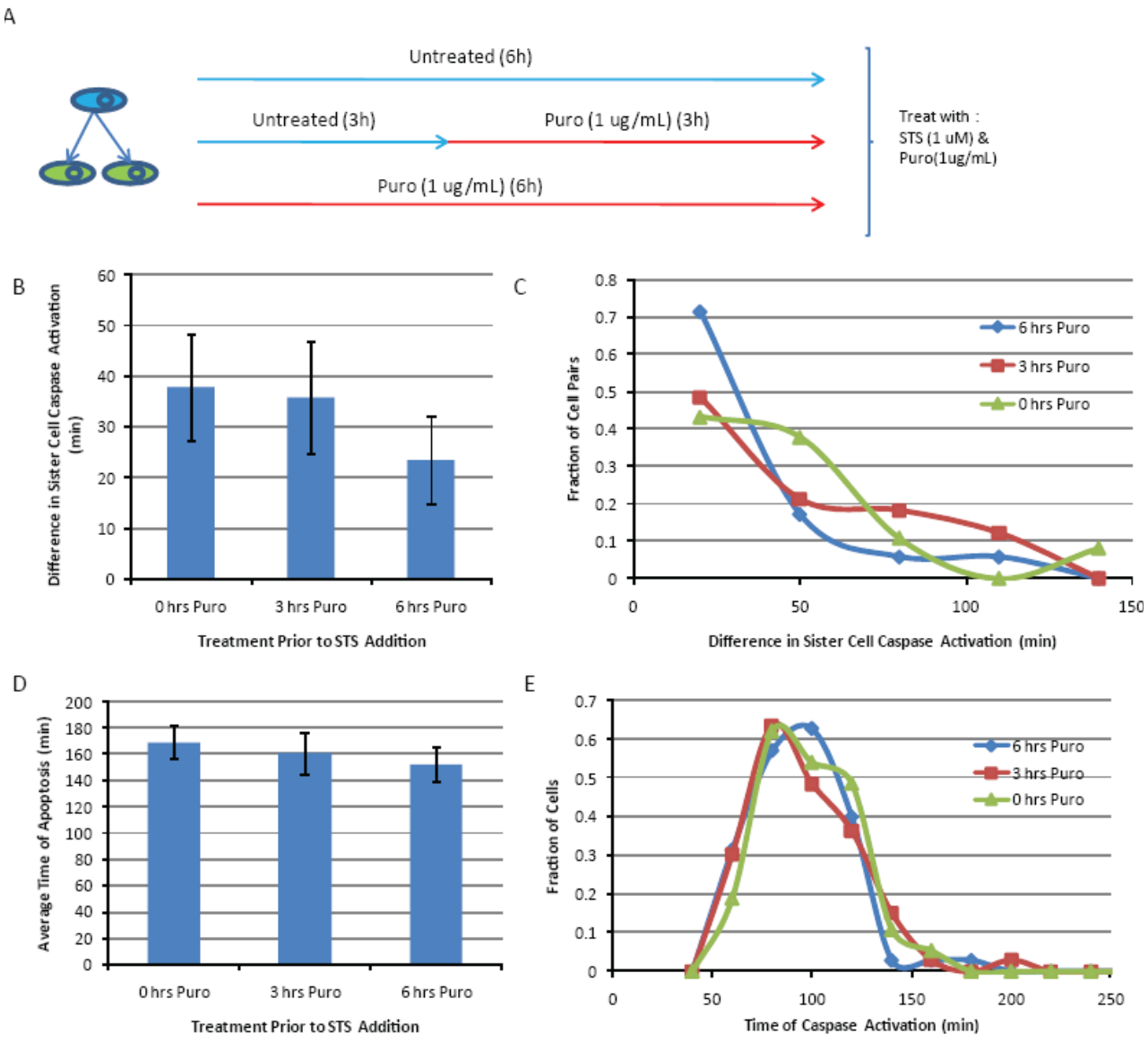
A
Untreated (6h)
Untreated (3h)
Puro (1 ug/mL) (3h)
Puro (1 ug/mL) (6h)
Treat with :
STS (1 uM) &
Puro(1ug/mL)
B
Difference in Sister Cell Caspase Activation (min)
0 hrs Puro
3 hrs Puro
6 hrs Puro
Treatment Prior to STS Addition
C
Fraction of Cell Pairs
6 hrs Puro
3 hrs Puro
0 hrs Puro
Difference in Sister Cell Caspase Activation (min)
D
Average Time of Apoptosis (min)
0 hrs Puro
3 hrs Puro
6 hrs Puro
Treatment Prior to STS Addition
E
Fraction of Cells
6 hrs Puro
3 hrs Puro
0 hrs Puro
Time of Caspase Activation (min)

**Figure 37**

# *Chapter Four: Cytochrome c is released in a wave*

## *Introduction*

Mitochondria play a central role in apoptosis, integrating signals from members of the Bcl-2 family (Danial and Korsmeyer, 2004), Opa and Parl (Pellegrini and Scorrano, 2007), and many other molecules. It has been proposed that mitochondria integrate these signals, resulting in changes in membrane permeability to pro-apoptotic proteins (Ow et al., 2008) and the fragmentation of mitochondria (ROUILLER, 1957; Zhuang et al., 1998).

Once released from the mitochondria, cytochrome *c* interacts with Apaf-1, resulting in the activation of caspases that in turn cleave several vital substrates, leading to biochemical and morphological features characteristic of apoptosis (Li et al., 1997). Membrane permeability to cytochrome *c* is considered a critical step in the progression of apoptosis. Along with cytochrome *c*, Smac is also released into the cytosol (Munoz-Pinedo et al., 2006). Once in the cytosol, Smac induces degradation of the inhibitor of apoptosis proteins (IAPs), thereby facilitating caspase activation (Du et al., 2000; Verhagen et al., 2000). Around the same time, the mitochondrial intermembrane becomes permeable to protons, causing loss of membrane potential ($\Delta\Psi_m$) (Munoz-Pinedo et al., 2006), and the mitochondria are observed to fragment and undergo changes

to their internal structure (Sun et al., 2007; Frezza et al., 2006). Furthermore, the precise temporal order of these events is not completely resolved (Martinou and Youle, 2006; Lakhani et al., 2006)

Although cytochrome *c* may be released in different cells at any time over a period of several hours, its release within a single cell is completed within several minutes (Goldstein et al., 2000). Thus, one of the major barriers to imaging the dynamics of cytochrome c is that its onset is so variable that when imaging is done at high temporal resolution, fluorescent tags are usually bleached before cytochrome c is initiated. This has limited the ability to resolve whether cytochrome *c* and Smac are released at different times or simultaneously (Munoz-Pinedo et al., 2006), or whether the increase in permeability of the outer (Waterhouse et al., 2001) or inner (Gottlieb et al., 2003) membrane occurs first.

Here, we show that cytochrome *c* release can be initiated at one, two, or multiple points in a cell and then propagates across the cell. This behavior was observed for apoptosis induced by a number of different drugs. Cytochrome *c* release took place before Smac release and loss of $\Delta\Psi_m$, which also occurred in waves, though lagging in time behind cytochrome *c* release. By analyzing individual mitochondria, we show that mitochondrial fission occurs after cytochrome *c* release. Additionally, we examine the dynamics of cytochrome *c* release from single mitochondria, showing that release occurs in a single step from single mitochondria. Finally, we show that the wave of cytochrome *c* release can be inhibited by thapsigargin (a blocker of the SERCA calcium pumps) but

not with BAPTA-AM, which buffers cytosolic calcium levels. These observations indicate that the signal for mitochondria to release cytochrome *c*, and, in some cases, the commitment to apoptosis does not take place simultaneously at all mitochondria, and does not occur spontaneously within the cell.

## *Results*

### *Wave of Cytochrome c – GFP Release in Single Cells*

Initiation of apoptosis in a population of cultured cells is asynchronous and distributed over several hours (Goldstein et al., 2000). Our observations in Chapter Three suggest that we can approximately predict the time when a cell will undergo apoptosis based on when its sister cell undergoes apoptosis (Figure 27). Furthermore, if we allow HeLa cells to divide on a dish for more than 40 hours, we see a local synchrony of apoptosis (Figure 14). Therefore, to obtain high temporal resolution images of cytochrome c GFP release, we plated HeLa cells and allowed them to divide for more than 40 hours, then we treated cells with an apoptotic drug, imaged clusters HeLa cells once every 2 minutes until one cell in a field released cytochrome c-GFP. At this point the acquisition rate was increased to once every 5-10 seconds to capture the release of cytochrome c-GFP in nearby cells that still had mitochondrial cytochrome c-GFP.

An example of the dynamics of cytochrome c-GFP release in HeLa cells treated with TNF-Related Apoptosis Inducing Ligand (TRAIL, 1 μg/mL) is shown in images from a time-lapse experiment (Figure 38). The release of cytochrome c-GFP was initiated at one end of the cell (indicated by the arrow), and in successive frames a wave of cytochrome c-GFP release swept across the cell. This continued for 90 seconds until cytochrome c-GFP was no longer localized to mitochondria in the cell. This result is consistent with a study published while our manuscript was in review, which also showed a spatial release of cytochrome c (Lartigue et al., 2008).

To determine whether the loss of cytochrome c-GFP fluorescence was a result of mitochondria moving out of the plane of focus, or a complete breakdown of mitochondria, we monitored cytochrome c-GFP simultaneously with the mitochondria marker mito-mCherry (Shaner et al., 2004; Rizzuto et al., 1995). During the loss of localized cytochrome c-GFP fluorescence, there were no discernable changes in the mito-mCherry fluorescence (Figure 38B). A wave of cytochrome c-GFP release was also observed using confocal microscopy (Figure 39).

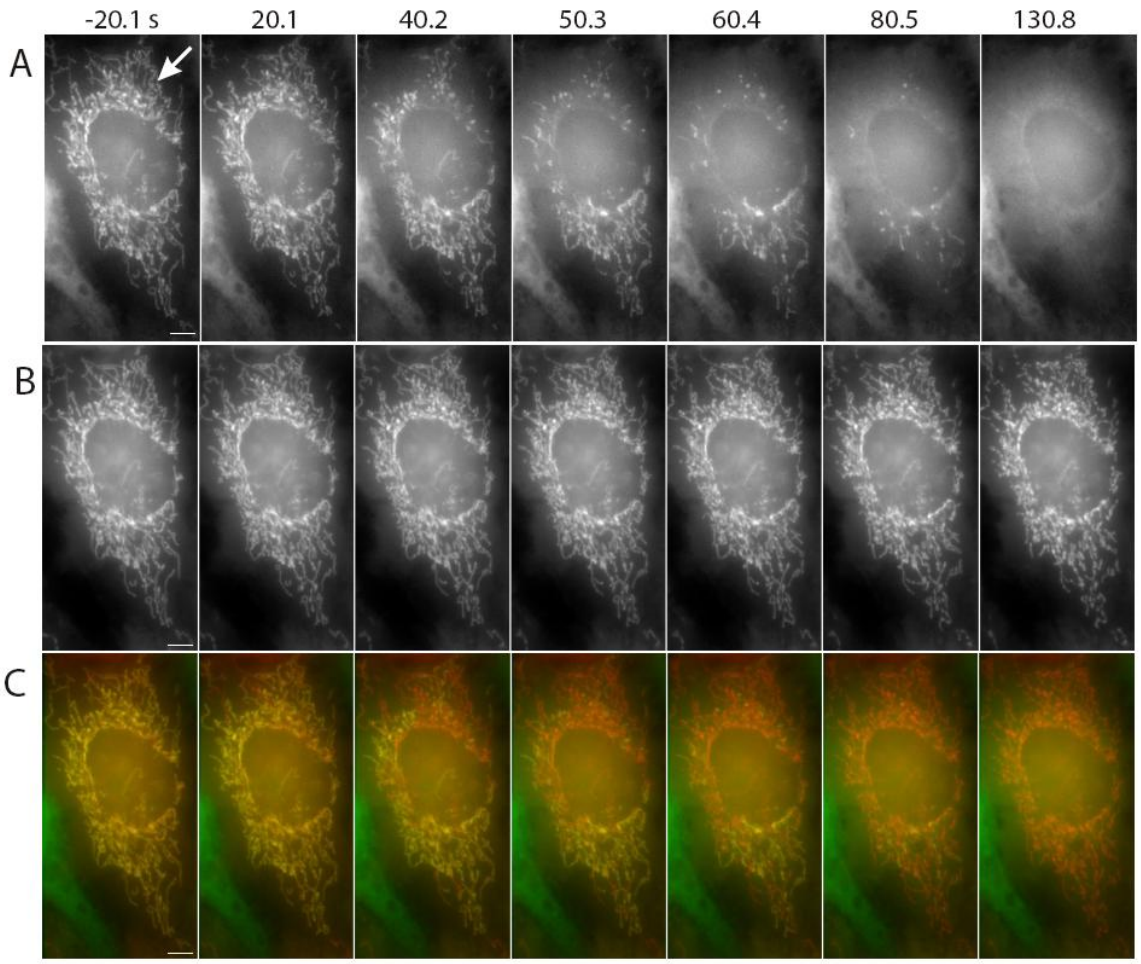


**Figure 38: Wave of cytochrome c GFP release in single cells. (A) Cytochrome c-GFP release shows a spatial pattern of release initiating at the arrow and progressing to the bottom of the cell and back to the lower portion of the nucleus. (B) Mito-mCherry fluorescence does not change in this time. Note that mitochondrial fragmentation can be observed. (C) Overlay of the two images with cytochrome c-GFP in green and mito-mCherry in red. Time in seconds with t = 0 indicating the time of first detectable release**

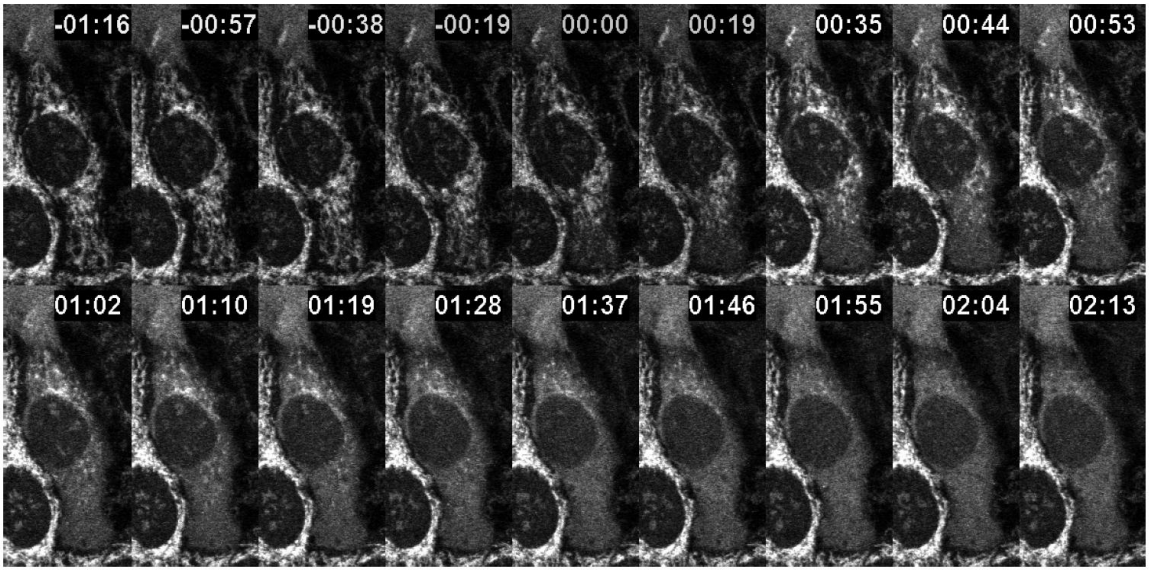


**Figure 39: Wave of cytochrome c-GFP release in HeLa cells using confocal microscopy. The top right shows a wave of release starting from the bottom and progressing to the top of the cell. Time in minutes:seconds.**

## *Quantification of Cytochrome c Release Waves*

The release of cytochrome c-GFP from mitochondria was quantified using the average intensity of GFP in regions of interest (ROIs) (Figure 40). Each ROI may contain more than one mitochondria because it was not always possible to discern individual mitochondrion in dense or out of focus regions of the cell. Therefore, the contents of ROIs are referred to as mitochondrial clusters. Most of the mitochondria in a cell were included within at least one ROI (Figure 40).

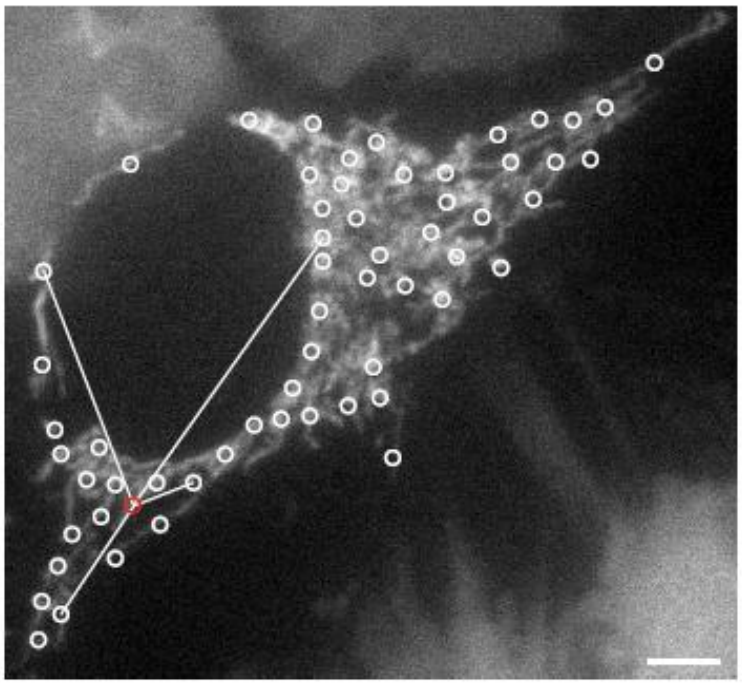

**Figure 40: A selected image before cytochrome c-GFP release demonstrating the ROI coverage. The circles represent the regions of interest (ROIs) chosen for analysis. The red circle is ROI in which the mitochondria released cytochrome c-GFP first. Therefore, the time of cytochrome c -GFP release from this region defined as t = 0 and all distance measurements are made relative to this region. The lines represent distance measurements from the first ROI to four other ROIs. This measurement is made for every ROI.**

In an individual ROI over time, the average intensity of the cytochrome c-GFP remained constant, then dropped to the local background level within 30 seconds (Figure 41A). In contrast, the mito-mCherry fluorescence remained at a constant level indicating that movement of the mitochondria out of the ROI is not responsible for the drop in

cytochrome c-GFP fluorescence (Figure 41A). In an individual cell, we observe that different ROI release cytochrome c-GFP at different times (Figure 41B for the cell shown in Figure 38).

To quantify the wave of release, we determined the first ROI in a cell to release cytochrome c (Figure 40, red ROI). The time of cytochrome c release from an ROI was defined as the point when the average intensity of the ROI began to decline irreversibly (for example see Figure 41C). The time of release from the first ROI was set to t=0 seconds, and all time measurements were made relative to this ROI. We next calculated the distances between the first ROI to release cytochrome c, and all other ROIs (see white lines in Figure 40). Finally, to represent the wave, we plotted the distance from the first ROI that released cytochrome c-GFP as a function of the time of ROI release (Figure 41D). A correlation plot of the distance of release as a function of the time of release for the cell shown in Figure 40 revealed a linear relationship indicating the wave like nature of cytochrome c release (Figure 41D).

**Figure 41: Quantification of cytochrome c-GFP release in a single cell. (A) The normalized intensity for one ROI versus time for both cytochrome c-GFP (black +) and mito-mCherry (gray ×). (B) Graph of cytochrome c-GFP loss from four separate regions. (C) The normalized cytochrome c-GFP intensity vs. time for an individual ROI. The black arrow indicates the time point selected as the release of cytochrome c-GFP. This point is selected because the fluorescence intensity declines irreversibly. The grey arrow indicates a point of decline which is not selected as the time of release because of the subsequent recovery. (D) Plot showing the distance of ROIs from the first ROI to release cytochrome c as a function of time of release (t=0 seconds for the first ROI to release cytochrome c). This plot corresponds to the cell shown in Figure 40.**

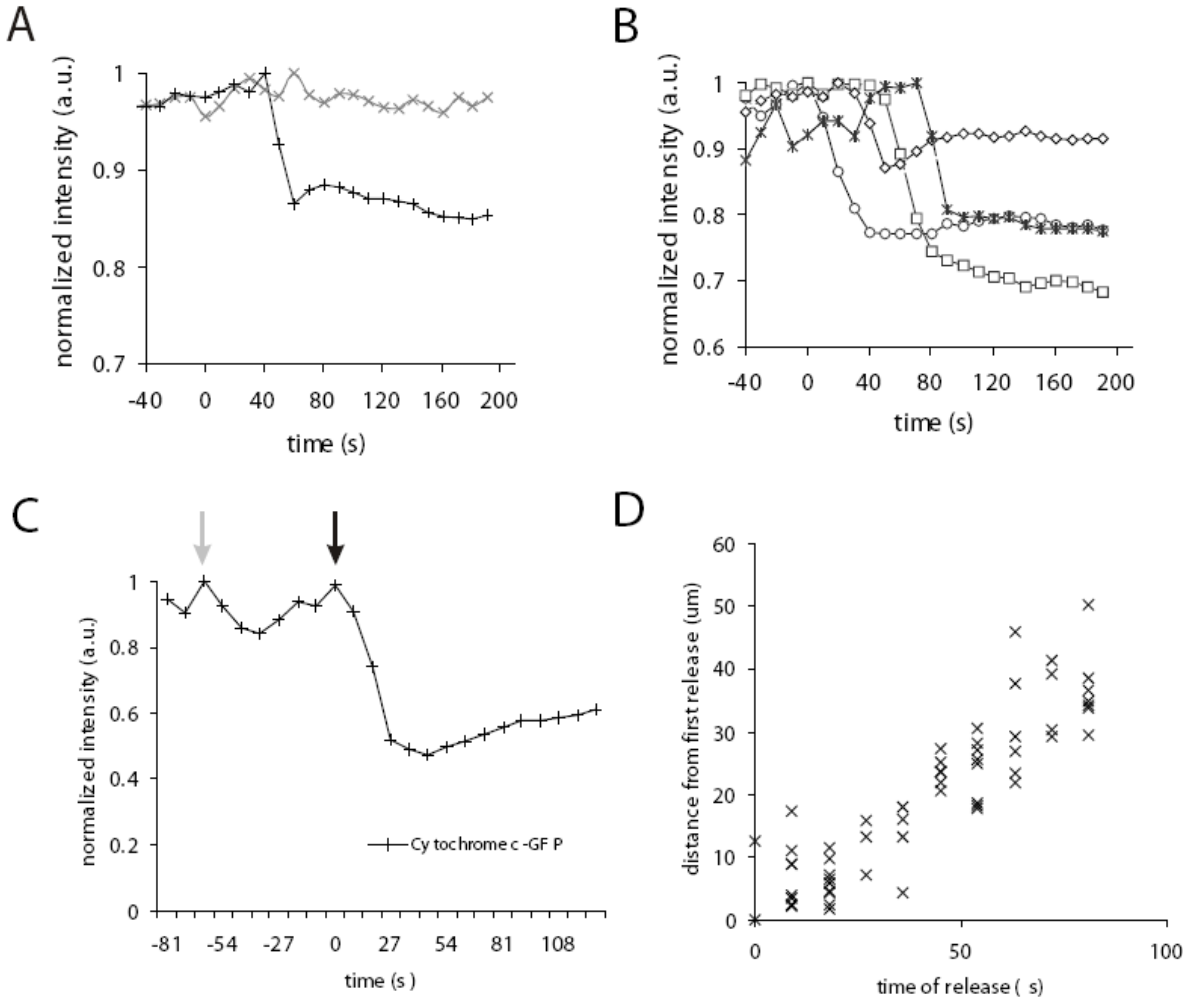
A
normalized intensity (a.u.)
1
0.9
0.8
0.7
-40
0
40
80
120
160
200
time (s)
B
normalized intensity (a.u.)
1
0.9
0.8
0.7
0.6
-40
0
40
80
120
160
200
time (s)
C
normalized intensity (a.u.)
1
0.8
0.6
0.4
0.2
0
-81
-54
-27
0
27
54
81
108
time (s)
Cytochrome c-GFP
D
distance from first release (um)
60
50
40
30
20
10
0
0
50
100
time of release (s)

**Figure 41**

This analysis quantitatively shows that cell-wide release of cytochrome c-GFP from mitochondria occurs as a propagating wave. To determine whether the wave of cytochrome c release is specific to a single mode of apoptosis, we observed the dynamics of cytochrome c release for cells treated with different agents that trigger apoptosis. Similar results were observed when apoptosis was induced with the death receptor ligand TRAIL (1 μg/mL) (Figure 38), protein kinase inhibitor staurosporine (STS, 2μM) (Figure 42) or the DNA damage inducing drug etoposide (ETO, 50μM) (data not shown). The observation of the cytochrome c release wave in multiple modes of apoptosis indicates that the wave is a general sub-cellular feature of apoptosis.

### *Patterns of cytochrome c release*

In characterizing the release of cytochrome c, three different patterns of release were observed (Figure 42). The first pattern is a wave initiated at a single point with the release of cytochrome c propagating in one direction across the cell (Figure 42A,B). The second pattern is two waves initiated at different points each propagating simultaneously across the cell (Figure 42C,D). The majority of cells treated with STS or ETO, and approximately half of cells treated with TRAIL (1 μg/mL) had a directional (one or two point) pattern of release (Table 3). Waves initiating at one or two points were observed in cells of oblong and round morphologies, indicating that cell shape did not induce a significant bias to the mode of release (Figure 42A, 43).

The third pattern of release of cytochrome c did not appear to be spatially coordinated, though similar to the other patterns, the cell-wide release was complete within minutes (Figure 42E,F). This could result from a wave that initiates at the top of the cell, furthest from the cover slip, and propagates perpendicular to the imaging plane, or from multiple spatially coordinated waves initiated at several points in the cell for which we lack the spatial and temporal sensitivity to resolve, or simply indicate an uncoordinated release.

We observed all three patterns of cytochrome c release with TRAIL, STS or ETO induced apoptosis (Table 3), indicating that the spatial patterns of release are not restricted to a single apoptotic paradigm. Furthermore, the wave of cytochrome c release was also observed in murine melanoma B16F0 cells (data not shown), demonstrating that the wave phenomena is not restricted to a single cell line. The release of cytochrome c in a wave that occurs at one, two or multiple points in the cell indicates that the initial trigger of the cytochrome c release wave can occur independently at multiple spatially distinct points in the cells. This indicates that the biochemical precursor of cytochrome c release is not a homogenous event within the cell, and instead is an accumulation of activated factors at spatially localize points in the cell.

**Figure 42: Spatial patterns of cytochrome c release. (A) Release initiating from one point in the cell. Release begins at the top of the cell and progresses down along the cell. (B) Distance correlation plot of the cell in A shows a linear relation. (C) Release initiating at two points in the cell. Release begins at the bottom of the cell, and also at the top of the cell. (D) Quantification of the release indicates two distinct linear relations consistent with two points of release. (E) Release that does not show a spatial pattern. (F) Quantification of the release in E.**

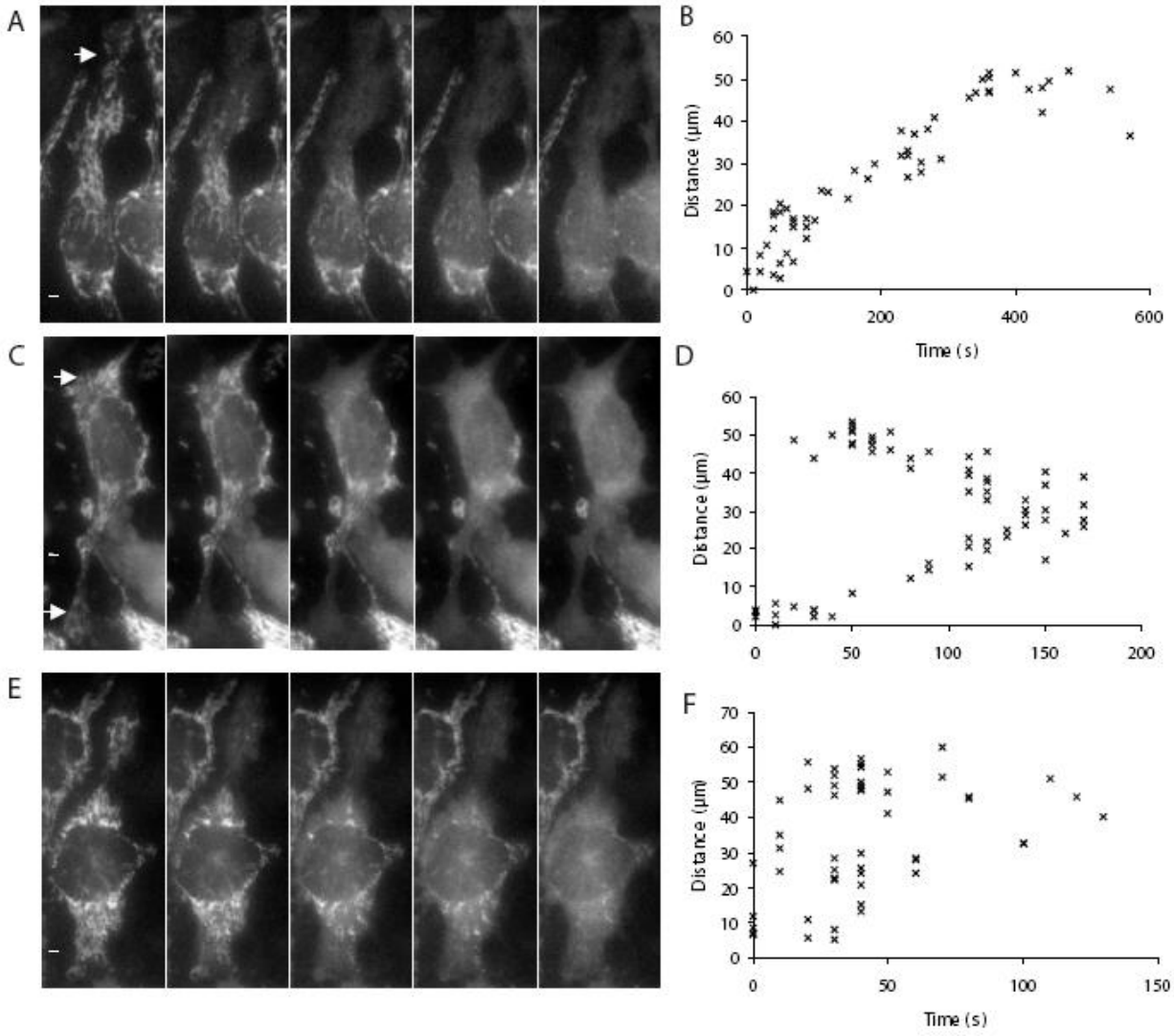
A
B
C
D
E
F
Distance (µm)
Time (s)
0
10
20
30
40
50
60
70
0
50
100
150
200
400
600

**Figure 42**

**Table 3: Different patterns of cytochrome c release in response to different stimuli**

| | Etoposide (n=10) | | Staurosporine (n=12) | | TRAIL (n= 20) | |
|---|---|---|---|---|---|---|
| | Number of cells | Total release time (sec) | Number of cells | Total release time (sec) | Number of cells | Total release time (sec) |
| **One Point** | 7 | 187 ± 95 | 4 | 306 ± 207 | 7 | 94 ± 34 |
| **Two Point** | 0 | - | 5 | 350 ± 93 | 2 | 115 ± 7 |
| **Random** | 3 | 66 ± 40 | 3 | 163 ± 35 | 11 | 62 ± 27 |
| **Total** | 10 | 151 ± 93 | 12 | 285 ± 154 | 20 | 79 ± 34 |

### *Dynamics of Loss of ΔΨm and Cytochrome c Release*

We next investigated the spatial and temporal relationships between events thought to be coincident with, or mechanistically linked to, cytochrome c release (Munoz-Pinedo et al., 2006). We first observed the dynamics of cytochrome c release relative to the loss of mitochondrial inner membrane potential ($\Delta\Psi_m$) as monitored by tetramethylrhodamine ethyl ester (TMRE). TMRE preferentially accumulates in actively respiring mitochondria (Ehrenberg et al., 1988), and during apoptosis TMRE is lost from the mitochondria at the same time as cytochrome c (Munoz-Pinedo et al., 2006). Although TMRE loss is temporally proximal to the release of cytochrome c, it has been observed that the pan-caspase inhibitor zVAD-fmk can delay the loss of TMRE relative to cytochrome c GFP (Goldstein et al., 2000).

HeLa cells were transfected with cytochrome c-GFP and loaded with TMRE. When these cells were treated with TRAIL (1 μg/mL), we observed that the

release of cytochrome c-GFP from the mitochondria preceded the loss of $\Delta\Psi_m$ (Figure 43A). Furthermore, the loss of $\Delta\Psi_m$ followed the same spatial patterns as cytochrome c release within the cell, though lagging in time (Figure 43A). This time delay was quantified monitoring cytochrome c release and TMRE loss from a single ROI (Figure 43B).

To demonstrate the lag between TMRE loss and cytochrome c release for the cell shown in Figure 43A, we plotted the correlation between distance from the first ROI to release and the time of release for both cytochrome c release and of TMRE loss (Figure 43C). This shows that TMRE has a similar distance-time release plot that differs in that it is shifted in the time axis. Furthermore, a correlation between the time of TMRE loss and cytochrome c release in this cell shows that TMRE loss occurs after cytochrome c release (Figure 43D). Finally, in 5 cells with a total of 150 ROI, we found that 146 of 150 ROI studied released cytochrome c-GFP before $\Delta\Psi_m$ loss (Figure 43E). The average time between cytochrome c release and $\Delta\Psi_m$ loss in TRAIL treated cells was 90 ± 42 seconds (Figure 43E), demonstrating that loss of $\Delta\Psi_m$ is not necessary for and does not occur before cytochrome c release. Note that 2.7% (4 of 150) of ROI show that TMRE loss occurs before cytochrome c release. This may result from an error in determining the time at which fluorescence irreversibly decreases in an ROI. These results demonstrate that cytochrome c is released from mitochondria before membrane potential is lost. Unlike previous reports, these experiments were conducted in the absence of biochemical inhibitors (Goldstein et al., 2000; Munoz-Pinedo et al., 2006).

**Figure 43: Mitochondrial release and loss of TMRE. HeLa cells treated with 2μM of STS. (A) Release of cytochrome c proceeds from left to right around the nucleus (top panel). TMRE loss occurs in approximately the same pattern but lagging in time (lower panel). (*B*) The average intensity in a single ROI of cytochrome *c*-GFP (*black* +) and TMRE (*gray* ×) versus time. (*C*) Correlation plot of distance of cytochrome *c*-GFP release and TMRE loss as a function of time. (*D*) Correlation of the time of cytochrome *c*-GFP release and the loss of potential for all regions. Gray line indicates simultaneity. (E) Histogram of the time difference between cytochrome c release and TMRE loss for 150 ROI in 5 HeLa cells treated with TRAIL (positive values indicate that cytochrome c is released before TMRE loss). The average release difference is 90 ± 42 seconds.**

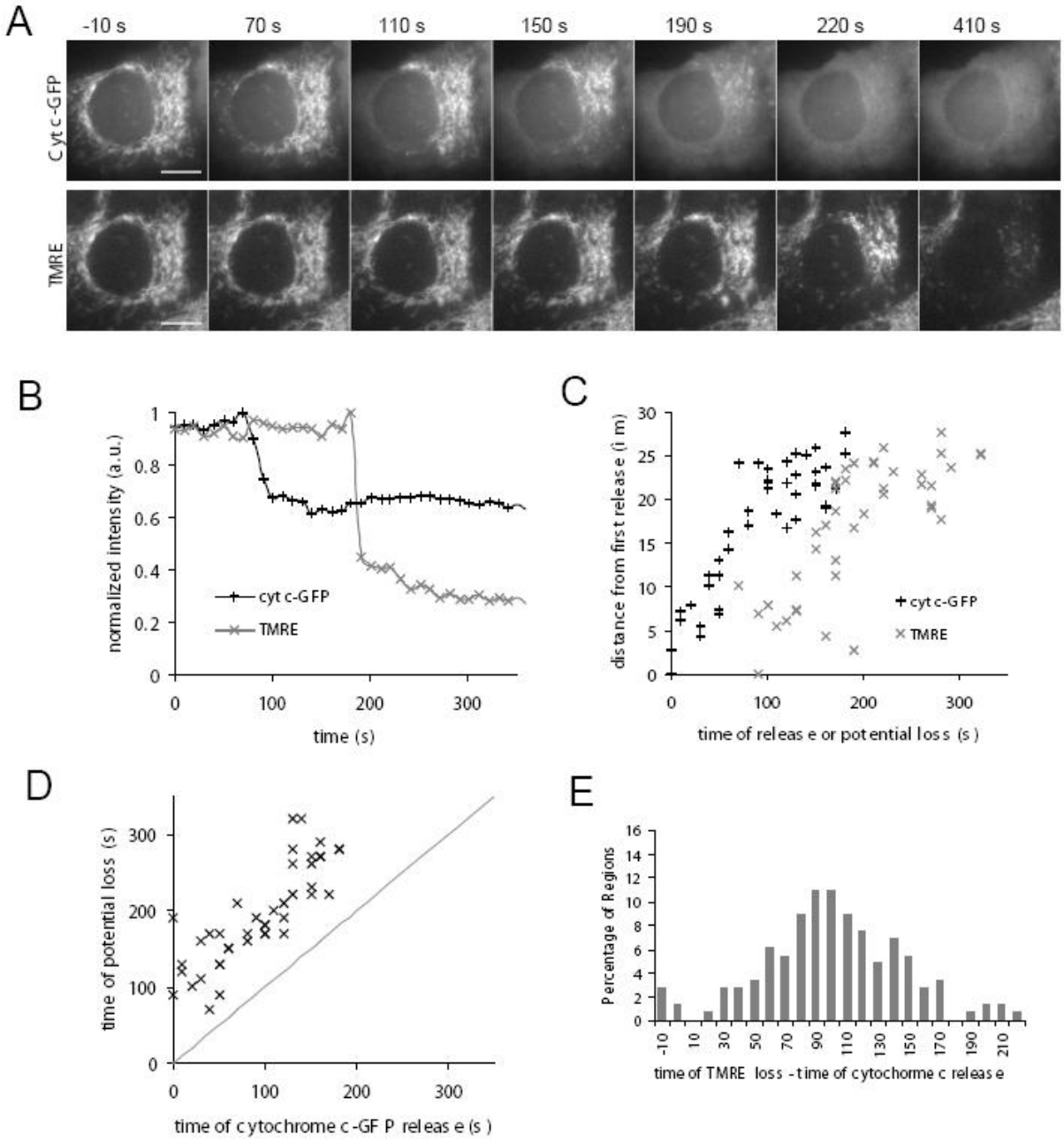
A
-10 s
70 s
110 s
150 s
190 s
220 s
410 s
Cyt c-GFP
TMRE
B
normalized intensity (a.u.)
cyt c-GFP
TMRE
time (s)
C
distance from first release (i m)
cyt c-GFP
TMRE
time of release or potential loss (s)
D
time of potential loss (s)
time of cytochrome c-GFP release (s)
E
Percentage of Regions
time of TMRE loss - time of cytochorme c release

**Figure 43**

### *Dynamics of Cytochrome c and Smac Release*

Next we observed the release of Smac, a mitochondrial protein that is released to the cytosol where it promotes apoptosis by inducing the degradation of the inhibitor of apoptosis proteins (IAPs) (Du et al., 2000; Verhagen et al., 2000). Previous work indicated that fluorescently-tagged Smac is simultaneously released with cytochrome c-GFP (Munoz-Pinedo et al., 2006). By simultaneously monitoring Smac-mCherry and cytochrome c-GFP at rates faster than previously published, we found that the release of Smac-mCherry followed the same spatial pattern as cytochrome c-GFP, but lagging in time (Figure 44).

We quantified the Smac delay using a similar analysis used to quantify the delay in TMRE loss (Figure 45). First we found that cytochrome c release preceded Smac release in a single ROI (Figure 45A). Next we plotted the distance of cytochrome c and Smac release as a function of time for the cell in Figure 44, and found that Smac release generally followed cytochrome c release (Figure 45B). This was also demonstrated by a correlation plot of the time of cytochrome c and Smac release (Figure 45C). Finally, by monitoring 312 ROI in 6 different cells, we found that Smac release followed cytochrome c-GFP release in 301 of 312 ROI with an average delay of 42 ± 29 seconds (Figure 45D). A few ROI (11 of 312; 3.5%) show that Smac is released before cytochrome c, which may result from an error of determining the time at which fluorescence irreversibly decreases in an ROI.

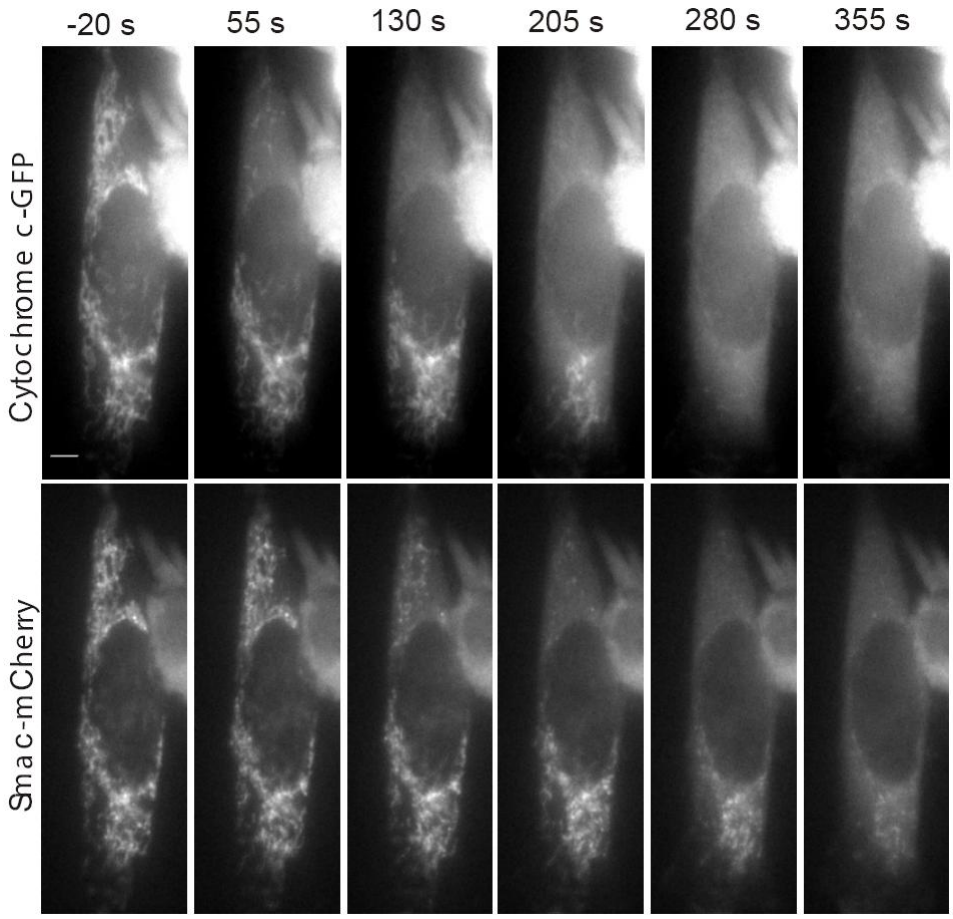


**Figure 44: Widefield time lapse images of cytochrome c-GFP release and Smac-mCherry release in the same cell. HeLa cells were treated with 2 μM of STS. Cytochrome c release starts at the top of the cells and propagates to the bottom of the cell. Smac release lags in time behind cytochrome c release, but follows a similar pattern.**

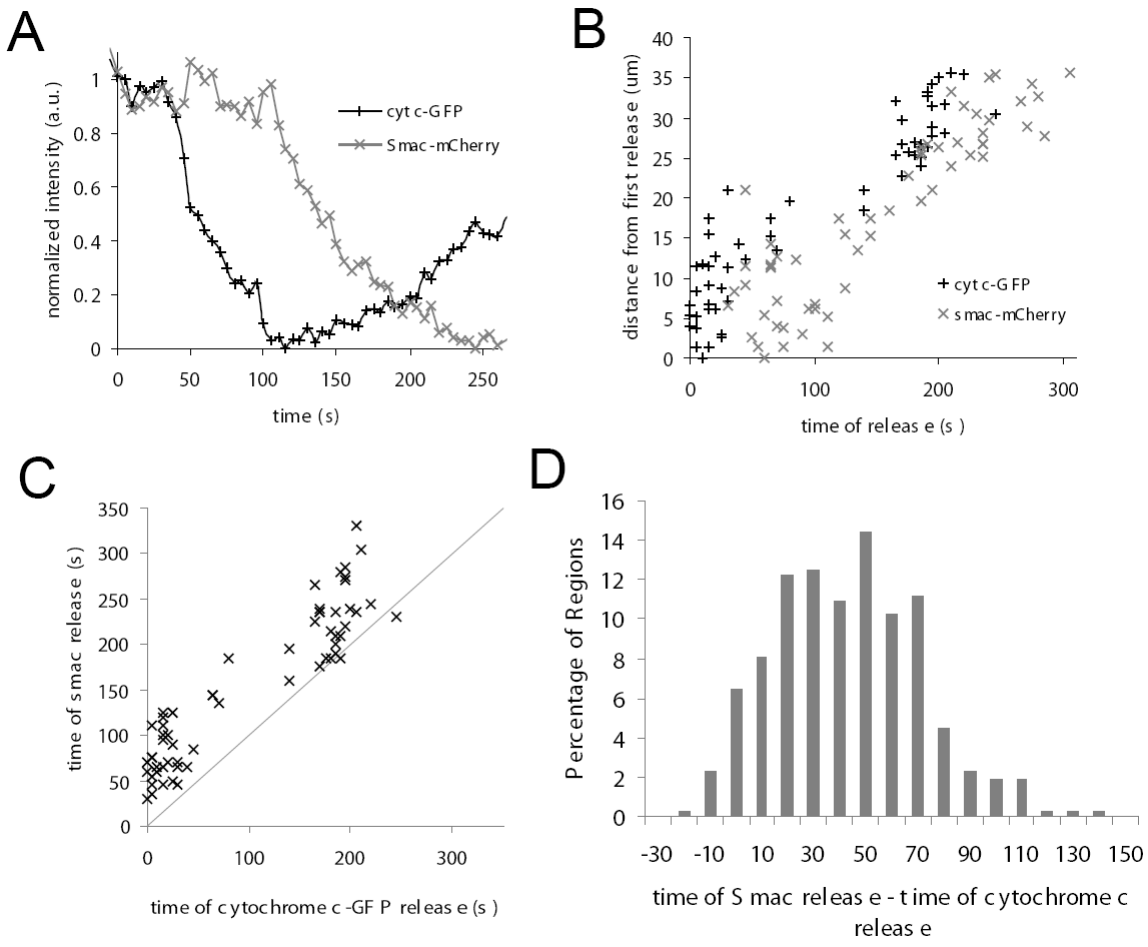


**Figure 45: Quantification of cytochrome c-GFP release and Smac-mCherry release in the same cell. HeLa cells were treated with 2 μM of STS. (A) The average intensity in a single ROI of cytochrome c-GFP (black +) and Smac-mCherry (gray ×) versus time. (B) Plot of cytochrome c-GFP release and Smac-mCherry release as a function of time. (C) Correlation of the time of cytochrome c-GFP release and the time of Smac-mCherry release for all regions. Dotted line indicates simultaneity. (D) Histogram of the time difference between cytochrome c release and Smac release for 312 ROI in 6 HeLa cells treated with TRAIL(positive values indicate that cytochrome c is released before Smac). The average release difference is 42 ± 28 seconds.**

We observe a delay between loss of $\Delta\Psi_m$ and Smac release, relative to cytochrome c release, and all three events occur in a similar spatial pattern. Although the release is distinct, the spatial and temporal similarity suggests that there is one underlying mechanism governing cytochrome c and Smac release and $\Delta\Psi_m$ loss from individual mitochondria. The delay observed between the Smac and cytochrome c waves could be a result of pores that preferentially release cytochrome c and then Smac. However, a delay could also be caused if Smac is oligomerized with itself or another protein (Du et al., 2000). The time between cytochrome c-GFP loss and loss of membrane potential could result from a delay associated with the breakdown of the electron transport chain, although there is evidence that loss of potential requires caspase activation (Goldstein et al., 2000; Goldstein et al., 2005).

### *Mitochondrial Fission*

We next investigated the temporal relationship between cytochrome c release and mitochondrial fission using the mitochondrial marker mito-mCherry (Figure 46). Mitochondrial fission proteins have been implicated in cytochrome c release during apoptosis (Suen et al., 2008; Frank et al., 2001; Karbowski et al., 2002). Furthermore, mitochondrial fragmentation is reported to occur simultaneously with, or within minutes of cytochrome c release (Karbowski et al., 2002).

To resolve the timing of these events, we first monitored individual mitochondria located primarily at the periphery of cells where there is lower spatial density of mitochondria. In HeLa cells treated with TRAIL (1μg/mL), we observed that cytochrome c-GFP was released prior to mitochondrial fission (24 mitochondria in 9 cells). A representative image of cytochrome c release and mitochondrial fission from a single mitochondria is shown in Figure 47.

Alterations in the mitochondrial morphology were observed in the time between cytochrome c release and prior to mitochondrial fission. The morphological alterations were characterized by the formation of multiple fluorescent aggregates with thinner intermediate connections (Figure 48A). These fluorescent aggregates and intermediate connections were quantified with a line scan of mitochondria (Figure 48B). The size, distribution, and duration of these aggregates varied between mitochondria (data not shown). In total we observed similar intermediate morphologies for 15 of 23 mitochondria observed.

The observation of alterations of mitochondrial morphology indicates that structural changes may precede complete mitochondria fission. These changes could be due to the restriction of mitochondria by proteins such as Fis1, and Drp1 (Karbowski et al., 2002) the formation of pores at the restriction sites (Kuwana et al., 2002) or the swelling of the inner membrane space (Sun et al., 2007).

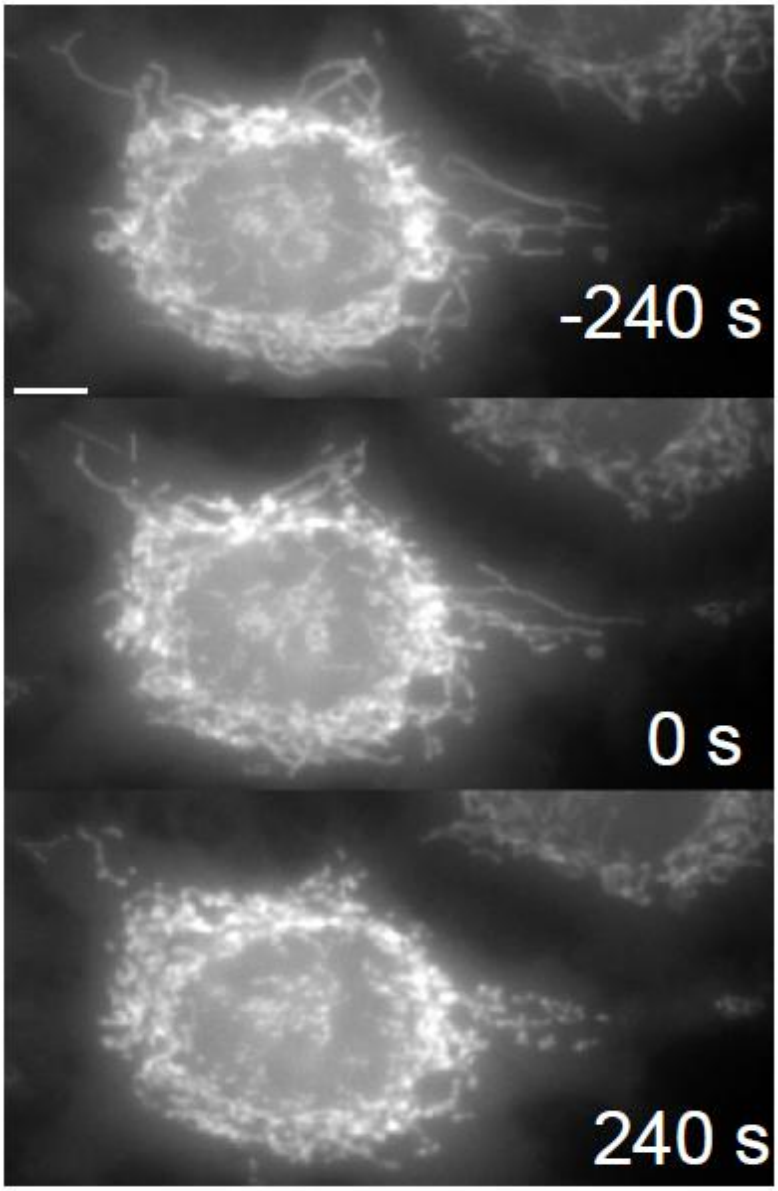


**Figure 46: Mitochondrial morphology before, during, and after cytochrome c-GFP release. Mito-mCherry showing mitochondrial morphology in a HeLa cell treated with TRAIL. Cytochrome c release began at t =0. Scale bar = 5µm**

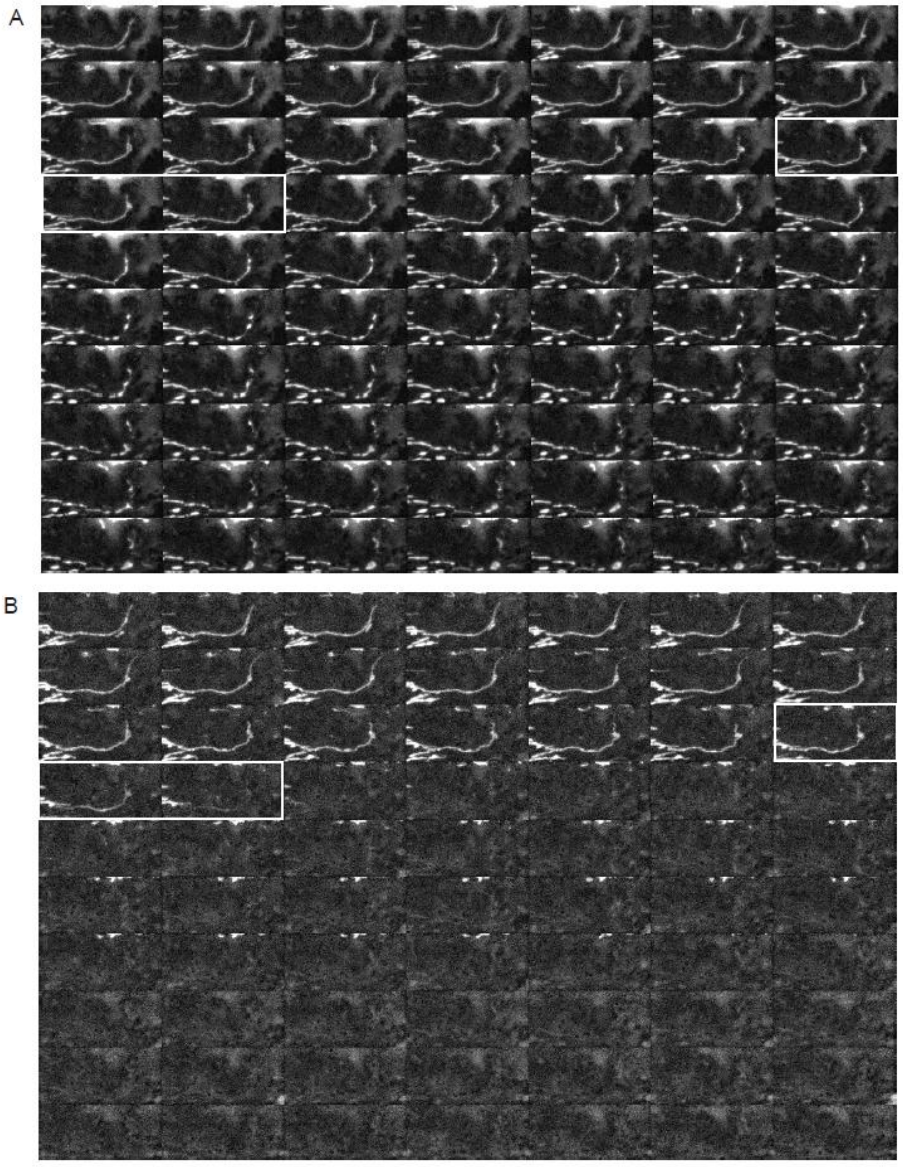


**Figure 47: Images of a single mitochondria undergoing cytochrome c release and mitochondrial fission. HeLa cells were transfected with (A) mito-mCherry and (B) cytochrome c-GFP and treated with 2μM of TRAIL. In white boxes are the frames where cytochrome c release is occurring. Images are taken every 5 seconds.**

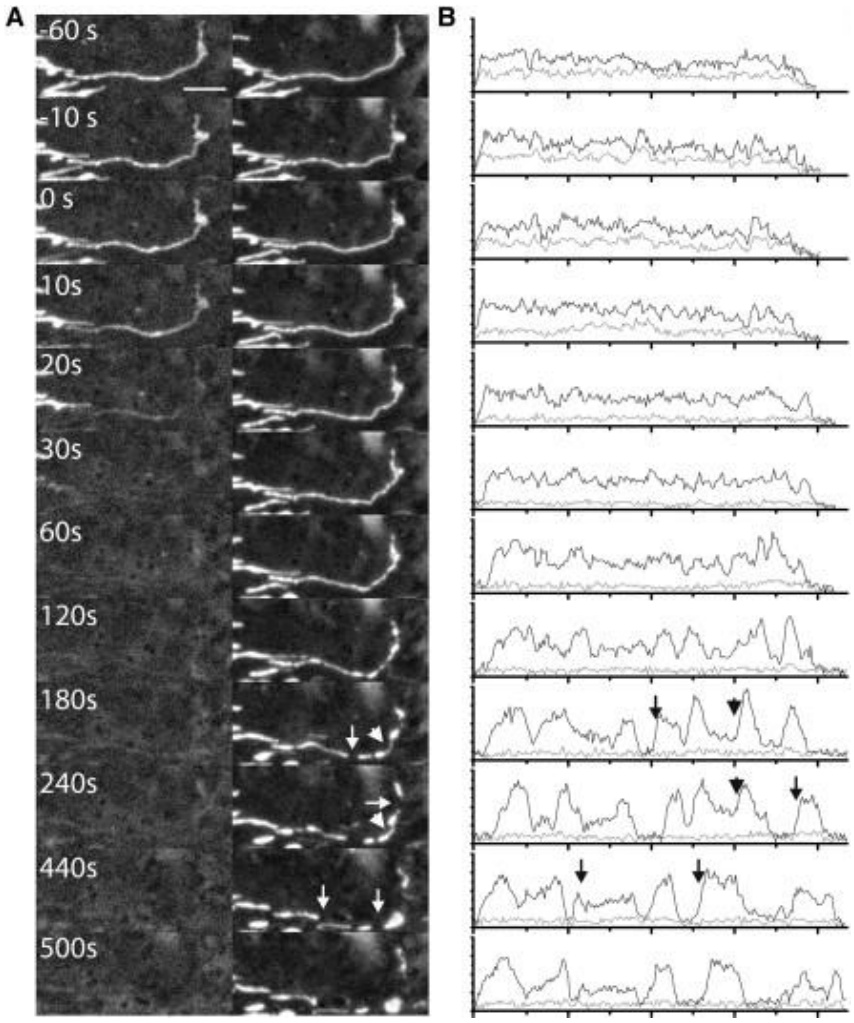


**Figure 48: Mitochondrial fission and release of cytochrome c from single mitochondria. HeLa cells transfected with cytochrome c-GFP and mito-mCherry, and treated with TRAIL. (A) Images of cytochrome c release and mitochondrial fission. Cytochrome c release begins at time t = 0. Arrows indicate sites of fission; arrowheads indicate sites of morphological changes. (B) Line scans of mitochondria from A with mito-mCherry in black and cytochrome c-GFP in gray. Arrows indicate corresponding positions of arrows on image.**

### *Release of Cytochrome c from individual mitochondria*

We imaged cytochrome c release from individual mitochondria to determine whether release occurred in a single step, as a two step process (Ott et al., 2002), or moved like a wave across each mitochondria. It has been shown that cytochrome c is localized to intra-cristae regions of the mitochondria with limited access to the intermembrane space (Scorrano et al., 2002). The release of cytochrome c from individual mitochondria is difficult to monitor because of the variable onset of apoptosis within single cells, and the rapid release of cytochrome c from individual mitochondria. Furthermore, the density of mitochondria makes it very difficult to discern individual mitochondria in wide field or confocal microscopy. To overcome the timing problem we imaged several single cells once every minute, and once cytochrome c was released in a single cell, we monitored adjacent cells once every ten seconds. These cells were then imaged every 10 seconds, until cytochrome c release was detected in single mitochondria and then we acquired images once every 400 ms.

For improved spatial resolution of individual mitochondria we imaged with total internal reflection microscopy (Axelrod, 1989), which illuminates only the very bottom of the cell within 200nm of the coverslip. This allows imaging of a subset of mitochondria with limited out of focus background fluorescence. Under these conditions we could monitor the cytochrome c-GFP throughout the length of the mitochondria (Figure 49A). Decrease in cytochrome c-GFP fluorescence appeared to initiate at the

same time through the entire mitochondria. A quantification of the fluorescence demonstrated that neither the time when cytochrome c release initiated nor the time course of release, were functions of the position along the mitochondria (Figure 49B).

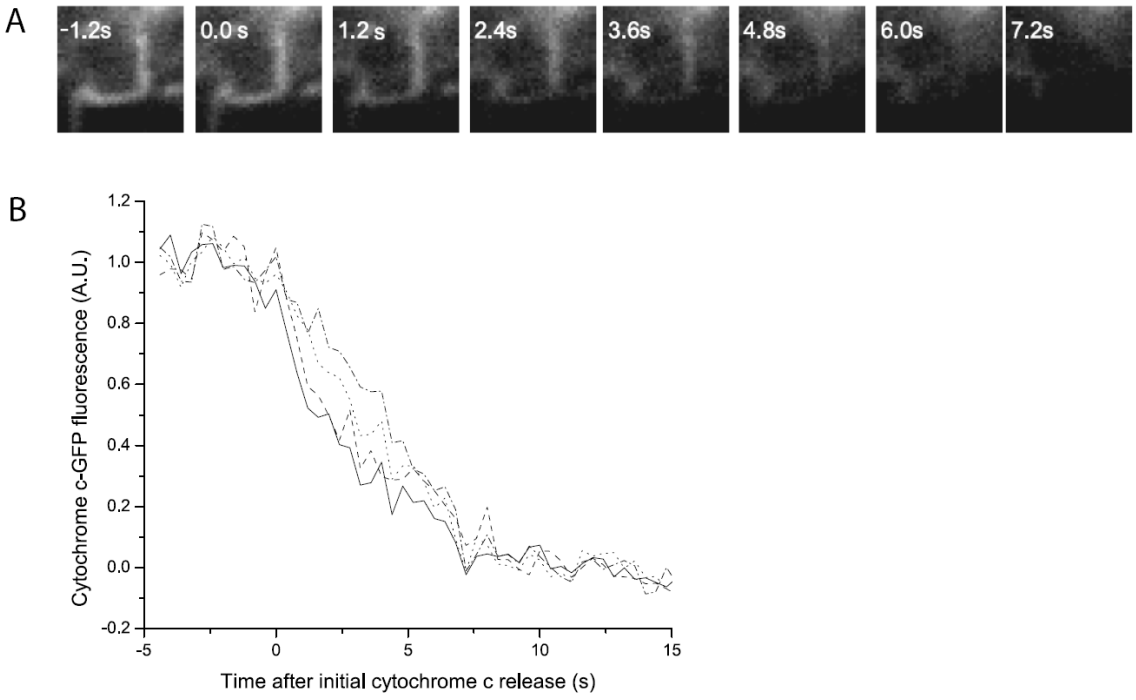


**Figure 49: (A) Release of cytochrome c-GFP from individual mitochondria as revealed by TIR microscopy. Cytochrome c release begins at time t = 0. (B) Quantification of cytochrome c release from different regions of the single mitochondria in A. Release appears to initiate at the same time throughout the mitochondria. Scale bars represent 5 μm.**

### *Inhibition of cytochrome c Release Wave*

The spatial waves of release illustrate that cytochrome c is not simultaneously released from all mitochondria in a single cell. Potential mechanisms to explain the spatial coordination of cytochrome c release include local activation of a precursor to release and a feed-forward loop that amplifies the initial loss of mitochondrial proteins. There is evidence suggesting a link between cytochrome c release, inositol 1,4,5 triphosphate receptor ($IP_3R$), and ER calcium stores (Boehning et al., 2005; Boehning et al., 2003). This potential role for calcium is consistent with the ability of the Bcl-2 family to modulate cellular calcium levels (Foyouzi-Youssefi et al., 2000; Palmer et al., 2004; Scorrano et al., 2003), as well as the observation of calcium waves in apoptotic cells (Pacher and Hajnoczky, 2001; Szabadkai et al., 2004).

We tested the effects of reducing the cytosolic calcium with BAPTA-AM and depleting ER calcium with thapsigargin (Palmer et al., 2004) on the spatial and temporal characteristics of cytochrome c release. HeLa cells expressing cytochrome c-GFP were treated with TRAIL (1 μg/mL) to induce apoptosis in the presence of extracellular EGTA (1.2mM). Once one cell in the field released cytochrome c, BAPTA-AM (1mM) was added to the bath. Calcium levels were stably reduced within 5 minutes of BAPTA-AM addition to media (data not shown). The time for 95% of the ROIs in a cell to release cytochrome c-GFP increased slightly from 112 ± 31 seconds for cells treated with TRAIL and EGTA, to 153 ± 49 seconds ($p=0.025$) for cells treated with BAPTA-AM (Figure

50A). There was a negligible change in the fraction of cells with a directional release (from 0.50 to 0.57, Figure 50B). The effects of thapsigargin (5μM), were larger in magnitude and significance. The time for a cell to release cytochrome c increased over four fold (112 ± 31 sec to 511 ± 245 sec, $p=2.2*10^{-6}$, Figure 50A) in cells that were treated with thapsigargin. Additionally, thapsigargin reduced the fraction of cells showing directional release patterns from 0.5 to 0.053) (Fig. 48B). Thus thapsigargin both disrupted the spatial wave of cytochrome c release and increased the duration of release by more than 6 minutes.

***Summary***

In this chapter, we described the spatial coordination of cytochrome *c* release, Smac release, and loss of $\Delta\Psi_m$. We observed that cytochrome c release occurs in a wave that can initiate from one point in the cell, two points in the cell, or randomly through the cell (Figure 42). The spatial wave of release could be observed with staurosporine, TRAIL and etoposide indicating that this is a phenomena that occurs in different modes of apoptosis. Smac release and loss of $\Delta\Psi_m$ lagged in time behind cytochrome c release. However, in single cells, Smac release, and loss of $\Delta\Psi_m$ exhibited the same spatial pattern as cytochrome *c* release (Figures 43, 45). Finally, we observed that mitochondria underwent fission after cytochrome *c* release (Figure 48). The wave of cytochrome *c* release was inhibited by treatment with thapsigargin (Figure 50).

**Figure 50: Thapsigargin, but not BAPTA, disrupts the wave of cytochrome *c* release. HeLa cells in 1.2 mM EGTA undergoing TRAIL-mediated apoptosis were treated with 1 mM BAPTA-AM (BAPTA) or 5 $\mu$M thapsigargin. (*A*) Duration of cytochrome *c* release (95% of all ROIs released). Thapsigargin increased the duration of release ($p = 2.2 \times 10^{-6}$), whereas BAPTA did not ($p = 0.025$). Thapsigargin, but not BAPTA, disrupts the wave of cytochrome c release. HeLa cells in 1.2 mM EGTA undergoing TRAIL-mediated apoptosis were treated with 1 mM BAPTA-AM (BAPTA) or 5 μM thapsigargin. (*B*) Bar graph showing the fraction of cells with directional release. Numbers indicate (directionally releasing cells)/(total cells).**

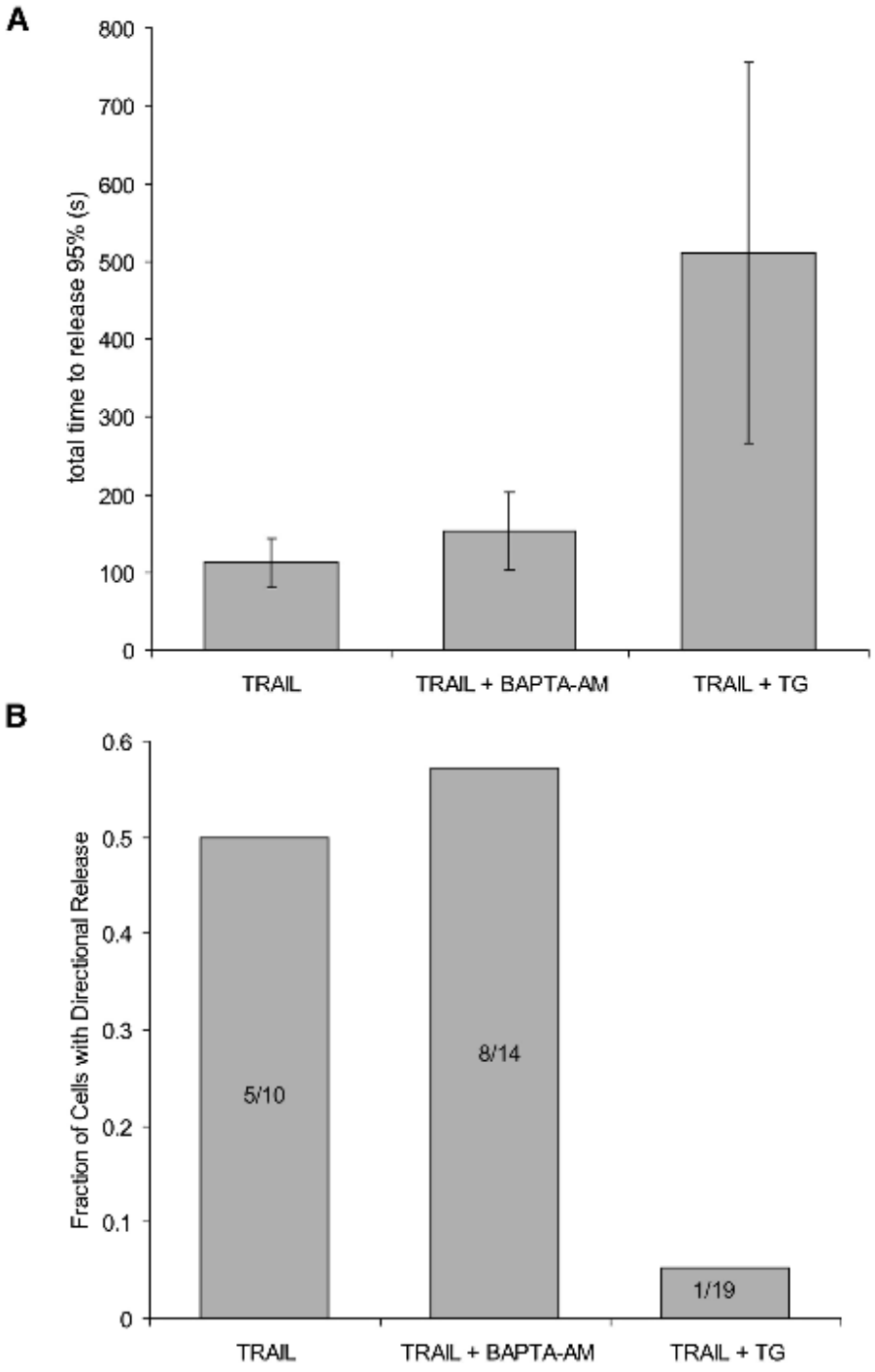
A
800
700
600
500
400
300
200
100
0
total time to release 95% (s)
TRAIL
TRAIL + BAPTA-AM
TRAIL + TG
B
0.6
0.5
0.4
0.3
0.2
0.1
0
Fraction of Cells with Directional Release
5/10
8/14
1/19
TRAIL
TRAIL + BAPTA-AM
TRAIL + TG

**Figure 50**

# Chapter Five: Conclusions and Future Directions

In this thesis we described the development of two new reporters for monitoring caspase activation in single cells (Chapter Two). This reporter was expressed in a population of cells where we observed a similarity in the time of caspase activation of related cells relative to the overall population (Chapter Three). This similarity in apoptosis timing was used to monitor mitochondrial apoptotic events in single cells with high temporal resolution where we observed the spatial pattern of cytochrome c release (Chapter Four). Below we discuss the implications of this work, and potential future directions.

## *Caspase Reporter*

The designed reporters (erDEVD and pmDEVD) relocalize from one organelle to another after caspase activation. The pmDEVD reporter consists of a single fluorophore which is relocalized from the plasma membrane to the cytosol after the activation of the caspases, and the erDEVD reporter relocalizes from the ER to the nucleus after caspase activation. On the basis of signal strength and kinetic properties the pmDEVD reporter is

comparable to or better than other genetically encoded caspase reporters (FRET, pCaspase-3, and erDEVD). Importantly, the reporter uses only a single fluorophore which enables simultaneous use of the pmDEVD reporter along with probes for other processes. Here, we were able to simultaneously monitor other events such as the cell cycle and cytochrome c release. Finally we determined that the expression of the pmDEVD reporter does not have an effect on the kinetics of downstream steps of apoptosis such as TUNEL staining.

The relocalization reporters can be modified to other proteases such as granzymes or initiator caspases by modifying the cleavage domain (Thornberry et al., 1997). This is potentially difficult owing to overlapping substrate specificities and low levels proteolytic activity in weaker proteases (such as the initiator caspases). To improve the reporter signal for detection of weaker proteases future modifications might include co-translational targeting to the plasma membrane, and the addition of a nuclear localization signal. This would aggregate the cleaved fluorophores in the nucleus which would be more easily detectable than if the reporter is localized to just the cytoplasm. Furthermore, to aid in the detection of weaker caspases, it may be useful to fuse protein-protein interaction domains such as CARD (for the detection of caspase-9) or DED domains (for the detection of caspase-8) to these reporters to help localize these weaker caspases to the reporter.

## *Sister Cell Apoptosis*

We observe that sister cells undergo activation of caspase-3/7 at similar times relative to the population. This similarity could not be correlated to the position of cells in the cell cycle, nor to the distance between cells. By investigating the similarity of apoptosis susceptibility over subsequent generations, we observe a divergence in the times of apoptosis as cells are more unrelated. A divergence in apoptosis susceptibility is also observed within single generations and is limited by blocking protein synthesis after division. These results suggest that the signal transduction in response to apoptotic stimuli reflects the internal state of the cell and therefore is deterministic.

### *Overview of variability*

A precise apoptotic response might be expected given its importance in executing developmental programs or ensuring destruction of aberrant cells. However, the time when a cell irreversibly commits to apoptosis can vary from 1 hour to over 20 hours depending on the type and strength of the apoptotic stimulus (Goldstein et al., 2000). Variability of cell fate decisions in clonally identical populations is also observed in phage lambda infection (Arkin et al., 1998), bacterial chemotaxis (Spudich and Koshland, Jr., 1976), cell differentiation (Abkowitz et al., 1996; Enver et al., 1998), and HIV-1 Tat transactivation (Weinberger et al., 2005). While phenotypic variability can be beneficial in certain scenarios such as in stress responses or environmental fluctuations (Kussell and

Leibler, 2005) it also imposes limits on the precise control of cellular fate. In the context of apoptosis, variability can be resolved into two components: a stochasticity in how biochemical signals are transduced after drug treatment, or a population-level heterogeneity of cellular factors (Kaern et al., 2005). It is difficult to experimentally resolve contributions of the different components owing to an inability to precisely replicate the biological conditions of a single cell.

*Entry into apoptosis is similar for cells in proximity*

When studying the times of apoptosis in a population, we noticed that the times for neighboring cells to enter apoptosis were highly correlated relative to more distant cells (Figure 14). One potential explanation for such a correlation would be secreted factors, which have been demonstrated to play a significant role in apoptosis. However, three independent tests demonstrated that there was no correlation between when caspases were activated and the physical distances between unrelated cells (Figures 23-26). Thus, the secreted factors may either be acting only on the secreting cell itself or on the culture as a whole, but not affecting the local microenvironment. Therefore while secreted factors play a role in the apoptosis decision, they may not be the underlying source of cell-cell variability.

Depending on the method of inducing apoptosis, previous work reported a correlation between apoptosis and the cell cycle (Stacey et al., 2000), or a lack of

correlation (Hueber et al., 1998; Cohen et al., 2008). Since recently divided cells both tend to be near each other and tend to be synchronized in the cell cycle, this might also account for the "local synchronization". This was tested with two different assays: Apoptosis was induced in a cell cycle synchronized population (double thymidine block) (Figure 16) or apoptosis was induced in an asynchronous population where the cell cycle phase was determined using a live cell reporter (Figure 20). In both assays there was no detectable correlation between cell cycle and apoptosis. .

*Entry into apoptosis is similar for related cells*

When neighboring cells were categorized into sister cells, cousins or unrelated cells, sister cells showed the greatest similarity for the time of entering apoptosis (Figure 26). Apoptosis times of sister cells are most similar right after division, and this similarity decreases over time (Figure 34). When weaker apoptotic insults were used we found that not only was the timing of apoptosis correlated for sister cells, but also the probably of apoptosing. Thus, fates were linked in sister cells (Figure 29) Although phenotypic similarities between sister cells have been shown with respect to the duration of the cell cycle (Dover and Potten, 1988; Nasmyth et al., 1979), and in some cases cell migration (Albrecht-Buehler, 1977) to our knowledge, this has not been shown with respect to apoptosis nor for any cellular phenotype in response to an exogenous trigger.

*Determinism in Apoptosis Signal Transduction*

The similarity of apoptosis times and the apoptotic fate of sister cells suggest that the time of apoptosis, and the fate of a single cell in response to an apoptosis stimulus is predictable. This predictability of apoptotic signal transduction suggests that cells which undergo apoptosis at a later time relative to the population may have molecular compositions that make the cell less susceptible to apoptosis, and do not result from stochastic events in apoptosis signal transduction.

While the difference in apoptosis time between sister cells is much smaller than expected if the entry to apoptosis was completely stochastic, the apoptosis times of sister cells was not identical (Figure 28). One explanation is that the biochemical signal transduction in response to apoptotic stimuli may have some stochastic steps. Alternatively, the dilution of factors during division may not be symmetric, or the molecular composition of daughter cells may diverge after division. The latter explanation is consistent results showing that as cells spend more time apart, their difference in caspase activation increases (Figure 34).

*Divergence of Apoptotic Susceptibility*

Sister and cousin cells underwent apoptosis at similar times but as cells became more distantly related, the difference in their times of apoptosis increased (Figure 32, 34). This divergence of apoptotic fate was observed to occur over a few generations,

suggesting that the molecular composition of the cell which predisposes cells to apoptosis is transient. A similar influence of lineage on phenotypic behavior is seen in the switching times of *S. cerevisiae* that were engineered to switch between galactose metabolizing and non-metabolizing states (Kaufmann et al., 2007).

Our results are reminiscent of prior results on the variability of gene expression in a lineage of mammalian cells (Sigal et al., 2006b). Sigal et al. calculated the kinetics and genealogical time over when the gene expression levels in a cell lineage reach the different expression levels found in the population. Our results build upon the demonstration of divergence in gene expression, to show a divergence of phenotype within a lineage. Strikingly, our half-time of divergence of the apoptosis response is on a similar scale as divergence in the gene expression study, thus suggesting that the divergence of gene expression levels in mammalian cells has a phenotypic consequence (Newman and Weissman, 2006).

*Divergence from New Protein Synthesis*

The similarity in apoptosis time between sister cells is observed for three distinct apoptosis inducing drugs (STS, TNFα, and ETO) and in different cell lines and in non-immortalized MEFs. This indicates that the mechanism generating diversity and persistence of the apoptotic state could be a few proteins common to the different apoptosis drugs, or could be a global mechanism affecting all proteins of which variation

in apoptosis signaling is only one consequence. The intragenerational variation in the apoptosis susceptibility could result from a gradual change in the cellular components which could reflect increasing differences in gene expression. Notably, Sigal et al. reported that variation in gene expression was found for distinct classes of proteins (Sigal et al., 2006b).

The divergence of apoptosis times of sister cells was inhibited by blocking protein synthesis after division, suggesting that variation in apoptosis is in part a result of a variation in protein synthesis just after division. Other molecular changes may contribute including the degradation of proteins, the post-translational modifications of proteins, and the localization of proteins. We propose that if the molecular composition of the cell, and the underlying biochemical network used to process apoptotic triggers is similar between sister cells at the time of treatment, the apoptosis times will be similar. However as the molecular composition of cells start to drift apart, so does the apoptotic response. Thus, while the biochemical reactions triggered by an apoptotic signal may be deterministic, the reactions that determine the molecular composition of the cell prior to the addition of an apoptosis drug may not be.

An understanding of the mechanisms of apoptosis will be aided by the development of techniques to monitor the expression and activity of different apoptotic proteins in single cells. Such reporters can be used along with the developed pmDEVD reporter, which uses only a single fluorophore, to correlate the times of reporter activation to time of caspase activation. This will help elucidate both the timing of events

and the determination of whether the variability between cells is the result of a specific apoptotic stage or of small variations in multiple stages.

Broadly, these results highlight the benefits of single cell assays in addition to monitoring population phenotypes. In a population, there is a substantial distribution in the onset of apoptosis. This is not just a stochastic transduction of an apoptotic signal, but a difference resulting from population heterogeneity. The determinism of signal transduction in single cells should enable the observation of processes that are too rapid to be continuously imaged such as cytochrome c or Smac release (Chapter Four). This can be potentially done by waiting for a cell to undergo apoptosis at low imaging frequency, then imaging its sister cell, or related cells at a higher frequency. The symmetry of division reproduces underlying biochemical networks that cells use to respond to external triggers. Exploiting this symmetry by comparing responses in sister cells enables an understanding of the reproducibility of the response of these signaling networks, and how biochemical signals are transduced. It remains to be seen whether this similarity extends to other phenotypes, and whether it extends to phenotypes in vivo.

## *Cytochrome c Release*

Rapid imaging during apoptosis revealed a spatial coordination of cytochrome *c* release, Smac release, and loss of $\Delta\Psi_m$. Three spatial patterns of cytochrome *c* release were observed: waves initiating at one or two points in the cell, and an apparent random

release. The release of Smac and loss of $\Delta\Psi_m$ exhibited a spatial pattern similar to that of cytochrome *c* release. Only one temporal pattern was observed: first, the mitochondria lost cytochrome *c* and then they lost Smac, which was followed by the loss of mitochondrial energetics, as assayed by the $\Delta\Psi_m$. The mitochondria underwent fission after cytochrome *c* release. The wave of cytochrome *c* release was inhibited by treatment with thapsigargin.

*Waves of cytochrome c release*

The cell-wide release of cytochrome *c*-GFP was previously observed to occur in an all-or-none manner (Goldstein et al., 2000) and, more recently, in a wave propagating across single or fused cells (Lartigue et al., 2008). The existence of a wave suggests that the upstream trigger of cytochrome *c* release is spatially localized. Though the identity of the trigger is unknown, possible triggers include the members of the Bcl-2 family (Youle and Strasser, 2008) and the initiator caspases. Here, we observed waves initiating not only at a single point in a cell, but also at two spatially distinct points in a cell (Figure 42). This indicates that although the trigger initiating the wave of cytochrome *c* release is spatially localized, it can occur in multiple locations independently within a single cell. Therefore, although there may be multiple points for the initiating pro-apoptotic trigger within the cell, cytochrome *c*-GFP release is initiated only when the concentration or activity of the precursor crosses a threshold.

*Other mitochondrial events*

The similar spatial pattern observed within each cell between the release of cytochrome *c*-GFP and Smac-mCherry and the subsequent loss of $\Delta\Psi_m$ suggests that although these events are not coincident, they are part of the same process. The temporal lag between the release of cytochrome *c*-GFP and Smac-mCherry could indicate different submitochondrial localizations of the proteins, different binding interactions that delay release of Smac-mCherry, or a pore that is selective for cytochrome *c*-GFP.

The temporal lag that was observed between the release of cytochrome *c*-GFP and the loss of TMRE shows that $\Delta\Psi_m$ and thus the integrity of the inner membrane permeability and mitochondrial energetics are maintained during cytochrome *c* release. Thus, loss of mitochondria energetics is unlikely to be a causal trigger for the loss of the proteins cytochrome *c* and Smac. This is consistent with a model in which apoptosis is initiated in the cytoplasm, permeabilizing the outer membrane, followed by inner membrane permeabilization and then loss of potential (Basanez et al., 1999). However, it is important to keep in mind that our experiments were done with fusion proteins, which may have different localizations than the endogenous proteins, resulting in different release dynamics.

*Mitochondrial morphological changes*

It has been proposed that the release of cytochrome *c* may be a consequence of fission of the mitochondria and the subsequent release of mitochondrial contents (Martinou and Youle, 2006). Here, we define mitochondrial fission as the point at which a break occurs in the mitochondria as observed by microscopy. The observation that cytochrome *c*-GFP release precedes mitochondrial fission (Figure 47) indicates that fission is not necessary for the release of cytochrome *c* from individual mitochondria. It is unlikely that there are significant tears in the mitochondrial membrane that we are not detecting due to limited optical resolution, since the mitochondria still maintain their membrane potential. However, it is possible that the tears are restricted to only the outer membrane. Alternatively, there may be local fissions, but the two halves of the mitochondria do not move apart until after the release of cytochrome *c* and Smac. This observation is consistent with evidence that multiple components of the mitochondrial fission machinery, such as Drp1, are involved in promoting the release of cytochrome *c*. It is also possible that these proteins are multifunctional and use different mechanisms in their roles to reshape mitochondria and to promote the release of proteins from mitochondria (Cassidy-Stone et al., 2008).

When we imaged single mitochondria expressing mito-mCherry, we observed a distinct mitochondrial morphology characterized by multiple fluorescent aggregates with thinner intermediate connections. This could result from the recruitment of proteins such as Bax, Drp1, or Fis1, which cause restrictions at localized mitochondrial sites

(Karbowski et al., 2002), or from alterations of internal mitochondria structures (Sun et al., 2007). This recruitment or alteration could be a precursor to mitochondrial fission.

*Cytochrome c release from a single mitochondria*

To gain insight into the release of cytochrome *c*, we imaged the release from individual mitochondria with subsecond resolution. This revealed that cytochrome *c* release from individual mitochondria occurs in a single step. This imaging technique will be beneficial for investigating events associated with cytochrome *c* release that are too fast to image by laser scanning confocal microscopy, and with a greater *z*-spatial resolution than that provided by wide-field or confocal microscopy.

*Wave mechanism*

One possible mechanism for the wave of cytochrome *c* release is a factor that diffuses across the cell, triggering the mitochondria to release cytochrome *c*. Alternatively, a wave could result from an initial release of cytochrome *c*, followed by a feed-forward loop that amplifies the initial release. A role for ER calcium in the feed-forward mechanism is supported by our experiments in cells treated with thapsigargin, which showed a prolonged duration and lack of spatial organization of cytochrome *c* release. This is consistent with previous work showing a link between cytochrome *c* and

calcium release from the ER, which in turn triggers cytochrome *c* release from the remaining mitochondria (Boehning et al., 2003; Boehning et al., 2005). However, loading the cytosol with 1 mM of BAPTA did not prolong or disrupt the spatial organization of the wave. This suggests that calcium signaling does not occur through the cytoplasm, and instead occurs through close contacts between the ER and the mitochondria (Rizzuto et al., 1998). Alternately, thapsigargin could have an off-target effect, perhaps by altering mitochondrial calcium levels, which has been observed with higher concentrations of thapsigargin (Vercesi et al., 1993). Ultimately, a biochemical dissection of the mechanisms of the wave will be required.

## *Future Directions*

### *Cytochrome c Release*

We observed that cytochrome c was released in a wave in response to STS, TRAIL and ETO, which trigger apoptosis through stress, death receptors and DNA damage pathways respectively. To gain insight into the origin points of the release wave, we could also use other methods to induce apoptosis that stimulate direct components of apoptosis pathways. One possibility would be to use Bcl-2 mimetics or inhibitors to determine whether these affect the wave or the number of starting points of the wave. For example, we could use the Bcl-2 inhibitor ABT-737 which is proposed to inhibit the anti-apoptotic activity of Bcl-2, Bcl-$X_L$ and Bcl-W and induce apoptosis (Oltersdorf et

al., 2005; Cragg et al., 2009), or we could use obatoclax which is proposed to inhibit the interaction between Mcl-1 and Bak (Nguyen et al., 2007), or more generally, we could express select BH3 peptides which induce release of mitochondrial proteins by directly acting on Bax or Bak (Letai et al., 2002; Walensky et al., 2006). If there is no spatial localization of these molecules or peptides in the cell, then if the spatial pattern of release in response to STS or TRAIL is caused by a gradient of Bax or Bak activation in the cell, the spatial pattern may not be present in response to ABT-737, obatoclax, or the BH3 peptides.

We were able to demonstrate that the application of thapsigargin to cells prior to inducing apoptosis was able to inhibit the wave of release, and slow down the overall release in the cell. However, thapsigargin is known to have off target effects (Vercesi et al., 1993), and without identifying specific molecules, or without inhibiting the wave using another inhibitor, it is not possible to rule out this effect. Some of the potential molecules involved in a feed-forward loop include calcium signaling molecules or molecules that are closely associated with both the mitochondria and the endoplasmic reticulum. For example, one of the possible interactions that was not investigated in Chapter Four is the interaction of cytochrome c with the $IP_3R$ (Boehning et al., 2003; Boehning et al., 2005). It has been demonstrated that cytochrome c interacts with amino acids 2621-2636 of type I $IP_3R$ thereby stimulating calcium release from the ER, which is proposed to induce further cytochrome c release (Boehning et al., 2003). A peptide comprising amino acids 2621-2636 of type I $IP_3R$ has been shown to bind to cytochrome c, and inhibit the interaction between cytochrome c and endogenous $IP_3R$ (Boehning et

al., 2005). It would be interesting to determine if this peptide could inhibit the wave of cytochrome c release.

A more general and less directed approach to identify molecules involved in wave propagation would involve performing a screen using a library of shRNA to determine which shRNAs would inhibit or modify the wave (Hitomi et al., 2008). This would require setting up a fluorescent assay to monitor the wave in a high-throughput way that would enable a screen in a reasonable time. Our approach to image the wave has been to wait for one cell to die, then to image rapidly. This was done with a 60x objective to get the maximal resolution to characterize the phenomenon. However, this level of resolution or prediction of apoptosis may not be necessary to observe the wave. At 10x resolution, it is possible to observe cytochrome c at different areas in the cell. Thus, while it may not be possible to resolve the detail of the waves, or all waves in all cells, it may still be possible to see fractional release.

The low-powered objective would enable the imaging of more cells. In imaging many cells, and by imaging at a time when most cells in the population are releasing cytochrome c (i.e. the maximum of the Gaussian), it may be possible to reproducibly observe a small percentage of cells undergoing spatial patterns of cytochrome c release. This would speed up the experimental time and reduce the effort for monitoring a wave of release and may enable a shRNA screen.

While we were able to monitor the release of cytochrome c in single cells, it is not clear if this is a process that occurs in vivo, or whether it is an artifact of cultured cells.

One way to test this would be to express a cytochrome c-GFP fusion in mice, and image cytochrome c GFP release in tissues undergoing apoptosis. Alternatively we could image cytochrome c homologs in other organisms such as *C. elegans* (ced-4), or *D. Melanogaster* (though it is not clear whether drosophila cytochrome c is released during apoptosis). In all of these instances, it would be interesting to determine whether the wave occurs at the same speed, and whether there is randomly occurring release.

### *Sister Cell Apoptosis*

While we find that sister cells undergo apoptosis at similar times, these times are not exactly the same. Our data shows that while blocking protein synthesis can reduce the dissimilarity, it does not completely eliminate the difference. Another source of dissimilarity is cell-cell variation caused by variation in protein degradation. Thus we could inhibit protein degradation using mg132 at various times after cell division and determine whether this has an effect on the divergence of sister cell apoptosis.

To isolate molecules responsible for the divergence, we could perform a shRNA screen. Again, this would require fully automating tracking the lineage of cells, the onset of apoptosis, and the subsequent analysis. It would then be possible to monitor which shRNA alters the similarity or the divergence of apoptosis times. It is possible that this will not only result in the identification of genes involved in apoptosis but possibly molecules involved in gene expression regulation and genomic stability.

Finally, to gain insight into what predisposes some cells to undergo apoptosis early relative to the population, we could isolate cells based on when they undergo apoptosis. One possibility is to perform this isolation using flow cytometry where we sort cells twice: first keeping cells that are alive, then sorting shortly afterwards to select cells that have undergone caspase activation in the time between the sorts. This would select for cells that have undergone apoptosis in this short interval. By assaying the gene expression of these cells it might be possible to identify specific molecules that are up or down regulated in early or late dying cells. This analysis presumes that there are subsets of molecules that are responsible, and that not all molecules are changing. For example, different cells may have different molecular reasons for their susceptibility, which could confound this experimental approach.

# *Chapter Six: Experimental Procedures*

## *General Methods*

### *Cell Culture*

HeLa, NIH3T3, MEF, B16F0, and HT1080 cells were maintained at 5% CO2 in DMEM (Gibco) containing 10% FBS (Gibco). Cells were maintained on 10 cm polystyrene dishes (Corning), and were passaged approximately every two days. For imaging, cells were plated on Mattek glass bottom dishes. Two different sized dishes were used depending on the nature of the experiment (10mm and 20mm). Long term multiwell imaging experiments were performed in 24 well dishes (BD Bioscience).

### *Induction of Apoptosis*

Apoptosis was induced with sFasL (BioVision, Mountain View, CA), TRAIL (BioVision), staurosporine (Sigma, St. Louis, MO), etoposide (BioVision), TNFα (BioVision), cycloheximide (Sigma). Drugs were mixed with media well prior to the addition of media to cells

### *Transfection*

Cells were transiently transfected with Lipofectamine 2000 (Invitrogen), or with Fugene (Roche). Fluorescence expression started to occur as early as 8 hours after Transfection.

### *Generation of Stable Cell Lines*

Stable cell lines were generated using lentiviral infection. Briefly cDNA was cloned into a pLNCX vector (Clontech). HEK293T Phoenix cells – which express viral coat proteins - were transfected with the pLNCX modified vector, thus producing viral particles. Supernatant containing viral particles were collected diluted 1:2 in DMEM and added to the target cells. Cells were allowed to grow over several days. Infection efficiency varied from ~ 5% to 20 %. Cells were selected using flow cytometry (Rockefeller FACS Center).

### *Fluorophores*

We used the fluorophores mCerulean, mCitrine, mCherry for the non-FRET constructs. CyPet and yPet (optimized from CFP and YFP respectively) were used in the FRET construct. mCherry and mCitrine were obtained from Roger Tsien (Shaner et al., 2004). CyPet and yPet obtained from Patrick Daugherty (Nguyen and Daugherty, 2005). mCerulean was obtained from David Piston (Rizzo et al., 2004).

### *Fluorescence Microscopy*

For widefield microscopy, we used an Olympus IX-81 microscope with Xenon lamp illumination source, and an Orca ER CCD camera (Hamamatsu). This microscope had an automated stage to enable the collection of data from multiple fields (Prior Scientific). The images were recorded using exposure times of 100-300ms. Image acquisition was performed using Metamorph software (Molecular Devices, Sunnyvale, CA). . The microscope was enclosed by a plexiglass chamber made by the Rockefeller High Energy Machine Shop. We used a 60x 1.2NA water immersion objective, a 40x 0.8 NA air objective and a 10X 0.6 NA air objective.

Filter settings were organized to enable the detection of multiple fluorophores in the same cell. All filters were purchased from Chroma. The filters are listed below:

**Table 5: Olympus IX81 Filters**

| **Fluorophore** | **Excitation Filter** | **Emission Filter** | **Dichroic** |
|---|---|---|---|
| DAPI | 360/40 | 400/LP | DAPI 61002 Polychroic |
| mCerulean | ET 430/24 | ET470/24 | CFP/YFP/mCherry 89006 polychroic |
| GFP | HQ 470/40 | HQ 520/50 | 495 long pass |
| mCitrine | ET 500/20 | ET 535/30 | CFP/YFP/mCherry 89006 polychroic |
| mCherry/TMRE | ET 577/25 | ET 632/60 | CFP/YFP/mCherry 89006 polychroic |

Long term imaging (between 24 and 96 hours) was performed in DMEM with 10% FBS, and in 5% $CO_2$. The temperature was maintained at 37$^oC$ using a homemade temperature box. Cells were imaged in Matek dishes or in 24-well dishes. Imaging in 24 well dishes was done to increase the number of cell conditions per experiment. Dishes (Mattek or 24 well dishes) were wrapped in parafilm or laboratory tape to minimize the loss of 5% $CO_2$ Media exchange was performed at least every 24 hours during imaging was performed using tubes inserted through the top of the dish. The 5% $CO_2$ was also perfused through the top of the dish. At least three fields per well was accquired over an experiment. Media exhange occured via tubes inserted through the top of the dishes. Untreated cells at 92 hours appeared normal.

Confocal microscopy differs from widefield microscopy in that it eliminates out focus light using a pinhole. Confocal imaging was performed on a Zeiss510 confocal microscope using a 60x objective. (BioImaging Facility, The Rockefeller University). Fluorophores were excited using a laser excitation source (Table 5). Cells were maintained at 37$^oC$ using a Warner Heating Chamber, and were imaged in Cell Imaging Media (Hanks BBS (Sigma) 9.8g/L, 10mM Hepes; 5% FBS; pH 7.4). Image acquisition was performed with Zeiss software. The following fluorophores were imaged with the following filters:

**Table 6: Confocal Microscopy Filters**

| Fluorophore | Excitation Filter | Emission Filter | Dichroic |
|---|---|---|---|
| mCerulean | 458 laser | 473-498 BP | 458/514 dichroic |
| GFP | | HQ 520/50 | 488/543 dichroic |
| mCitrine | 514 laser | 550/50 BP | 458/514 dichroic |
| mCherry/TMRE | 543 laser | 560 LP | 488/543 dichroic |

We also used total internal reflection microscopy to image single mitochondria releasing cytochrome c at rapid time resolution. Excitation was with a 488nm (Spectra Physics) and 561nm (Melles Griot) laser for GFP and mCherry respectively, a 488/561 polychroic mirror, a Cairn OptosplitIII image splitter (Cairn Research) with a 580lp dichroic to split the channels and emission filter 525/50 for GFP and 632/60 for mCherry, and an OrcaER CCD camera. The TIR microscope was controlled with Metamorph software . All filters and dichroics are from Chroma.

## *Chapter Two Methods*

### *Plasmid Design*

This outlines the cloning details to make the constructs. All primers are listed in 5' → 3' format. All primers were ordered from Genelink. The pmDEVD reporter was anchored to the plasma membrane by using the N-terminal palmitoylation site from GAP-43. This was PCR amplified from pECFPmem (Clontech) using the primers:

Forward: GCGCGCTAGCAATAGATCTTGTTTAGTGAACATGCT GTGCTGTATGAGA

Reverse: GATGAGGACCAAAAGATCTCATCGTCTGAATTGTCT GGTGATGAAGTTGATGGATCTTCTGGTTCTGAATTCG CGC

The DEVD site is contained in the reverse primer. This was inserted into the pECFP-C1 vector in the restriction sites NheI and EcoRI. Fluorescent proteins were swapped by digesting with EcoRI and XhoI, and inserting fluorescent proteins PCR amplified with the primers:

Forward: GCGCGAATTCTCATCTACCGGTATGGTGAGCAAGGG CGAG

Reverse: ATGGACGAGCTGTACAAGCTCGAGCATAACTAAGGA TCCGCGC

This encodes the construct shown in Figure 5:

Palmitoylation- sselsg**devd**gssgsefssstg-Fluorophore

The pmControl construct is a variant of pmDEVD without the DEVD. This was made by PCR amplifying the palmitoylation site with primers that did not contain the DEVD site:

Forward: GCGCGCTAGCAATAGATCTTGTTTAGTGAACATGCT GTGCTGTATGAGA

Reverse: GATGAGGACCAAAAGATCTCATCGTCTGAATTGTCT GGTGGATCTTCTGGTTCTGAATTCGCGC

This resulted in the construct:

Palmitoylation-sselsggssgstg-Fluorophore

pCaspase-3 sensor was initially distributed by Clontech with a GFP, which limits the simultaneous observation of other fluorophores. We first amplified the NES from the pCaspase-3 sensor and in the process added a DEVD domain, and an EcoRI site. This was inserted into the NheI and AgeI sites in pECFP-C1. Next, we amplified mCherry and inserted this into the AgeI and XhoI sites. Next, the NLS from the pCaspase-3 sensor was amplified and inserted between the XhoI and BamHI sites. Finally to create a control plasmid, we inserted amplified mCerulean using the control primers, and inserted these between the EcoRI and XhoI sites. The primers used are below:

NES Primers:

Forward: GCGCGCTAGCAATAGATCTTGTTTAGTGAACATGAA CCTGGTGGACCTC

Reverse: GAGCTGGACGAGCAGCAGGAATTCTCATCGTCTGAA TTGTCTGGTGATGAAGTTGATGGATCTTCTGGTTCTT CATCTACCGGTGCGC

Fluorescent Protein Primer:

Forward: GCGCACCGGTATGGTGAGCAAGGGCGAG

Reverse: ATGGACGAGCTGTACAAGCTCGAGCATAACTAAGGA TCCGCGC

NLS Primers:

Forward: GCGCCTCGAGTCTGATCCAAAAAAGAAGAGA

Reverse: GGATCCACCGGATCTAGATAAGGATCCGCGC

Control Primer

Forward: GCGCGAATTCTCATCGTCTGAATTGTCTGGTGGATCT TCTGGTTCT

Reverse: ATGGACGAGCTGTACAAGCTCGAGCATAACTAAGGA TCCGCGC

To create the erDEVD reporter, the first transmembrane domain of Sec63 was PCR amplified from a cDNA library using the primers:

Forward: GCGCGCTAGCATGGCCGGGCAGCAGTTC

Reverse: TGGTATCGTAAGCTTTCTGAA TTCGCGC

This was inserted into the aforementioned pCaspase-3 vector, excising the NES resulting in:

Sec63(1-68)-sselsg**devd**gssgstg-Fluorophore-NLS(3)

The erControl construct was created by inserting the Sec63 (aa 1-68) into the pCaspase-3 Control reporter using the erDEVD primers, and the restriction sites EcoRI, and NheI. This resulted in the following construct:

Sec63(1-68)- sselsggssgstg -Fluorophore-NLS(3)

This FRET-DEVD construct was made using the CyPet and yPet vectors which have been optimized to produce a large change in FRET. This was created by PCR

amplifying CyPet using the primers below and inserting into the NheI and BamHI restriction enzyme sites of pEGFP-C1

Forward: GCGCGCTAGCATGGTGAGCAAGGGAGAG

Reverse: ATGGACGAACTGTACAAATCCTCGTCCGAGCTCAGC
GGAGATGAGGTCGATGGATCCCCAAA

Subsequently yPet was amplified using the primers below and placed into the BamHI and HindIII sites in the previous vector.

Forward: TTTGGGGATCCAGCGGAAGCGAATTCTCTTCAACCG
GTATGGTGAGCAAAGGCGAAGAG

Reverse: AACGAGCTCTATAAGTAAAAGCTTGCGC

The DEVD site is contained in the primers:

CyPet–sselsg**devd**gssgsef-yPet

### *Reporter Quantification*

Analysis of changes in live single cell fluorescence (for initial reporter characterization experiments) were quantified in Metamorph. To quantify changes in the pmDEVD reporter, a single region within the cytoplasm was chosen. Fluorescent proteins fused to the palmitoylation domain localize to the Golgi as well as the plasma membrane. Therefore in choosing a cytoplasmic region to quantify the changes in fluorescence, the Golgi aggregate fluorescence was avoided. To quantify fluorescent changes in the erDEVD reporter and the pCaspase-3 sensor, we monitored nuclear fluorescence. Finally changes in the FRET-DEVD construct were quantified by monitoring the ratio of CFP/YFP in a single cytoplasmic region. During all quantification, a background subtraction of each fluorescent channel was performed.

### *TUNEL Staining*

TUNEL staining was performed to assay double stranded breaks. Cells were transiently transfected with the pmDEVD reporter, treated with staurosporine (2µM), fixed at different time points, and were stained. TUNEL staining of STS (2µM) treated HeLa cells was performed in glass bottom 96 well plates (BDBiosciences). We analyzed untreated cells, thereby determining a fluorescence range for non-apoptotic cells, and we also monitored cells that were treated for 8 hours with STS, and determined an apoptotic

range. In each well we determined whether cells were TUNEL positive, and transfected with the pmDEVD-mCherry reporter. In each well this was continued until we counted 50 transfected cells, and 50 untransfected cells. The percentage of TUNEL positive cells for transfected and untransfected cells was calculated, and averaged over three wells for each time point.

## *Chapter Three Methods*

### *Plasmids*

The G1/S cell cycle reporter consists of the PSLD domain (amino acids 957-1087 of human DNA Helicase B) fused to mCitrine. The reporter is in the nucleus in G1 phase, and translocates to the cytoplasm during the G1/S transition when PSLD is phosphorylated by CyclinE-CDK2. The PSLD domain from Human DNA Helicase B was PCRed from a HeLa cDNA library using the primers below. This was inserted into a vector similar to pEGFP-C1 (between XhoI and EcoRI) with mCitrine in the place of EGFP.

Forward: GCGCCTCGAGCTTCTAGCGGCGCACCTCCA

Reverse: GATAATCAAGAAACTTAGGAATTCGCGC

The triple repeat of the SV40 NLS was PCR amplified from pEYFP-Nuc and placed into a vector similar to pEGFP-C1 with mCerulean in the place of EGFP between the restriction sites XhoI and EcoRI.

### *Correlation between Inter-Cell distance and Caspase-3/7 activation*

The determination of the position of cells and their times of apoptosis was performed in Metamorph and Excel. The time of caspase-3/7 activation was determined by circling a region which was approximately the center of cells and determining when fluorescence irreversibly increased above background. When this did not give a clear result (potentially owing to movement of the cell) the time of caspase-3/7 activity was visually determined by looking at the time-lapse images. If the onset of caspase-3/7 activation was still not clear, the cell was excluded from the analysis. The center of the circled region was recorded as the position of the cell. The position of cells was the position at the time of drug treatment.

Analysis of the distance between cells and their times of apoptosis was performed in MatLab. The program would get the position and times of apoptosis of all cells in a field. Distance was calculated as the distance between the approximate center of cells, and not the edges of cells. For every cell pairing the distance and the absolute value of the difference of caspase-3/7 activation in the cells was calculated. This data was binned based on distance producing plots such as Figure 15. Error bars indicate the 95% confidence interval of the mean so as to visualize the confidence in the average and not the distribution.

For analysis of inter-cell distance and caspase-3/7 activation for cells that were not sister or cousin cells, we performed the same analysis as above, but excluded sister or cousin comparisons from the calculation.

Analysis of plating at different times and correlating distance to difference in caspase activation was performed as above. The times of the actual caspase activation difference was normalized to the caspase activation difference for cells whose position were randomly reassigned (null hypothesis). This was a result of variability in the time difference for cells that are very far apart at the different plating times.

### *Cell Cycle Analyses*

Long term imaging was performed on the Olympus IX-81 in widefield microscopy. The analysis of the time of onset of caspase-3/7 activation was performed in Metamorph. The specific time of caspase-3/7 activation, as measured by pmDEVD-mCherry, was determined as the time when the cytosolic fluorescence irreversibly increased above the basal level. Cell tracking and the analysis of the G1/S transition was performed in Imaris (using the Spot Module). Specifically, the nucleus was tracked using Cerulean-NLS. For a single cell, this resulted in a moving region of interest marking the nucleus. The nuclear fluorescence of the mCitrine-PSLD reporter was quantified in this moving region of interest, and the time course data was exported to Excel. The time of the G1/S transition was characterized as the time when the mCitrine-PSLD nuclear

fluorescence irreversibly decreased from the basal G1 levels (see Figure 18 for an example of the PSLD-mCitrine time course data). After the addition of the drugs the cells were not as dynamic, therefore the nuclear tracking was not required to measure the pmDEVD-mCherry reporter.

Alternatively, cell cycles were synchronized with a double thymidine block (15 hr block, 10 hr release, 15 hr block) and released for variable times (Figure 165). Controls to determine DNA content was performed with Hoechst staining (Sigma). Briefly, cells were trypisined, fixed in 4% PFA, and stained with Hoechst (1ug/mL, 20 min), and analyzed with BD LSRII flow cytometry analyzer (BS BioScience). One way ANOVA performed in Excel (Fig. S5)

### *Analysis of Sister Cells and Cell Lineage*

Sister cell pairs were visually determined by monitoring division up to 36 hours before drug treatment. Comparisons of the average time of apoptosis for different cell types and different stimuli (Figure 28) was calculated in Excel. The randomized differences were calculated by taking actual times of apoptosis and randomly pairing these in Excel.

Cell death of only part of the population (44% of the population) was induced by using a 1μM STS treatment for 45 minutes. Cells were washed 3 times in fresh DMEM after treatment. Within 36 hours of drug treatment there were some cells that did not

divide or undergo apoptosis. We counted these non-apoptotic, non-dividing cells as surviving. Chi-squared test was performed with p calculated for 2 degrees of freedom (Figure 29).

Analysis of the difference in apoptosis between related cells was performed in MatLab (Figure 31). The time of apoptosis of each cell, and a four number identifier of the ancestry of each cell was inputted into the program. Cells that shared the same first number were sister cells, cells that shared the same second number, but not the same first number were cousin cells, etc. The program would then calculate the difference in the time of caspase-3/7 activation for each pairing of cells, and store it in 4 different arrays depending on the relationships between the cell (i.e. if cells were sister cells, data was stored in array 1, if cells were cousin cells, data was stored in array 2, etc.). Histograms were plotted in Excel. Data fit for the memory of the cell was performed using the Marquadt-Levenberg Algorithm in Origin or non-linear least squares fit algorithm in MatLab using all the data points, and not the average data points. One way ANOVA of clonal cell lines was performed in Excel (Figure 33).

### *Intergenerational Differences of Caspase Activation*

A subset of sister cells from Figure 34. 4A was re-analyzed to determine both the time of apoptosis, and the time since division. Cells were fit to recovering exponential curve as performed in MatLab with calculations for the 95% CI of the fit (Figure 34).

Cells were grouped into bins of 500 minutes to demonstrate intra-generational trends using Excel (Figure 34). Error bars of said binned data represent 95% confidence interval of the mean.

### *Protein Synthesis Inhibition*

Protein synthesis was inhibited using Cycloheximide (C7698), and Puromycin (Sigma P7255). Treatment regimes are shown in Figure 35 and 37A. S9A,10A. Media with CHX or puromycin was added through the top of the dish.

## *Chapter Four Methods*

### *Plasmids*

Plasmids (Cytochrome c-GFP, Mito-mCherry, and Smac-mCherry) were transfected using Lipofectamine 2000 (Invitrogen). TMRE (Molecular Probes) was added at a concentration of 25 ng/mL for 15 minutes prior to drug addition. Cytochrome-c GFP vector was obtained from Douglas Green (Goldstein et al., 2000). Smac-mCherry was made by inserting mCherry in the place of CFP in the Smac-CFP vector (from Richard Youle). mCherry was obtained from Roger Tsien, and was placed into a vector similar to EGFP-C1 (mCherry-C1, made by Florence Koeppel). mCherry was cut using EcoRI and XhoI restriction enzyme sites and inserted into the corresponding region of Smac-CFP. Mito-mCherry (a fluorescent fusion of the localization tag of cytochrome c oxidase IV) was made by inserting mCherry in the place of DsRed in the mito-DsRed vector (Rizzuto et al., 1995). This was done by inserting mCherry from mCherry-C1 into mitoDsRed using the sites AgeI and XhoI.

Cells were transfected with cytochrome c-GFP 72 hours before addition of the apoptotic drug to allow time for proper cytochrome c-GFP localization. In experiments involving co-expression of Smac-mCherry or mito-mCherry, cells were transfected a second time 24 hours before the beginning of imaging. An area containing at least 2 transfected cells was imaged at once every 2 minutes until one cell in the field of view released cytochrome c. Then the rate of imaging was increased to once every 10 seconds.

### *Microscopy Controls*

Microscopy controls: Cells were imaged under experimental conditions in the absence of any apoptotic trigger and the release of cytochrome c-GFP from the mitochondria was never observed indicating that the release of cytochrome c-GFP was not a consequence of the imaging conditions.

Untreated cells loaded with TMRE were imaged and used to set excitation intensity and exposure times that did not induce spontaneous mitochondrial depolarizations from free-radical production (Huser et al., 1998). Cells were imaged under experimental conditions in the absence of any apoptotic trigger and the release of cytochrome c-GFP from the mitochondria was never observed indicating that the release of cytochrome c-GFP was not a consequence of the imaging conditions.

### *Image and Data Analysis*

Data was analyzed with Metamorph. The FRET ratio was calculated as CFP/YFP after background subtraction. Analysis of the cell cycle reporters were conducted using Spot Detection in Imaris (Bitplane, Saint Paul, MN). Analysis of the differences in times of apoptosis relative to both lineage and distance were performed in MatLab and Excel. Curve fitting was performed in Origin using the Marquardt-Levenberg Algorithm or

MatLab. Flow cytometry was performed using the BD FACS Aria, and BDLSRII (BD Biosciences, Flow Cytometry Facility at The Rockefeller University).

Image analysis was performed with Metamorph software (Universal Imaging). Circular regions of interest (ROIs) with an area of 3μm were selected on the cytochrome c-GFP image. Many ROIs were selected such that a majority of the mitochondria were included within at least one ROI. The ROIs were then transferred to the other channel. The average intensity of each ROI over time was calculated. The time of release for the ROI was selected by eye as the time when the intensity began to decline irreversibly. If such a point could not be determined, the ROI was discarded. The x,y location of each ROI was recorded and the linear distances were calculated from the ROI that had the first cytochrome c release. (see Figure 40).

### *Statistical Analysis*

All data were analyzed with excel software (Microsoft). The analysis was performed using the Student's t-test.

### *BAPTA-AM and Thapsigargin Experiments*

Media Changes: BAPTA-AM and Thapsigargin experiments required media changes during imaging. These experiments were performed in MatTek dishes, and

media exchange occurred via syringes connected to thin tubing inserted through the top of the MatTek dish.

BAPTA-AM (1mM) (Alexis) and thapsigargin (5μM) (Sigma) were used to alter calcium signaling. To reduce extracellular calcium levels, we added EGTA (1.2 mM) (Sigma) to CIM. We conducted three different experiments. The control experiment was the addition of TRAIL (1 μg/mL) to cells. In these experiments EGTA and TRAIL were added to cells in CIM.

The second experiment required the addition of BAPTA-AM (1mM) to quench cytosolic calcium. BAPTA-AM was not added at the beginning of the experiment. BAPTA-AM addition was delayed to minimize unintended consequences of the 1mM concentration. Instead, TRAIL and EGTA were added to cells in CIM, and after the first cell released cytochrome c BAPTA-AM was added. During the addition all media was removed from the MatTek dish, and replaced with fresh CIM, TRAIL, EGTA, and BAPTA-AM. Analysis was conducted on cells that began to release cytochrome c at least 5 minutes after the addition of BAPTA-AM. Control experiments showed that this is an appropriate time to ensure cytosolic calcium buffering.

The third experiment involved adding thapsigargin to deplete the endoplasmic reticulum (ER) calcium. Previous studies in HeLa cells indicated that Tg takes approximately 20 minutes to deplete ER calcium (Palmer et al., 2004). Tg and EGTA were added to the CIM at the beginning of the experiment (prior to the addition of

TRAIL). After 20 minutes the media was removed and replaced with CIM containing TRAIL, EGTA, and thapsigargin.

References

Abkowitz,J.L., Catlin,S.N., and Guttorp,P. (1996). Evidence that hematopoiesis may be a stochastic process in vivo. Nat. Med. *2*, 190-197.

Acehan,D., Jiang,X., Morgan,D.G., Heuser,J.E., Wang,X., and Akey,C.W. (2002). Three-dimensional structure of the apoptosome: implications for assembly, procaspase-9 binding, and activation. Mol. Cell *9*, 423-432.

Adams,J.M. and Cory,S. (2007). The Bcl-2 apoptotic switch in cancer development and therapy. Oncogene *26*, 1324-1337.

Albrecht-Buehler,G. (1977). Daughter 3T3 cells. Are they mirror images of each other? J. Cell Biol. *72*, 595-603.

Alexander,C., Votruba,M., Pesch,U.E., Thiselton,D.L., Mayer,S., Moore,A., Rodriguez,M., Kellner,U., Leo-Kottler,B., Auburger,G., Bhattacharya,S.S., and Wissinger,B. (2000). OPA1, encoding a dynamin-related GTPase, is mutated in autosomal dominant optic atrophy linked to chromosome 3q28. Nat. Genet. *26*, 211-215.

Alnemri,E.S., Livingston,D.J., Nicholson,D.W., Salvesen,G., Thornberry,N.A., Wong,W.W., and Yuan,J. (1996). Human ICE/CED-3 protease nomenclature. Cell *87*, 171.

Andrews,D.L. (1989). A Unified Theory of Radiative and Radiationless Molecular-Energy Transfer. Chemical Physics *135*, 195-201.

Annis,M.G., Soucie,E.L., Dlugosz,P.J., Cruz-Aguado,J.A., Penn,L.Z., Leber,B., and Andrews,D.W. (2005). Bax forms multispanning monomers that oligomerize to permeabilize membranes during apoptosis. EMBO J. *24*, 2096-2103.

Antignani,A. and Youle,R.J. (2006). How do Bax and Bak lead to permeabilization of the outer mitochondrial membrane? Curr. Opin. Cell Biol. *18*, 685-689.

Arkin,A., Ross,J., and McAdams,H.H. (1998). Stochastic kinetic analysis of developmental pathway bifurcation in phage lambda-infected Escherichia coli cells. Genetics *149*, 1633-1648.

Arstila,A.U. and Trump,B.F. (1968). Studies on cellular autophagocytosis. The formation of autophagic vacuoles in the liver after glucagon administration. Am. J. Pathol. *53*, 687-733.

Axelrod,D. (1989). Total internal reflection fluorescence microscopy. Methods Cell Biol. *30*, 245-270.

Baines,C.P., Kaiser,R.A., Sheiko,T., Craigen,W.J., and Molkentin,J.D. (2007). Voltage-dependent anion channels are dispensable for mitochondrial-dependent cell death. Nat. Cell Biol. *9*, 550-555.

Baird,G.S., Zacharias,D.A., and Tsien,R.Y. (2000). Biochemistry, mutagenesis, and oligomerization of DsRed, a red fluorescent protein from coral. Proc. Natl. Acad. Sci. U. S. A *97*, 11984-11989.

Bakhshi,A., Jensen,J.P., Goldman,P., Wright,J.J., McBride,O.W., Epstein,A.L., and Korsmeyer,S.J. (1985). Cloning the chromosomal breakpoint of t(14;18) human lymphomas: clustering around JH on chromosome 14 and near a transcriptional unit on 18. Cell *41*, 899-906.

Baliga,B.C., Read,S.H., and Kumar,S. (2004). The biochemical mechanism of caspase-2 activation. Cell Death. Differ. *11*, 1234-1241.

Barkett,M. and Gilmore,T.D. (1999). Control of apoptosis by Rel/NF-kappaB transcription factors. Oncogene *18*, 6910-6924.

Basanez,G., Nechushtan,A., Drozhinin,O., Chanturiya,A., Choe,E., Tutt,S., Wood,K.A., Hsu,Y., Zimmerberg,J., and Youle,R.J. (1999). Bax, but not Bcl-xL, decreases the lifetime of planar phospholipid bilayer membranes at subnanomolar concentrations. Proc. Natl. Acad. Sci. U. S. A *96*, 5492-5497.

Basanez,G., Zhang,J., Chau,B.N., Maksaev,G.I., Frolov,V.A., Brandt,T.A., Burch,J., Hardwick,J.M., and Zimmerberg,J. (2001). Pro-apoptotic cleavage products of Bcl-xL form cytochrome c-conducting pores in pure lipid membranes. J. Biol. Chem. *276*, 31083-31091.

Bereiter-Hahn,J. and Voth,M. (1994). Dynamics of mitochondria in living cells: shape changes, dislocations, fusion, and fission of mitochondria. Microsc. Res. Tech. *27*, 198-219.

Bernardi,P. and Azzone,G.F. (1981). Cytochrome c as an electron shuttle between the outer and inner mitochondrial membranes. J. Biol. Chem. *256*, 7187-7192.

Boatright,K.M., Renatus,M., Scott,F.L., Sperandio,S., Shin,H., Pedersen,I.M., Ricci,J.E., Edris,W.A., Sutherlin,D.P., Green,D.R., and Salvesen,G.S. (2003). A unified model for apical caspase activation. Mol. Cell *11*, 529-541.

Boatright,K.M. and Salvesen,G.S. (2003). Mechanisms of caspase activation. Curr. Opin. Cell Biol. *15*, 725-731.

Boehning,D., Patterson,R.L., Sedaghat,L., Glebova,N.O., Kurosaki,T., and Snyder,S.H. (2003). Cytochrome c binds to inositol (1,4,5) trisphosphate receptors, amplifying calcium-dependent apoptosis. Nat. Cell Biol. *5*, 1051-1061.

Boehning,D., van Rossum,D.B., Patterson,R.L., and Snyder,S.H. (2005). A peptide inhibitor of cytochrome c/inositol 1,4,5-trisphosphate receptor binding blocks intrinsic and extrinsic cell death pathways. Proc. Natl. Acad. Sci. U. S. A *102*, 1466-1471.

Boldin,M.P., Goncharov,T.M., Goltsev,Y.V., and Wallach,D. (1996). Involvement of MACH, a novel MORT1/FADD-interacting protease, in Fas/APO-1- and TNF receptor-induced cell death. Cell *85*, 803-815.

Boyd,J.M., Gallo,G.J., Elangovan,B., Houghton,A.B., Malstrom,S., Avery,B.J., Ebb,R.G., Subramanian,T., Chittenden,T., Lutz,R.J., and . (1995). Bik, a novel death-inducing protein shares a distinct sequence motif with Bcl-2 family proteins and interacts with viral and cellular survival-promoting proteins. Oncogene *11*, 1921-1928.

Burri,L., Strahm,Y., Hawkins,C.J., Gentle,I.E., Puryer,M.A., Verhagen,A., Callus,B., Vaux,D., and Lithgow,T. (2005). Mature DIABLO/Smac is produced by the IMP protease complex on the mitochondrial inner membrane. Mol. Biol. Cell *16*, 2926-2933.

Campbell,R.E., Tour,O., Palmer,A.E., Steinbach,P.A., Baird,G.S., Zacharias,D.A., and Tsien,R.Y. (2002). A monomeric red fluorescent protein. Proc. Natl. Acad. Sci. U. S. A *99*, 7877-7882.

Carrington,P.E., Sandu,C., Wei,Y., Hill,J.M., Morisawa,G., Huang,T., Gavathiotis,E., Wei,Y., and Werner,M.H. (2006). The structure of FADD and its mode of interaction with procaspase-8. Mol. Cell *22*, 599-610.

Carswell,E.A., Old,L.J., Kassel,R.L., Green,S., Fiore,N., and Williamson,B. (1975). An endotoxin-induced serum factor that causes necrosis of tumors. Proc. Natl. Acad. Sci. U. S. A *72*, 3666-3670.

Cassidy-Stone,A., Chipuk,J.E., Ingerman,E., Song,C., Yoo,C., Kuwana,T., Kurth,M.J., Shaw,J.T., Hinshaw,J.E., Green,D.R., and Nunnari,J. (2008). Chemical inhibition of the mitochondrial division dynamin reveals its role in Bax/Bak-dependent mitochondrial outer membrane permeabilization. Dev. Cell *14*, 193-204.

Cerretti,D.P., Kozlosky,C.J., Mosley,B., Nelson,N., Van Ness,K., Greenstreet,T.A., March,C.J., Kronheim,S.R., Druck,T., Cannizzaro,L.A., and . (1992). Molecular cloning of the interleukin-1 beta converting enzyme. Science *256*, 97-100.

Chai,J., Wu,Q., Shiozaki,E., Srinivasula,S.M., Alnemri,E.S., and Shi,Y. (2001). Crystal structure of a procaspase-7 zymogen: mechanisms of activation and substrate binding. Cell *107*, 399-407.

Chalfie,M., Tu,Y., Euskirchen,G., Ward,W.W., and Prasher,D.C. (1994). Green fluorescent protein as a marker for gene expression. Science *263*, 802-805.

Chen,L., Willis,S.N., Wei,A., Smith,B.J., Fletcher,J.I., Hinds,M.G., Colman,P.M., Day,C.L., Adams,J.M., and Huang,D.C. (2005). Differential targeting of prosurvival Bcl-2 proteins by their BH3-only ligands allows complementary apoptotic function. Mol. Cell *17*, 393-403.

Chen,P., Nordstrom,W., Gish,B., and Abrams,J.M. (1996). grim, a novel cell death gene in Drosophila. Genes Dev. *10*, 1773-1782.

Cheng,E.H., Sheiko,T.V., Fisher,J.K., Craigen,W.J., and Korsmeyer,S.J. (2003). VDAC2 inhibits BAK activation and mitochondrial apoptosis. Science *301*, 513-517.

Cheng,E.H., Wei,M.C., Weiler,S., Flavell,R.A., Mak,T.W., Lindsten,T., and Korsmeyer,S.J. (2001). BCL-2, BCL-X(L) sequester BH3 domain-only molecules preventing BAX- and BAK-mediated mitochondrial apoptosis. Mol. Cell *8*, 705-711.

Chipuk,J.E. and Green,D.R. (2008). How do BCL-2 proteins induce mitochondrial outer membrane permeabilization? Trends Cell Biol. *18*, 157-164.

Chipuk,J.E., Moldoveanu,T., Llambi,F., Parsons,M.J., and Green,D.R. (2010). The BCL-2 family reunion. Mol. Cell *37*, 299-310.

Chittenden,T., Flemington,C., Houghton,A.B., Ebb,R.G., Gallo,G.J., Elangovan,B., Chinnadurai,G., and Lutz,R.J. (1995). A conserved domain in Bak, distinct from BH1 and BH2, mediates cell death and protein binding functions. EMBO J. *14*, 5589-5596.

Clarke,P.G. and Clarke,S. (1996). Nineteenth century research on naturally occurring cell death and related phenomena. Anat. Embryol. (Berl) *193*, 81-99.

Cleary,M.L. and Sklar,J. (1985). Nucleotide sequence of a t(14;18) chromosomal breakpoint in follicular lymphoma and demonstration of a breakpoint-cluster region near a transcriptionally active locus on chromosome 18. Proc. Natl. Acad. Sci. U. S. A *82*, 7439-7443.

Cohen,A.A., Geva-Zatorsky,N., Eden,E., Frenkel-Morgenstern,M., Issaeva,I., Sigal,A., Milo,R., Cohen-Saidon,C., Liron,Y., Kam,Z., Cohen,L., Danon,T., Perzov,N., and Alon,U. (2008). Dynamic Proteomics of Individual Cancer Cells in Response to a Drug. Science.

Cragg,M.S., Harris,C., Strasser,A., and Scott,C.L. (2009). Unleashing the power of inhibitors of oncogenic kinases through BH3 mimetics. Nat. Rev. Cancer *9*, 321-326.

Crook,N.E., Clem,R.J., and Miller,L.K. (1993). An apoptosis-inhibiting baculovirus gene with a zinc finger-like motif. J. Virol. *67*, 2168-2174.

Danial,N.N. and Korsmeyer,S.J. (2004). Cell death: critical control points. Cell *116*, 205-219.

Deng,J., Carlson,N., Takeyama,K., Dal Cin,P., Shipp,M., and Letai,A. (2007). BH3 profiling identifies three distinct classes of apoptotic blocks to predict response to ABT-737 and conventional chemotherapeutic agents. Cancer Cell *12*, 171-185.

Deveraux,Q.L., Roy,N., Stennicke,H.R., Van Arsdale,T., Zhou,Q., Srinivasula,S.M., Alnemri,E.S., Salvesen,G.S., and Reed,J.C. (1998). IAPs block apoptotic events induced by caspase-8 and cytochrome c by direct inhibition of distinct caspases. EMBO J. *17*, 2215-2223.

Dix,M.M., Simon,G.M., and Cravatt,B.F. (2008). Global mapping of the topography and magnitude of proteolytic events in apoptosis. Cell *134*, 679-691.

Dover,R. and Potten,C.S. (1988). Heterogeneity and cell cycle analyses from time-lapse studies of human keratinocytes in vitro. J. Cell Sci. *89 ( Pt 3)*, 359-364.

Du,C., Fang,M., Li,Y., Li,L., and Wang,X. (2000). Smac, a mitochondrial protein that promotes cytochrome c-dependent caspase activation by eliminating IAP inhibition. Cell *102*, 33-42.

Dussmann,H., Rehm,M., Concannon,C.G., Anguissola,S., Wurstle,M., Kacmar,S., Voller,P., Huber,H.J., and Prehn,J.H. (2010). Single-cell quantification of Bax activation and mathematical modelling suggest pore formation on minimal mitochondrial Bax accumulation. Cell Death. Differ. *17*, 278-290.

Eckelman,B.P., Salvesen,G.S., and Scott,F.L. (2006). Human inhibitor of apoptosis proteins: why XIAP is the black sheep of the family. EMBO Rep. *7*, 988-994.

Ehrenberg,B., Montana,V., Wei,M.D., Wuskell,J.P., and Loew,L.M. (1988). Membrane potential can be determined in individual cells from the nernstian distribution of cationic dyes. Biophys. J. *53*, 785-794.

Ellis,H.M. and Horvitz,H.R. (1986). Genetic control of programmed cell death in the nematode C. elegans. Cell *44*, 817-829.

Ellis,R.E., Yuan,J.Y., and Horvitz,H.R. (1991). Mechanisms and functions of cell death. Annu. Rev. Cell Biol. *7*, 663-698.

ENNIS,H.L. and LUBIN,M. (1964). CYCLOHEXIMIDE: ASPECTS OF INHIBITION OF PROTEIN SYNTHESIS IN MAMMALIAN CELLS. Science *146*, 1474-1476.

Enver,T., Heyworth,C.M., and Dexter,T.M. (1998). Do stem cells play dice? Blood *92*, 348-351.

Foyouzi-Youssefi,R., Arnaudeau,S., Borner,C., Kelley,W.L., Tschopp,J., Lew,D.P., Demaurex,N., and Krause,K.H. (2000). Bcl-2 decreases the free Ca2+ concentration within the endoplasmic reticulum. Proc. Natl. Acad. Sci. U. S. A *97*, 5723-5728.

Frank,S., Gaume,B., Bergmann-Leitner,E.S., Leitner,W.W., Robert,E.G., Catez,F., Smith,C.L., and Youle,R.J. (2001). The role of dynamin-related protein 1, a mediator of mitochondrial fission, in apoptosis. Dev. Cell *1*, 515-525.

Frey,T.G. and Mannella,C.A. (2000). The internal structure of mitochondria. Trends Biochem. Sci. *25*, 319-324.

Frezza,C., Cipolat,S., Martins,d.B., Micaroni,M., Beznoussenko,G.V., Rudka,T., Bartoli,D., Polishuck,R.S., Danial,N.N., De Strooper,B., and Scorrano,L. (2006). OPA1 controls apoptotic cristae remodeling independently from mitochondrial fusion. Cell *126*, 177-189.

Fu,J., Jin,Y., and Arend,L.J. (2003). Smac3, a novel Smac/DIABLO splicing variant, attenuates the stability and apoptosis-inhibiting activity of X-linked inhibitor of apoptosis protein. J. Biol. Chem. *278*, 52660-52672.

Fuentes-Prior,P. and Salvesen,G.S. (2004). The protein structures that shape caspase activity, specificity, activation and inhibition. Biochem. J. *384*, 201-232.

Fulda,S. and Debatin,K.M. (2006). Extrinsic versus intrinsic apoptosis pathways in anticancer chemotherapy. Oncogene *25*, 4798-4811.

Giam,M., Huang,D.C., and Bouillet,P. (2008). BH3-only proteins and their roles in programmed cell death. Oncogene *27 Suppl 1*, S128-S136.

Glucksmann (1951). Cell deaths in normal vertebrate ontogeny. Biol. Rev. Cambridge Philos. Soc. ***26***, 59-86.

Goldstein,J.C., Munoz-Pinedo,C., Ricci,J.E., Adams,S.R., Kelekar,A., Schuler,M., Tsien,R.Y., and Green,D.R. (2005). Cytochrome c is released in a single step during apoptosis. Cell Death. Differ. *12*, 453-462.

Goldstein,J.C., Waterhouse,N.J., Juin,P., Evan,G.I., and Green,D.R. (2000). The coordinate release of cytochrome c during apoptosis is rapid, complete and kinetically invariant. Nat. Cell Biol. *2*, 156-162.

Gottlieb,E., Armour,S.M., Harris,M.H., and Thompson,C.B. (2003). Mitochondrial membrane potential regulates matrix configuration and cytochrome c release during apoptosis. Cell Death. Differ. *10*, 709-717.

Goyal,L., McCall,K., Agapite,J., Hartwieg,E., and Steller,H. (2000). Induction of apoptosis by Drosophila reaper, hid and grim through inhibition of IAP function. EMBO J. *19*, 589-597.

Grether,M.E., Abrams,J.M., Agapite,J., White,K., and Steller,H. (1995). The head involution defective gene of Drosophila melanogaster functions in programmed cell death. Genes Dev. *9*, 1694-1708.

Griesbeck,O., Baird,G.S., Campbell,R.E., Zacharias,D.A., and Tsien,R.Y. (2001). Reducing the environmental sensitivity of yellow fluorescent protein. Mechanism and applications. J. Biol. Chem. *276*, 29188-29194.

Gross,A., Jockel,J., Wei,M.C., and Korsmeyer,S.J. (1998). Enforced dimerization of BAX results in its translocation, mitochondrial dysfunction and apoptosis. EMBO J. *17*, 3878-3885.

Gu,J., Xia,X., Yan,P., Liu,H., Podust,V.N., Reynolds,A.B., and Fanning,E. (2004). Cell cycle-dependent regulation of a human DNA helicase that localizes in DNA damage foci. Mol. Biol. Cell *15*, 3320-3332.

Hakem,R., Hakem,A., Duncan,G.S., Henderson,J.T., Woo,M., Soengas,M.S., Elia,A., de la Pompa,J.L., Kagi,D., Khoo,W., Potter,J., Yoshida,R., Kaufman,S.A., Lowe,S.W.,

Penninger,J.M., and Mak,T.W. (1998). Differential requirement for caspase 9 in apoptotic pathways in vivo. Cell *94*, 339-352.

Hamburger,V. and Levi-Montalcini,R. (1949). Proliferation, differentiation and degeneration in the spinal ganglia of the chick embryo under normal and experimental conditions. J. Exp. Zool. *111*, 457-501.

Hansen,T.M., Smith,D.J., and Nagley,P. (2006). Smac/DIABLO is not released from mitochondria during apoptotic signalling in cells deficient in cytochrome c. Cell Death. Differ. *13*, 1181-1190.

Hao,Z., Duncan,G.S., Chang,C.C., Elia,A., Fang,M., Wakeham,A., Okada,H., Calzascia,T., Jang,Y., You-Ten,A., Yeh,W.C., Ohashi,P., Wang,X., and Mak,T.W. (2005). Specific ablation of the apoptotic functions of cytochrome C reveals a differential requirement for cytochrome C and Apaf-1 in apoptosis. Cell *121*, 579-591.

Harada,H., Becknell,B., Wilm,M., Mann,M., Huang,L.J., Taylor,S.S., Scott,J.D., and Korsmeyer,S.J. (1999). Phosphorylation and inactivation of BAD by mitochondria-anchored protein kinase A. Mol. Cell *3*, 413-422.

Heim,R., Cubitt,A.B., and Tsien,R.Y. (1995). Improved green fluorescence. Nature *373*, 663-664.

Heim,R., Prasher,D.C., and Tsien,R.Y. (1994). Wavelength mutations and posttranslational autoxidation of green fluorescent protein. Proc. Natl. Acad. Sci. U. S. A *91*, 12501-12504.

Hitomi,J., Christofferson,D.E., Ng,A., Yao,J., Degterev,A., Xavier,R.J., and Yuan,J. (2008). Identification of a molecular signaling network that regulates a cellular necrotic cell death pathway. Cell *135*, 1311-1323.

Hockenbery,D., Nunez,G., Milliman,C., Schreiber,R.D., and Korsmeyer,S.J. (1990). Bcl-2 is an inner mitochondrial membrane protein that blocks programmed cell death. Nature *348*, 334-336.

Honarpour,N., Du,C., Richardson,J.A., Hammer,R.E., Wang,X., and Herz,J. (2000). Adult Apaf-1-deficient mice exhibit male infertility. Dev. Biol. *218*, 248-258.

Hoppins,S., Lackner,L., and Nunnari,J. (2007). The machines that divide and fuse mitochondria. Annu. Rev. Biochem. *76*, 751-780.

Hsu,Y.T., Wolter,K.G., and Youle,R.J. (1997). Cytosol-to-membrane redistribution of Bax and Bcl-X(L) during apoptosis. Proc. Natl. Acad. Sci. U. S. A *94*, 3668-3672.

Hsu,Y.T. and Youle,R.J. (1997). Nonionic detergents induce dimerization among members of the Bcl-2 family. J. Biol. Chem. *272*, 13829-13834.

Hu,Y., Ding,L., Spencer,D.M., and Nunez,G. (1998). WD-40 repeat region regulates Apaf-1 self-association and procaspase-9 activation. J. Biol. Chem. *273*, 33489-33494.

Huang,Y., Rich,R.L., Myszka,D.G., and Wu,H. (2003). Requirement of both the second and third BIR domains for the relief of X-linked inhibitor of apoptosis protein (XIAP)-mediated caspase inhibition by Smac. J. Biol. Chem. *278*, 49517-49522.

Hubner,A., Barrett,T., Flavell,R.A., and Davis,R.J. (2008). Multisite phosphorylation regulates Bim stability and apoptotic activity. Mol. Cell *30*, 415-425.

Hueber,A., Durka,S., and Weller,M. (1998). CD95-mediated apoptosis: no variation in cellular sensitivity during cell cycle progression. FEBS Lett. *432*, 155-157.

Huser,J., Rechenmacher,C.E., and Blatter,L.A. (1998). Imaging the permeability pore transition in single mitochondria. Biophys. J. *74*, 2129-2137.

Janes,K.A., Gaudet,S., Albeck,J.G., Nielsen,U.B., Lauffenburger,D.A., and Sorger,P.K. (2006). The response of human epithelial cells to TNF involves an inducible autocrine cascade. Cell *124*, 1225-1239.

Ji,C., Marnett,L.J., and Pietenpol,J.A. (1997). Cell cycle re-entry following chemically-induced cell cycle synchronization leads to elevated p53 and p21 protein levels. Oncogene *15*, 2749-2753.

Kaern,M., Elston,T.C., Blake,W.J., and Collins,J.J. (2005). Stochasticity in gene expression: from theories to phenotypes. Nat. Rev. Genet. *6*, 451-464.

Kalderon,D., Roberts,B.L., Richardson,W.D., and Smith,A.E. (1984). A short amino acid sequence able to specify nuclear localization. Cell *39*, 499-509.

Kandasamy,K., Srinivasula,S.M., Alnemri,E.S., Thompson,C.B., Korsmeyer,S.J., Bryant,J.L., and Srivastava,R.K. (2003). Involvement of proapoptotic molecules Bax and Bak in tumor necrosis factor-related apoptosis-inducing ligand (TRAIL)-induced mitochondrial disruption and apoptosis: differential regulation of cytochrome c and Smac/DIABLO release. Cancer Res. *63*, 1712-1721.

Karbowski,M., Lee,Y.J., Gaume,B., Jeong,S.Y., Frank,S., Nechushtan,A., Santel,A., Fuller,M., Smith,C.L., and Youle,R.J. (2002). Spatial and temporal association of Bax with mitochondrial fission sites, Drp1, and Mfn2 during apoptosis. J. Cell Biol. *159*, 931-938.

Karbowski,M., Norris,K.L., Cleland,M.M., Jeong,S.Y., and Youle,R.J. (2006). Role of Bax and Bak in mitochondrial morphogenesis. Nature *443*, 658-662.

Kaufmann,B.B., Yang,Q., Mettetal,J.T., and van Oudenaarden,A. (2007). Heritable stochastic switching revealed by single-cell genealogy. PLoS. Biol. *5*, e239.

Kerr,J.F. (1969). An electron-microscope study of liver cell necrosis due to heliotrine. J. Pathol. *97*, 557-562.

Kerr,J.F. (1970). An electron microscopic study of liver cell necrosis due to albitocin. Pathology *2*, 251-259.

Kerr,J.F. (1971). Shrinkage necrosis: a distinct mode of cellular death. J. Pathol. *105*, 13-20.

Kerr,J.F., Wyllie,A.H., and Currie,A.R. (1972). Apoptosis: a basic biological phenomenon with wide-ranging implications in tissue kinetics. Br. J. Cancer *26*, 239-257.

Kim,H., Rafiuddin-Shah,M., Tu,H.C., Jeffers,J.R., Zambetti,G.P., Hsieh,J.J., and Cheng,E.H. (2006). Hierarchical regulation of mitochondrion-dependent apoptosis by BCL-2 subfamilies. Nat. Cell Biol. *8*, 1348-1358.

Kluck,R.M., Bossy-Wetzel,E., Green,D.R., and Newmeyer,D.D. (1997). The release of cytochrome c from mitochondria: a primary site for Bcl-2 regulation of apoptosis. Science *275*, 1132-1136.

Kokoszka,J.E., Waymire,K.G., Levy,S.E., Sligh,J.E., Cai,J., Jones,D.P., MacGregor,G.R., and Wallace,D.C. (2004). The ADP/ATP translocator is not essential for the mitochondrial permeability transition pore. Nature *427*, 461-465.

Kornbluth,S. and White,K. (2005). Apoptosis in Drosophila: neither fish nor fowl (nor man, nor worm). J. Cell Sci. *118*, 1779-1787.

Kroemer,G., Galluzzi,L., and Brenner,C. (2007). Mitochondrial membrane permeabilization in cell death. Physiol Rev. *87*, 99-163.

Kuida,K., Haydar,T.F., Kuan,C.Y., Gu,Y., Taya,C., Karasuyama,H., Su,M.S., Rakic,P., and Flavell,R.A. (1998). Reduced apoptosis and cytochrome c-mediated caspase activation in mice lacking caspase 9. Cell *94*, 325-337.

Kuida,K., Zheng,T.S., Na,S., Kuan,C., Yang,D., Karasuyama,H., Rakic,P., and Flavell,R.A. (1996). Decreased apoptosis in the brain and premature lethality in CPP32-deficient mice. Nature *384*, 368-372.

Kumar,S. (2007). Caspase function in programmed cell death. Cell Death. Differ. *14*, 32-43.

Kussell,E. and Leibler,S. (2005). Phenotypic diversity, population growth, and information in fluctuating environments. Science *309*, 2075-2078.

Kuwana,T., Mackey,M.R., Perkins,G., Ellisman,M.H., Latterich,M., Schneiter,R., Green,D.R., and Newmeyer,D.D. (2002). Bid, Bax, and lipids cooperate to form supramolecular openings in the outer mitochondrial membrane. Cell *111*, 331-342.

LaCasse,E.C., Mahoney,D.J., Cheung,H.H., Plenchette,S., Baird,S., and Korneluk,R.G. (2008). IAP-targeted therapies for cancer. Oncogene *27*, 6252-6275.

Lacasse,E.C., Mahoney,D.J., Cheung,H.H., Plenchette,S., Baird,S., and Korneluk,R.G. (2008). IAP-targeted therapies for cancer. Oncogene *27*, 6252-6275.

Lakhani,S.A., Masud,A., Kuida,K., Porter,G.A., Jr., Booth,C.J., Mehal,W.Z., Inayat,I., and Flavell,R.A. (2006). Caspases 3 and 7: key mediators of mitochondrial events of apoptosis. Science *311*, 847-851.

Lanford,R.E., Kanda,P., and Kennedy,R.C. (1986). Induction of nuclear transport with a synthetic peptide homologous to the SV40 T antigen transport signal. Cell *46*, 575-582.

Lartigue,L., Medina,C., Schembri,L., Chabert,P., Zanese,M., Tomasello,F., Dalibart,R., Thoraval,D., Crouzet,M., Ichas,F., and De Giorgi,F. (2008). An intracellular wave of cytochrome c propagates and precedes Bax redistribution during apoptosis. J. Cell Sci. *121*, 3515-3523.

Lee,K.H., Feig,C., Tchikov,V., Schickel,R., Hallas,C., Schutze,S., Peter,M.E., and Chan,A.C. (2006). The role of receptor internalization in CD95 signaling. EMBO J. *25*, 1009-1023.

Lei,K. and Davis,R.J. (2003). JNK phosphorylation of Bim-related members of the Bcl2 family induces Bax-dependent apoptosis. Proc. Natl. Acad. Sci. U. S. A *100*, 2432-2437.

Letai,A., Bassik,M.C., Walensky,L.D., Sorcinelli,M.D., Weiler,S., and Korsmeyer,S.J. (2002). Distinct BH3 domains either sensitize or activate mitochondrial apoptosis, serving as prototype cancer therapeutics. Cancer Cell *2*, 183-192.

Levi-Montalcini,R. (1987). The nerve growth factor: thirty-five years later. EMBO J. *6*, 1145-1154.

Li,H., Zhu,H., Xu,C.J., and Yuan,J. (1998). Cleavage of BID by caspase 8 mediates the mitochondrial damage in the Fas pathway of apoptosis. Cell *94*, 491-501.

Li,K., Li,Y., Shelton,J.M., Richardson,J.A., Spencer,E., Chen,Z.J., Wang,X., and Williams,R.S. (2000). Cytochrome c deficiency causes embryonic lethality and attenuates stress-induced apoptosis. Cell *101*, 389-399.

Li,P., Nijhawan,D., Budihardjo,I., Srinivasula,S.M., Ahmad,M., Alnemri,E.S., and Wang,X. (1997). Cytochrome c and dATP-dependent formation of Apaf-1/caspase-9 complex initiates an apoptotic protease cascade. Cell *91*, 479-489.

Liu,X., Kim,C.N., Yang,J., Jemmerson,R., and Wang,X. (1996). Induction of apoptotic program in cell-free extracts: requirement for dATP and cytochrome c. Cell *86*, 147-157.

Liu,X., Zou,H., Slaughter,C., and Wang,X. (1997). DFF, a heterodimeric protein that functions downstream of caspase-3 to trigger DNA fragmentation during apoptosis. Cell *89*, 175-184.

Livet,J., Weissman,T.A., Kang,H., Draft,R.W., Lu,J., Bennis,R.A., Sanes,J.R., and Lichtman,J.W. (2007). Transgenic strategies for combinatorial expression of fluorescent proteins in the nervous system. Nature *450*, 56-62.

Lockshin,R.A. (1969). Programmed cell death. Activation of lysis by a mechanism involving the synthesis of protein. J. Insect Physiol *15*, 1505-1516.

Loewer,A. and Lahav,G. (2006). Cellular conference call: external feedback affects cell-fate decisions. Cell *124*, 1128-1130.

Lomonosova,E. and Chinnadurai,G. (2008). BH3-only proteins in apoptosis and beyond: an overview. Oncogene *27 Suppl 1*, S2-19.

Lovell,J.F., Billen,L.P., Bindner,S., Shamas-Din,A., Fradin,C., Leber,B., and Andrews,D.W. (2008). Membrane binding by tBid initiates an ordered series of events culminating in membrane permeabilization by Bax. Cell *135*, 1074-1084.

Majno,G. and Joris,I. (1995). Apoptosis, oncosis, and necrosis. An overview of cell death. Am. J. Pathol. *146*, 3-15.

Martinez-Caballero,S., Dejean,L.M., Kinnally,M.S., Oh,K.J., Mannella,C.A., and Kinnally,K.W. (2009). Assembly of the mitochondrial apoptosis-induced channel, MAC. J. Biol. Chem. *284*, 12235-12245.

Martinou,J.C. and Youle,R.J. (2006). Which came first, the cytochrome c release or the mitochondrial fission? Cell Death. Differ. *13*, 1291-1295.

Matz,M.V., Fradkov,A.F., Labas,Y.A., Savitsky,A.P., Zaraisky,A.G., Markelov,M.L., and Lukyanov,S.A. (1999). Fluorescent proteins from nonbioluminescent Anthozoa species. Nat. Biotechnol. *17*, 969-973.

McAdams,H.H. and Arkin,A. (1998). Simulation of prokaryotic genetic circuits. Annu. Rev. Biophys. Biomol. Struct. *27*, 199-224.

McDonnell,T.J. and Korsmeyer,S.J. (1991). Progression from lymphoid hyperplasia to high-grade malignant lymphoma in mice transgenic for the t(14; 18). Nature *349*, 254-256.

McLaughlin,R.E. and Denny,J.B. (1999). Palmitoylation of GAP-43 by the ER-Golgi intermediate compartment and Golgi apparatus. Biochim. Biophys. Acta *1451*, 82-92.

McStay,G.P., Salvesen,G.S., and Green,D.R. (2008). Overlapping cleavage motif selectivity of caspases: implications for analysis of apoptotic pathways. Cell Death. Differ. *15*, 322-331.

Meyer,H.A., Grau,H., Kraft,R., Kostka,S., Prehn,S., Kalies,K.U., and Hartmann,E. (2000). Mammalian Sec61 is associated with Sec62 and Sec63. J. Biol. Chem. *275*, 14550-14557.

Micheau,O. and Tschopp,J. (2003). Induction of TNF receptor I-mediated apoptosis via two sequential signaling complexes. Cell *114*, 181-190.

Mittl,P.R., Di Marco,S., Krebs,J.F., Bai,X., Karanewsky,D.S., Priestle,J.P., Tomaselli,K.J., and Grutter,M.G. (1997). Structure of recombinant human CPP32 in complex with the tetrapeptide acetyl-Asp-Val-Ala-Asp fluoromethyl ketone. J. Biol. Chem. *272*, 6539-6547.

Muchmore,S.W., Sattler,M., Liang,H., Meadows,R.P., Harlan,J.E., Yoon,H.S., Nettesheim,D., Chang,B.S., Thompson,C.B., Wong,S.L., Ng,S.L., and Fesik,S.W. (1996). X-ray and NMR structure of human Bcl-xL, an inhibitor of programmed cell death. Nature *381*, 335-341.

Munoz-Pinedo,C., Guio-Carrion,A., Goldstein,J.C., Fitzgerald,P., Newmeyer,D.D., and Green,D.R. (2006). Different mitochondrial intermembrane space proteins are released during apoptosis in a manner that is coordinately initiated but can vary in duration. Proc. Natl. Acad. Sci. U. S. A *103*, 11573-11578.

Muzio,M., Chinnaiyan,A.M., Kischkel,F.C., O'Rourke,K., Shevchenko,A., Ni,J., Scaffidi,C., Bretz,J.D., Zhang,M., Gentz,R., Mann,M., Krammer,P.H., Peter,M.E., and Dixit,V.M. (1996). FLICE, a novel FADD-homologous ICE/CED-3-like protease, is recruited to the CD95 (Fas/APO-1) death--inducing signaling complex. Cell *85*, 817-827.

Nasmyth,K., Nurse,P., and Fraser,R.S. (1979). The effect of cell mass on the cell cycle timing and duration of S-phase in fission yeast. J. Cell Sci. *39*, 215-233.

Nechushtan,A., Smith,C.L., Lamensdorf,I., Yoon,S.H., and Youle,R.J. (2001). Bax and Bak coalesce into novel mitochondria-associated clusters during apoptosis. J. Cell Biol. *153*, 1265-1276.

Newman,J.R. and Weissman,J.S. (2006). Systems biology: many things from one. Nature *444*, 561-562.

Newmeyer,D.D., Farschon,D.M., and Reed,J.C. (1994). Cell-free apoptosis in Xenopus egg extracts: inhibition by Bcl-2 and requirement for an organelle fraction enriched in mitochondria. Cell *79*, 353-364.

Nguyen,A.W. and Daugherty,P.S. (2005). Evolutionary optimization of fluorescent proteins for intracellular FRET. Nat. Biotechnol. *23*, 355-360.

Nguyen,M., Marcellus,R.C., Roulston,A., Watson,M., Serfass,L., Murthy,M., Sr., Goulet,D., Viallet,J., Belec,L., Billot,X., Acoca,S., Purisima,E., Wiegmans,A., Cluse,L., Johnstone,R.W., Beauparlant,P., and Shore,G.C. (2007). Small molecule obatoclax (GX15-070) antagonizes MCL-1 and overcomes MCL-1-mediated resistance to apoptosis. Proc. Natl. Acad. Sci. U. S. A *104*, 19512-19517.

Okada,H., Suh,W.K., Jin,J., Woo,M., Du,C., Elia,A., Duncan,G.S., Wakeham,A., Itie,A., Lowe,S.W., Wang,X., and Mak,T.W. (2002). Generation and characterization of Smac/DIABLO-deficient mice. Mol. Cell Biol. *22*, 3509-3517.

Oltersdorf,T., Elmore,S.W., Shoemaker,A.R., Armstrong,R.C., Augeri,D.J., Belli,B.A., Bruncko,M., Deckwerth,T.L., Dinges,J., Hajduk,P.J., Joseph,M.K., Kitada,S., Korsmeyer,S.J., Kunzer,A.R., Letai,A., Li,C., Mitten,M.J., Nettesheim,D.G., Ng,S., Nimmer,P.M., O'Connor,J.M., Oleksijew,A., Petros,A.M., Reed,J.C., Shen,W., Tahir,S.K., Thompson,C.B., Tomaselli,K.J., Wang,B., Wendt,M.D., Zhang,H., Fesik,S.W., and Rosenberg,S.H. (2005). An inhibitor of Bcl-2 family proteins induces regression of solid tumours. Nature *435*, 677-681.

Ott,M., Robertson,J.D., Gogvadze,V., Zhivotovsky,B., and Orrenius,S. (2002). Cytochrome c release from mitochondria proceeds by a two-step process. Proc. Natl. Acad. Sci. U. S. A *99*, 1259-1263.

Ott,M., Zhivotovsky,B., and Orrenius,S. (2007). Role of cardiolipin in cytochrome c release from mitochondria. Cell Death. Differ. *14*, 1243-1247.

Ow,Y.P., Green,D.R., Hao,Z., and Mak,T.W. (2008). Cytochrome c: functions beyond respiration. Nat. Rev. Mol. Cell Biol. *9*, 532-542.

Pacher,P. and Hajnoczky,G. (2001). Propagation of the apoptotic signal by mitochondrial waves. EMBO J *20*, 4107-4121.

Palade,G.E. (1953). An electron microscope study of the mitochondrial structure. J. Histochem. Cytochem. *1*, 188-211.

Palmer,A.E., Jin,C., Reed,J.C., and Tsien,R.Y. (2004). Bcl-2-mediated alterations in endoplasmic reticulum Ca2+ analyzed with an improved genetically encoded fluorescent sensor. Proc. Natl. Acad. Sci. U. S. A *101*, 17404-17409.

Pedrola,L., Espert,A., Wu,X., Claramunt,R., Shy,M.E., and Palau,F. (2005). GDAP1, the protein causing Charcot-Marie-Tooth disease type 4A, is expressed in neurons and is associated with mitochondria. Hum. Mol. Genet. *14*, 1087-1094.

Pellegrini,L. and Scorrano,L. (2007). A cut short to death: Parl and Opa1 in the regulation of mitochondrial morphology and apoptosis. Cell Death. Differ. *14*, 1275-1284.

Pop,C. and Salvesen,G.S. (2009). Human caspases: activation, specificity, and regulation. J. Biol. Chem. *284*, 21777-21781.

Porter,K.R., Claude,A., and Fullam,E.F. (1945). A STUDY OF TISSUE CULTURE CELLS BY ELECTRON MICROSCOPY : METHODS AND PRELIMINARY OBSERVATIONS. J. Exp. Med. *81*, 233-246.

Prasher,D.C., Eckenrode,V.K., Ward,W.W., Prendergast,F.G., and Cormier,M.J. (1992). Primary structure of the Aequorea victoria green-fluorescent protein. Gene *111*, 229-233.

Rao,C.V., Wolf,D.M., and Arkin,A.P. (2002). Control, exploitation and tolerance of intracellular noise. Nature *420*, 231-237.

Raychaudhuri,S., Willgohs,E., Nguyen,T.N., Khan,E.M., and Goldkorn,T. (2008). Monte Carlo simulation of cell death signaling predicts large cell-to-cell stochastic fluctuations through the type 2 pathway of apoptosis. Biophys. J. *95*, 3559-3562.

Rehm,M., Dussmann,H., and Prehn,J.H. (2003). Real-time single cell analysis of Smac/DIABLO release during apoptosis. J. Cell Biol. *162*, 1031-1043.

Renatus,M., Stennicke,H.R., Scott,F.L., Liddington,R.C., and Salvesen,G.S. (2001). Dimer formation drives the activation of the cell death protease caspase 9. Proc. Natl. Acad. Sci. U. S. A *98*, 14250-14255.

Riedl,S.J., Fuentes-Prior,P., Renatus,M., Kairies,N., Krapp,S., Huber,R., Salvesen,G.S., and Bode,W. (2001). Structural basis for the activation of human procaspase-7. Proc. Natl. Acad. Sci. U. S. A *98*, 14790-14795.

Rizzo,M.A., Springer,G.H., Granada,B., and Piston,D.W. (2004). An improved cyan fluorescent protein variant useful for FRET. Nat. Biotechnol. *22*, 445-449.

Rizzuto,R., Brini,M., Pizzo,P., Murgia,M., and Pozzan,T. (1995). Chimeric green fluorescent protein as a tool for visualizing subcellular organelles in living cells. Curr. Biol. *5*, 635-642.

Rizzuto,R., Pinton,P., Carrington,W., Fay,F.S., Fogarty,K.E., Lifshitz,L.M., Tuft,R.A., and Pozzan,T. (1998). Close contacts with the endoplasmic reticulum as determinants of mitochondrial Ca2+ responses. Science *280*, 1763-1766.

Roberts,D.L., Merrison,W., MacFarlane,M., and Cohen,G.M. (2001). The inhibitor of apoptosis protein-binding domain of Smac is not essential for its proapoptotic activity. J. Cell Biol. *153*, 221-228.

Rodriguez,J. and Lazebnik,Y. (1999). Caspase-9 and APAF-1 form an active holoenzyme. Genes Dev. *13*, 3179-3184.

Rotonda,J., Nicholson,D.W., Fazil,K.M., Gallant,M., Gareau,Y., Labelle,M., Peterson,E.P., Rasper,D.M., Ruel,R., Vaillancourt,J.P., Thornberry,N.A., and Becker,J.W. (1996). The three-dimensional structure of apopain/CPP32, a key mediator of apoptosis. Nat. Struct. Biol. *3*, 619-625.

ROUILLER,C. (1957). [Electron microscopy for the study of the normal & pathological liver.]. Ann. Anat. Pathol. (Paris) *2*, 548-562.

Roy,N., Deveraux,Q.L., Takahashi,R., Salvesen,G.S., and Reed,J.C. (1997). The c-IAP-1 and c-IAP-2 proteins are direct inhibitors of specific caspases. EMBO J. *16*, 6914-6925.

Saito,M., Korsmeyer,S.J., and Schlesinger,P.H. (2000). BAX-dependent transport of cytochrome c reconstituted in pure liposomes. Nat. Cell Biol. *2*, 553-555.

Salvesen,G.S. and Duckett,C.S. (2002). IAP proteins: blocking the road to death's door. Nat. Rev. Mol. Cell Biol. *3*, 401-410.

Schultz,B.E. and Chan,S.I. (2001). Structures and proton-pumping strategies of mitochondrial respiratory enzymes. Annu. Rev. Biophys. Biomol. Struct. *30*, 23-65.

Scorrano,L., Ashiya,M., Buttle,K., Weiler,S., Oakes,S.A., Mannella,C.A., and Korsmeyer,S.J. (2002). A distinct pathway remodels mitochondrial cristae and mobilizes cytochrome c during apoptosis. Dev. Cell *2*, 55-67.

Scorrano,L., Oakes,S.A., Opferman,J.T., Cheng,E.H., Sorcinelli,M.D., Pozzan,T., and Korsmeyer,S.J. (2003). BAX and BAK regulation of endoplasmic reticulum Ca2+: a control point for apoptosis. Science *300*, 135-139.

Scott,F.L., Denault,J.B., Riedl,S.J., Shin,H., Renatus,M., and Salvesen,G.S. (2005). XIAP inhibits caspase-3 and -7 using two binding sites: evolutionarily conserved mechanism of IAPs. EMBO J. *24*, 645-655.

Shaner,N.C., Campbell,R.E., Steinbach,P.A., Giepmans,B.N., Palmer,A.E., and Tsien,R.Y. (2004). Improved monomeric red, orange and yellow fluorescent proteins derived from Discosoma sp. red fluorescent protein. Nat. Biotechnol. *22*, 1567-1572.

Shaner,N.C., Steinbach,P.A., and Tsien,R.Y. (2005). A guide to choosing fluorescent proteins. Nat. Methods *2*, 905-909.

Shi,Y. (2004). Caspase activation: revisiting the induced proximity model. Cell *117*, 855-858.

Shimizu,S., Narita,M., and Tsujimoto,Y. (1999). Bcl-2 family proteins regulate the release of apoptogenic cytochrome c by the mitochondrial channel VDAC. Nature *399*, 483-487.

Shimomura,O. (2009). Discovery of green fluorescent protein (GFP) (Nobel Lecture). Angew. Chem. Int. Ed Engl. *48*, 5590-5602.

Shiozaki,E.N., Chai,J., Rigotti,D.J., Riedl,S.J., Li,P., Srinivasula,S.M., Alnemri,E.S., Fairman,R., and Shi,Y. (2003). Mechanism of XIAP-mediated inhibition of caspase-9. Mol. Cell *11*, 519-527.

SIEGEL,M.R. and SISLER,H.D. (1963). INHIBITION OF PROTEIN SYNTHESIS IN VITRO BY CYCLOHEXIMIDE. Nature *200*, 675-676.

Siegel,R.M., Muppidi,J.R., Sarker,M., Lobito,A., Jen,M., Martin,D., Straus,S.E., and Lenardo,M.J. (2004). SPOTS: signaling protein oligomeric transduction structures are early mediators of death receptor-induced apoptosis at the plasma membrane. J. Cell Biol. *167*, 735-744.

Sigal,A., Milo,R., Cohen,A., Geva-Zatorsky,N., Klein,Y., Alaluf,I., Swerdlin,N., Perzov,N., Danon,T., Liron,Y., Raveh,T., Carpenter,A.E., Lahav,G., and Alon,U. (2006a). Dynamic proteomics in individual human cells uncovers widespread cell-cycle dependence of nuclear proteins. Nat. Methods *3*, 525-531.

Sigal,A., Milo,R., Cohen,A., Geva-Zatorsky,N., Klein,Y., Liron,Y., Rosenfeld,N., Danon,T., Perzov,N., and Alon,U. (2006b). Variability and memory of protein levels in human cells. Nature *444*, 643-646.

Skene,J.H. and Virag,I. (1989). Posttranslational membrane attachment and dynamic fatty acylation of a neuronal growth cone protein, GAP-43. J. Cell Biol. *108*, 613-624.

Slater,E.C. (1977). Mechanism of oxidative phosphorylation. Annu. Rev. Biochem. *46*, 1015-1026.

Slee,E.A., Harte,M.T., Kluck,R.M., Wolf,B.B., Casiano,C.A., Newmeyer,D.D., Wang,H.G., Reed,J.C., Nicholson,D.W., Alnemri,E.S., Green,D.R., and Martin,S.J. (1999). Ordering the cytochrome c-initiated caspase cascade: hierarchical activation of caspases-2, -3, -6, -7, -8, and -10 in a caspase-9-dependent manner. J. Cell Biol. *144*, 281-292.

Spencer,S.L., Gaudet,S., Albeck,J.G., Burke,J.M., and Sorger,P.K. (2009). Non-genetic origins of cell-to-cell variability in TRAIL-induced apoptosis. Nature *459*, 428-432.

Spudich,J.L. and Koshland,D.E., Jr. (1976). Non-genetic individuality: chance in the single cell. Nature *262*, 467-471.

Srinivasula,S.M., Hegde,R., Saleh,A., Datta,P., Shiozaki,E., Chai,J., Lee,R.A., Robbins,P.D., Fernandes-Alnemri,T., Shi,Y., and Alnemri,E.S. (2001). A conserved XIAP-interaction motif in caspase-9 and Smac/DIABLO regulates caspase activity and apoptosis. Nature *410*, 112-116.

Stacey,D.W., Hitomi,M., and Chen,G. (2000). Influence of cell cycle and oncogene activity upon topoisomerase IIalpha expression and drug toxicity. Mol. Cell Biol. *20*, 9127-9137.

Stennicke,H.R., Deveraux,Q.L., Humke,E.W., Reed,J.C., Dixit,V.M., and Salvesen,G.S. (1999). Caspase-9 can be activated without proteolytic processing. J. Biol. Chem. *274*, 8359-8362.

Stennicke,H.R., Jurgensmeier,J.M., Shin,H., Deveraux,Q., Wolf,B.B., Yang,X., Zhou,Q., Ellerby,H.M., Ellerby,L.M., Bredesen,D., Green,D.R., Reed,J.C., Froelich,C.J., and Salvesen,G.S. (1998). Pro-caspase-3 is a major physiologic target of caspase-8. J. Biol. Chem. *273*, 27084-27090.

Stennicke,H.R., Renatus,M., Meldal,M., and Salvesen,G.S. (2000). Internally quenched fluorescent peptide substrates disclose the subsite preferences of human caspases 1, 3, 6, 7 and 8. Biochem. J. *350 Pt 2*, 563-568.

Strasser,A., Harris,A.W., Bath,M.L., and Cory,S. (1990). Novel primitive lymphoid tumours induced in transgenic mice by cooperation between myc and bcl-2. Nature *348*, 331-333.

Suda,T., Takahashi,T., Golstein,P., and Nagata,S. (1993). Molecular cloning and expression of the Fas ligand, a novel member of the tumor necrosis factor family. Cell *75*, 1169-1178.

Suen,D.F., Norris,K.L., and Youle,R.J. (2008). Mitochondrial dynamics and apoptosis. Genes Dev. *22*, 1577-1590.

Sulston,J.E. (1976). Post-embryonic development in the ventral cord of Caenorhabditis elegans. Philos. Trans. R. Soc. Lond B Biol. Sci. *275*, 287-297.

Sulston,J.E. and Horvitz,H.R. (1977). Post-embryonic cell lineages of the nematode, Caenorhabditis elegans. Dev. Biol. *56*, 110-156.

Sulston,J.E., Schierenberg,E., White,J.G., and Thomson,J.N. (1983). The embryonic cell lineage of the nematode Caenorhabditis elegans. Dev. Biol. *100*, 64-119.

Sun,M.G., Williams,J., Munoz-Pinedo,C., Perkins,G.A., Brown,J.M., Ellisman,M.H., Green,D.R., and Frey,T.G. (2007). Correlated three-dimensional light and electron microscopy reveals transformation of mitochondria during apoptosis. Nat. Cell Biol. *9*, 1057-1065.

Suzuki,M., Youle,R.J., and Tjandra,N. (2000). Structure of Bax: coregulation of dimer formation and intracellular localization. Cell *103*, 645-654.

Szabadkai,G., Simoni,A.M., Chami,M., Wieckowski,M.R., Youle,R.J., and Rizzuto,R. (2004). Drp-1-dependent division of the mitochondrial network blocks intraorganellar Ca2+ waves and protects against Ca2+-mediated apoptosis. Mol. Cell *16*, 59-68.

Takemoto,K., Kuranaga,E., Tonoki,A., Nagai,T., Miyawaki,A., and Miura,M. (2007). Local initiation of caspase activation in Drosophila salivary gland programmed cell death in vivo. Proc. Natl. Acad. Sci. U. S. A *104*, 13367-13372.

Taneja,P., Gu,J., Peng,R., Carrick,R., Uchiumi,F., Ott,R.D., Gustafson,E., Podust,V.N., and Fanning,E. (2002). A dominant-negative mutant of human DNA helicase B blocks the onset of chromosomal DNA replication. J. Biol. Chem. *277*, 40853-40861.

Tata,J.R. (1966). Requirement for RNA and protein synthesis for induced regression of the tadpole tail in organ culture. Dev. Biol. *13*, 77-94.

Tauber,A.I. (2003). Metchnikoff and the phagocytosis theory. Nat. Rev. Mol. Cell Biol. *4*, 897-901.

Thornberry,N.A., Bull,H.G., Calaycay,J.R., Chapman,K.T., Howard,A.D., Kostura,M.J., Miller,D.K., Molineaux,S.M., Weidner,J.R., Aunins,J., and . (1992). A novel heterodimeric cysteine protease is required for interleukin-1 beta processing in monocytes. Nature *356*, 768-774.

Thornberry,N.A., Rano,T.A., Peterson,E.P., Rasper,D.M., Timkey,T., Garcia-Calvo,M., Houtzager,V.M., Nordstrom,P.A., Roy,S., Vaillancourt,J.P., Chapman,K.T., and Nicholson,D.W. (1997). A combinatorial approach defines specificities of members of the caspase family and granzyme B. Functional relationships established for key mediators of apoptosis. J. Biol. Chem. *272*, 17907-17911.

Timmer,J.C. and Salvesen,G.S. (2007). Caspase substrates. Cell Death. Differ. *14*, 66-72.

Tinel,A. and Tschopp,J. (2004). The PIDDosome, a protein complex implicated in activation of caspase-2 in response to genotoxic stress. Science *304*, 843-846.

Traut,R.R. and Monro,R.E. (1964). The puromycin reaction and its relation to protein synthesis. J. Mol. Biol. *10*, 63-72.

Tu,S., McStay,G.P., Boucher,L.M., Mak,T., Beere,H.M., and Green,D.R. (2006). In situ trapping of activated initiator caspases reveals a role for caspase-2 in heat shock-induced apoptosis. Nat. Cell Biol. *8*, 72-77.

Varfolomeev,E.E., Schuchmann,M., Luria,V., Chiannilkulchai,N., Beckmann,J.S., Mett,I.L., Rebrikov,D., Brodianski,V.M., Kemper,O.C., Kollet,O., Lapidot,T., Soffer,D., Sobe,T., Avraham,K.B., Goncharov,T., Holtmann,H., Lonai,P., and Wallach,D. (1998). Targeted disruption of the mouse Caspase 8 gene ablates cell death induction by the TNF receptors, Fas/Apo1, and DR3 and is lethal prenatally. Immunity. *9*, 267-276.

Vaux,D.L., Cory,S., and Adams,J.M. (1988). Bcl-2 gene promotes haemopoietic cell survival and cooperates with c-myc to immortalize pre-B cells. Nature *335*, 440-442.

Vaux,D.L. and Korsmeyer,S.J. (1999). Cell death in development. Cell *96*, 245-254.

Vaux,D.L., Weissman,I.L., and Kim,S.K. (1992). Prevention of programmed cell death in Caenorhabditis elegans by human bcl-2. Science *258*, 1955-1957.

Veis,D.J., Sorenson,C.M., Shutter,J.R., and Korsmeyer,S.J. (1993). Bcl-2-deficient mice demonstrate fulminant lymphoid apoptosis, polycystic kidneys, and hypopigmented hair. Cell *75*, 229-240.

Vercesi,A.E., Moreno,S.N., Bernardes,C.F., Meinicke,A.R., Fernandes,E.C., and Docampo,R. (1993). Thapsigargin causes Ca2+ release and collapse of the membrane potential of Trypanosoma brucei mitochondria in situ and of isolated rat liver mitochondria. J. Biol. Chem. *268*, 8564-8568.

Verhagen,A.M., Ekert,P.G., Pakusch,M., Silke,J., Connolly,L.M., Reid,G.E., Moritz,R.L., Simpson,R.J., and Vaux,D.L. (2000). Identification of DIABLO, a mammalian protein that promotes apoptosis by binding to and antagonizing IAP proteins. Cell *102*, 43-53.

Walensky,L.D., Pitter,K., Morash,J., Oh,K.J., Barbuto,S., Fisher,J., Smith,E., Verdine,G.L., and Korsmeyer,S.J. (2006). A stapled BID BH3 helix directly binds and activates BAX. Mol. Cell *24*, 199-210.

Wang,C. and Youle,R.J. (2009). The role of mitochondria in apoptosis*. Annu. Rev. Genet. *43*, 95-118.

Wang,K., Yin,X.M., Chao,D.T., Milliman,C.L., and Korsmeyer,S.J. (1996). BID: a novel BH3 domain-only death agonist. Genes Dev. *10*, 2859-2869.

Waterhouse,N.J., Goldstein,J.C., von Ahsen,O., Schuler,M., Newmeyer,D.D., and Green,D.R. (2001). Cytochrome c maintains mitochondrial transmembrane potential and ATP generation after outer mitochondrial membrane permeabilization during the apoptotic process. J. Cell Biol. *153*, 319-328.

Wei,M.C., Lindsten,T., Mootha,V.K., Weiler,S., Gross,A., Ashiya,M., Thompson,C.B., and Korsmeyer,S.J. (2000). tBID, a membrane-targeted death ligand, oligomerizes BAK to release cytochrome c. Genes Dev. *14*, 2060-2071.

Wei,M.C., Zong,W.X., Cheng,E.H., Lindsten,T., Panoutsakopoulou,V., Ross,A.J., Roth,K.A., MacGregor,G.R., Thompson,C.B., and Korsmeyer,S.J. (2001). Proapoptotic BAX and BAK: a requisite gateway to mitochondrial dysfunction and death. Science *292*, 727-730.

Weinberger,L.S., Burnett,J.C., Toettcher,J.E., Arkin,A.P., and Schaffer,D.V. (2005). Stochastic gene expression in a lentiviral positive-feedback loop: HIV-1 Tat fluctuations drive phenotypic diversity. Cell *122*, 169-182.

Wertz,I.E. and Dixit,V.M. (2008). Ubiquitin-mediated regulation of TNFR1 signaling. Cytokine Growth Factor Rev. *19*, 313-324.

White,K., Grether,M.E., Abrams,J.M., Young,L., Farrell,K., and Steller,H. (1994). Genetic control of programmed cell death in Drosophila. Science *264*, 677-683.

Wiley,S.R., Schooley,K., Smolak,P.J., Din,W.S., Huang,C.P., Nicholl,J.K., Sutherland,G.R., Smith,T.D., Rauch,C., Smith,C.A., and . (1995). Identification and characterization of a new member of the TNF family that induces apoptosis. Immunity. *3*, 673-682.

Willis,S.N., Chen,L., Dewson,G., Wei,A., Naik,E., Fletcher,J.I., Adams,J.M., and Huang,D.C. (2005). Proapoptotic Bak is sequestered by Mcl-1 and Bcl-xL, but not Bcl-2, until displaced by BH3-only proteins. Genes Dev. *19*, 1294-1305.

Willis,S.N., Fletcher,J.I., Kaufmann,T., van Delft,M.F., Chen,L., Czabotar,P.E., Ierino,H., Lee,E.F., Fairlie,W.D., Bouillet,P., Strasser,A., Kluck,R.M., Adams,J.M., and Huang,D.C. (2007). Apoptosis initiated when BH3 ligands engage multiple Bcl-2 homologs, not Bax or Bak. Science *315*, 856-859.

Wilson,R., Goyal,L., Ditzel,M., Zachariou,A., Baker,D.A., Agapite,J., Steller,H., and Meier,P. (2002). The DIAP1 RING finger mediates ubiquitination of Dronc and is indispensable for regulating apoptosis. Nat. Cell Biol. *4*, 445-450.

Wright,M.E., Han,D.K., and Hockenbery,D.M. (2000). Caspase-3 and inhibitor of apoptosis protein(s) interactions in Saccharomyces cerevisiae and mammalian cells. FEBS Lett. *481*, 13-18.

Wu,G., Chai,J., Suber,T.L., Wu,J.W., Du,C., Wang,X., and Shi,Y. (2000). Structural basis of IAP recognition by Smac/DIABLO. Nature *408*, 1008-1012.

Xu,X., Gerard,A.L., Huang,B.C., Anderson,D.C., Payan,D.G., and Luo,Y. (1998). Detection of programmed cell death using fluorescence energy transfer. Nucleic Acids Res. *26*, 2034-2035.

Yan,N. and Shi,Y. (2005). Mechanisms of apoptosis through structural biology. Annu. Rev. Cell Dev. Biol. *21*, 35-56.

Yang,J., Liu,X., Bhalla,K., Kim,C.N., Ibrado,A.M., Cai,J., Peng,T.I., Jones,D.P., and Wang,X. (1997). Prevention of apoptosis by Bcl-2: release of cytochrome c from mitochondria blocked. Science *275*, 1129-1132.

Yoshida,H., Kong,Y.Y., Yoshida,R., Elia,A.J., Hakem,A., Hakem,R., Penninger,J.M., and Mak,T.W. (1998). Apaf1 is required for mitochondrial pathways of apoptosis and brain development. Cell *94*, 739-750.

Youle,R.J. and Strasser,A. (2008). The BCL-2 protein family: opposing activities that mediate cell death. Nat. Rev. Mol. Cell Biol. *9*, 47-59.

Yuan,J., Shaham,S., Ledoux,S., Ellis,H.M., and Horvitz,H.R. (1993). The C. elegans cell death gene ced-3 encodes a protein similar to mammalian interleukin-1 beta-converting enzyme. Cell *75*, 641-652.

Zha,H., Aime-Sempe,C., Sato,T., and Reed,J.C. (1996a). Proapoptotic protein Bax heterodimerizes with Bcl-2 and homodimerizes with Bax via a novel domain (BH3) distinct from BH1 and BH2. J. Biol. Chem. *271*, 7440-7444.

Zha,J., Harada,H., Yang,E., Jockel,J., and Korsmeyer,S.J. (1996b). Serine phosphorylation of death agonist BAD in response to survival factor results in binding to 14-3-3 not BCL-X(L). Cell *87*, 619-628.

Zhuang,J., Dinsdale,D., and Cohen,G.M. (1998). Apoptosis, in human monocytic THP.1 cells, results in the release of cytochrome c from mitochondria prior to their ultracondensation, formation of outer membrane discontinuities and reduction in inner membrane potential. Cell Death. Differ. *5*, 953-962.

Zong,W.X., Li,C., Hatzivassiliou,G., Lindsten,T., Yu,Q.C., Yuan,J., and Thompson,C.B. (2003). Bax and Bak can localize to the endoplasmic reticulum to initiate apoptosis. J. Cell Biol. *162*, 59-69.

Zou,H., Henzel,W.J., Liu,X., Lutschg,A., and Wang,X. (1997). Apaf-1, a human protein homologous to C. elegans CED-4, participates in cytochrome c-dependent activation of caspase-3. Cell *90*, 405-413.

Zou,H., Li,Y., Liu,X., and Wang,X. (1999). An APAF-1.cytochrome c multimeric complex is a functional apoptosome that activates procaspase-9. J. Biol. Chem. *274*, 11549-11556.